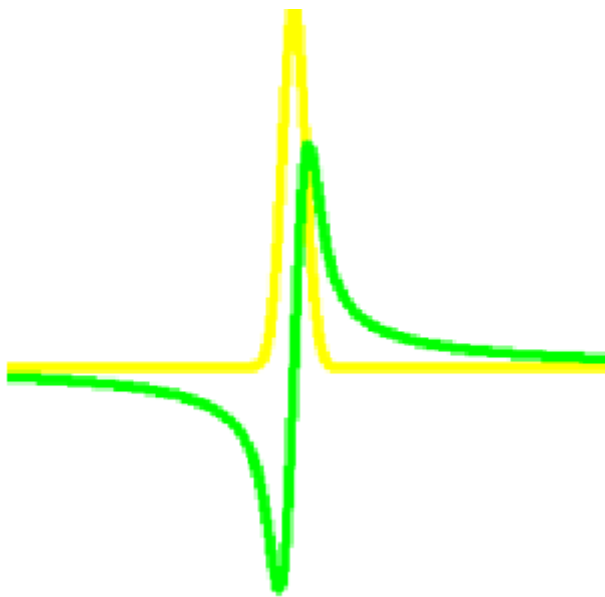


Numerical evaluation of the Hilbert transform in nonlinear optics

Krzysztof Parjaszewski



Dedication

To my Family.

Abstract

The motivation for this work comes from the real problem stated by physicists and chemists employing theoretical models to describe the interaction between light and matter due to the low-level and intense light irradiation. We are interested in the light behaviour both in the frequency and time domains. In the frequency domain the behaviour of light can be described with the Hilbert transform, but to build a valid models - we need to handle two important problems. The first problem concerns the numerical evaluation of the Hilbert Transform, which is defined with the singular and improper integral. The

second problem concerns the question stated by physicists: How to properly use these mathematical tools in a typical experiment and in the construction of a model useful in optical research? We present comparison of several implementations of the numerical calculations of the Hilbert transform:

- Numerical trapezoidal rule mixed with the Simpson's rule and the cubic interpolation,
- Newton-Cotes quadrature of the sixth degree,
- Clenshaw-Curtis quadrature,
- Hilbert transform based on fast Hartley transforms,
- a method based on approximation with the orthonormal Hermite polynomials and Hermite functions,
- a method based on approximation with the Fourier series.

We also test two out-of-the-box MATLAB-implemented routines `quadgk` and `hilbert` - based on the fast Fourier transform. The given physical models for both linear and nonlinear optics are analyzed and validated. We formulate hints for good practises for scientists interested in the subject of optical experiments. Finally, we make conclusions about the numerical stability, advantages and disadvantages of the developed implementations in further research on nonlinear optics.

Keywords

numerical integration, Cauchy principal value integral, Hilbert transform, nonlinear optics, Kramers-Kronig relations, optical dispersion relations

Promoters

Nonlinear optics

Professor Marek Samoć

Institute of Physical and Theoretical Chemistry
Wrocław University of Technology, PL-50-370 Wrocław
Wybrzeże Wyspiańskiego 27, Poland
+48-71-320-4466 — E-mail: Marek.Samoc@pwr.wroc.pl

Numerical analysis

Paweł Keller PhD

Numerical Analysis Research Group, Institute of Computer Science
University of Wrocław, PL-50-383 Wrocław
Joliot-Curie 15, Poland
+48-71-375-7813 — E-mail: Pawel.Keller@ii.uni.wroc.pl

Reviewer

Professor Stanisław Lewanowicz

Numerical Analysis Research Group, Institute of Computer Science
University of Wrocław, PL-50-383 Wrocław
Joliot-Curie 15, Poland
+48-71-375-7813 — E-mail: Stanislaw.Lewanowicz@ii.uni.wroc.pl

Author

Krzysztof Parjaszewski

Institute of Computer Science
University of Wrocław, PL-50-383 Wrocław
Joliot-Curie 15, Poland
+48-660-070-043 — E-mail: Krzysztof.Parjaszewski@gmail.com

1 Practical motivations

Physics and chemistry are two scientific domains strictly connected with mathematics and the numerical analysis. Playing with the experimental results and theoretical models scientists need the tools allowing them to validate or falsify their hypothesis, conclusions and observations (Figure 1.0.1).

The first motivation for this thesis was the problem stated by physicians and chemists about the complex physical quantity called the optical susceptibility denoted with χ :

$$\chi = \Re(\chi) + \Im(\chi). \quad (1.0.1)$$

The real part of the optical susceptibility is related with an optical phenomena - the refraction of light. The imaginary part of the susceptibility is connected with the absorption of light. In many models these two physical quantities are connected to each other with the modified Hilbert transform called the Kramers-Kronig relations:

$$\Re(\chi) \xrightarrow{\mathcal{H}} \Im(\chi). \quad (1.0.2)$$

The scientists require both mathematical and numerical tools to better understand the properties of the light beam interaction with matter.

In this thesis we have prepared and discussed several tools that evaluate the Hilbert transform, which together with the proper physical models, help to find a connection between the real and imaginary part of the optical susceptibility.

The subject of this thesis is not only an academic exercise - in the last twenty years the global interest in photonics, and especially application of light in modern devices for information transfer, storage and processing - including the construction of super-fast all-optical computers - is steadily increasing. Recent years have seen much focus on the science and technology of photonics on nano scale.

This thesis consists of three important fragments. In the first fragment we have prepared the introduction into the mathematical calculations (Chapter 2) and the overview of the theoretical physical models we will be using to check the prepared numerical methods

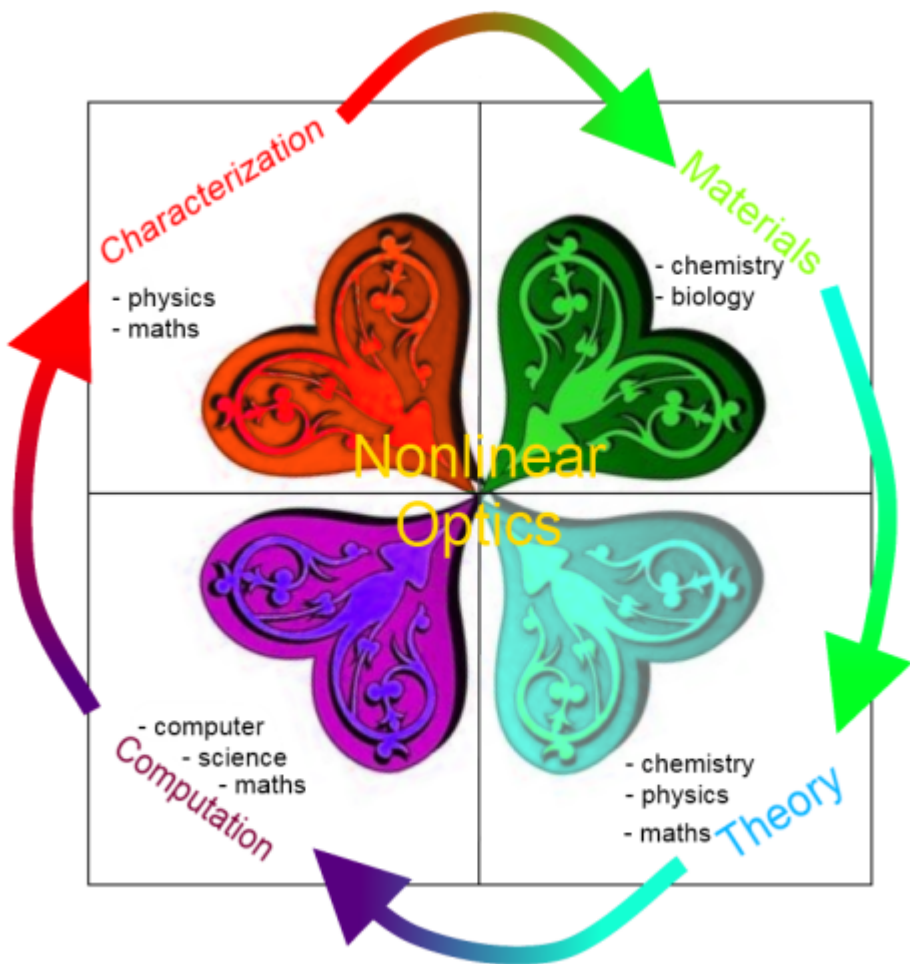


Figure 1.0.1: Nonlinear optics derives from many fundamental disciplines: biology, chemistry, maths, physics and computer science.

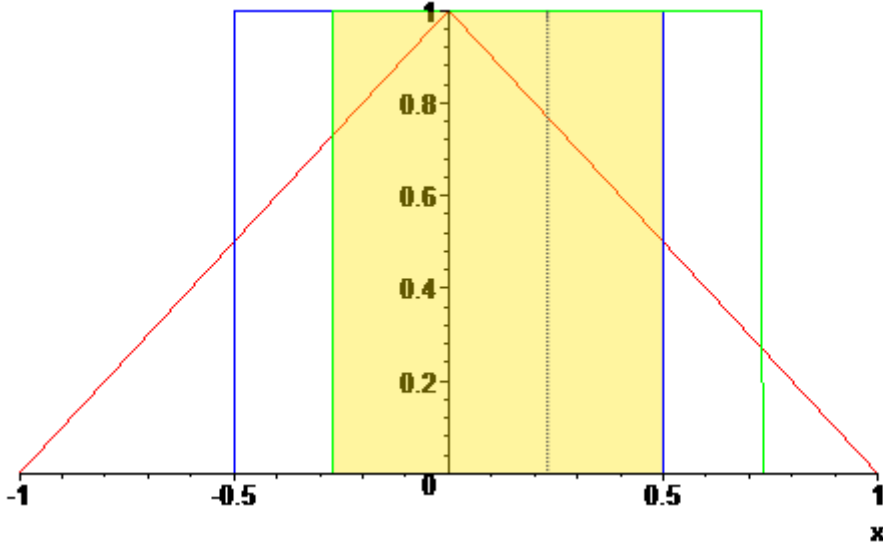


Figure 2.1.1: The example of convolution: the rectangle-like function overlaps another, equal rectangle-like function to create a triangle-like convolution as the result. In fact - the result is the modified trapezoid for the general case.

(Chapter 3). In the second fragment of this thesis we have prepared the short description of each Hilbert transform evaluating methods (Chapters 4 - 10). In the last fragment we have compared the obtained results (Chapter 11) and drew the final conclusions (Chapter 12). You can also find the attached source code in the document appendices.

The second motivation for this Thesis was to prepare a set of numerical tools for the advanced optical experiment called the Z-Scan experiment, which has been described in the Appendix B.

2 Mathematical calculations

2.1 Hilbert transform - introduction

To define the Hilbert transform we will need to firstly define the convolution operator $*$. In the area of functional analysis in mathematics the convolution is defined as the integral of a product of two functions, but one of them is shifted and reversed [5]:

$$(f * g)(x) \stackrel{\text{def}}{=} \int_{-\infty}^{\infty} f(\omega) g(x - \omega) d\omega. \quad (2.1.1)$$

The result of the convolution of two functions f and g is a third function h than can be described as the area overlap. The example has been presented on the Figure (2.1.1).

Now we are ready to define the Hilbert transform. In fact it is a convolution of given function $f(x)$ with the function $h(x) = \frac{1}{x\pi}$. The Hilbert transform has been presented in the equation (2.1.2)

$$\mathcal{H}[f(x)] \stackrel{\text{def}}{=} \int_{-\infty}^{\infty} f(\omega) h(x - \omega) d\omega = \frac{1}{\pi} \int_{-\infty}^{\infty} \frac{f(\omega)}{(x - \omega)} d\omega. \quad (2.1.2)$$

$f(x)$	$\mathcal{H}[f(x)]$
$\sin(x)$	$\cos(x)$
$\cos(x)$	$-\sin(x)$
$\frac{1}{1+x^2}$	$-\frac{x}{1+x^2}$
e^{-x^2}	$e^{-x^2} \frac{-2}{\sqrt{\pi}} \int_0^x e^{t^2} dt$
$\frac{\sin(x)}{x}$	$\frac{\cos(x)-1}{x}$
$\Pi(x) \equiv \begin{cases} 0 & \text{for } x > \frac{1}{2} \\ \frac{1}{2} & \text{for } x = \frac{1}{2} \\ 1 & \text{for } x < \frac{1}{2} \end{cases}$	$\frac{1}{\pi} \ln \left \frac{x-\frac{1}{2}}{x+\frac{1}{2}} \right $
$\delta(x) \equiv \frac{1}{\pi} \lim_{\epsilon \rightarrow 0} \frac{\epsilon}{x^2 + \epsilon^2}$	$-\frac{1}{\pi x}$

Table 1: The table presents example pair of functions with their Hilbert transforms.

It is important to stress that the dashed integral: \oint used in the equation (2.1.2) means the Cauchy principal value integral. It is the integration method for certain improper integrals like $h(x) = \frac{1}{x\pi}$. The Cauchy principal value was designed to omit the singularity and it is a less rigorous integration method than the Riemann integral. For the example singular $h(x)$ it is defined as in the equation (2.1.3):

$$\oint_{-\infty}^{\infty} \frac{f(\omega)}{(x-\omega)} d\omega = \lim_{a \rightarrow \infty} \int_{-a}^a \frac{f(\omega)}{(x-\omega)} d\omega. \quad (2.1.3)$$

More information about the Cauchy principal value integral can be easily found in the literature [16].

We have presented several pairs of functions and their Hilbert transforms in the Table (1) [46].

2.2 Fourier transform and its application

In this thesis we will very often use the description of a function in the time or in the frequency domain. The Fourier transform is a mathematical translation tool between those two domains and therefore is has many applications in modern physics and of course in optics.

Let $f : \mathbb{R} \rightarrow \mathbb{R}$ be a function of time. We can also call this function a signal. When we will search for the frequency function, also named the frequency spectrum, we can apply the Hilbert transform on the time-domain f function: $\mathcal{H}[f(t)] = \widehat{f}(\omega)$.

The one-dimensional Fourier transform is defined in the equation (2.2.1):

$$\widehat{f}(\omega) = \mathcal{F}[f(t)] \stackrel{\text{def}}{=} \int_{-\infty}^{\infty} f(t) e^{-2\pi i t \omega} dt. \quad (2.2.1)$$

We will also use the inverse Fourier transform as defined in the equation (2.2.2):

$$f(t) = \mathcal{F}^{-1}[\widehat{f}(\omega)] \stackrel{\text{def}}{=} \int_{-\infty}^{\infty} \widehat{f}(\omega) e^{-2\pi i \omega t} d\omega. \quad (2.2.2)$$

A typical example of a implemented Fourier transform can be find in the typical radio display called the equalizer as in the Figure (2.2.1).



Figure 2.2.1: The typical radio display - showing the proper wavelengths used in the current fragment of a music track.

The sound wave behaves in a similar way to the light wave. We can investigate properties of a light in the time domain - but we can also ask a question what different wavelengths is the investigated light beam created of. We will easily find the Fourier transform a good mathematical tool for answering such question. More information about the Fourier transform and its application can be easily found in the literature, for instance in Trott [41].

2.3 Lebesgue and Hardy spaces

We shall also define the Lebesgue and the Hardy spaces for the next calculations. The Lebesgue space is also called the L^p and is a function space described in the functional analysis. We can now define a function $f : \mathbb{S} \rightarrow \mathbb{D}$. The function f belongs to the L^p space if it is measurable and if raised to the p^{th} power it has a finite integral on \mathbb{S} with the measure μ . The formal definition has been presented in the equation 2.3.1:

$$\|f\|_p \equiv \left(\int_S |f|^p d\mu \right)^{\frac{1}{p}} < \infty. \quad (2.3.1)$$

Instead of \mathbb{S} we will often use the set of real numbers. The L^2 space, also named the set of quadratically integrable functions is commonly used in physics. When we have the frequency domain of a light signal it must belong to the L^2 space. Otherwise its energy would be considered as infinite. The Hardy spaces are a part of research interests in the complex analysis. They can be defined on domains like discs or circles, but they can also be defined for domains like the upper-half plane. We will take a closer look only for the third case.

The upper-half plane \mathbb{H} is the set of complex numbers defined as in equation (2.3.2):

$$\mathbb{H} = \{x + iy \mid y > 0; x, y \in \mathbb{R}\}. \quad (2.3.2)$$

The complex analysis very often investigates properties of the holomorphic functions. We say a function $f : \mathbb{C} \rightarrow \mathbb{C}$ is holomorphic when it has a complex derivative in each point of its domain and also in a small neighbourhood for each of domain points. For the complex function f the complex derivative is defined with a limit - very similar as for the real function - as in equation (2.3.3):

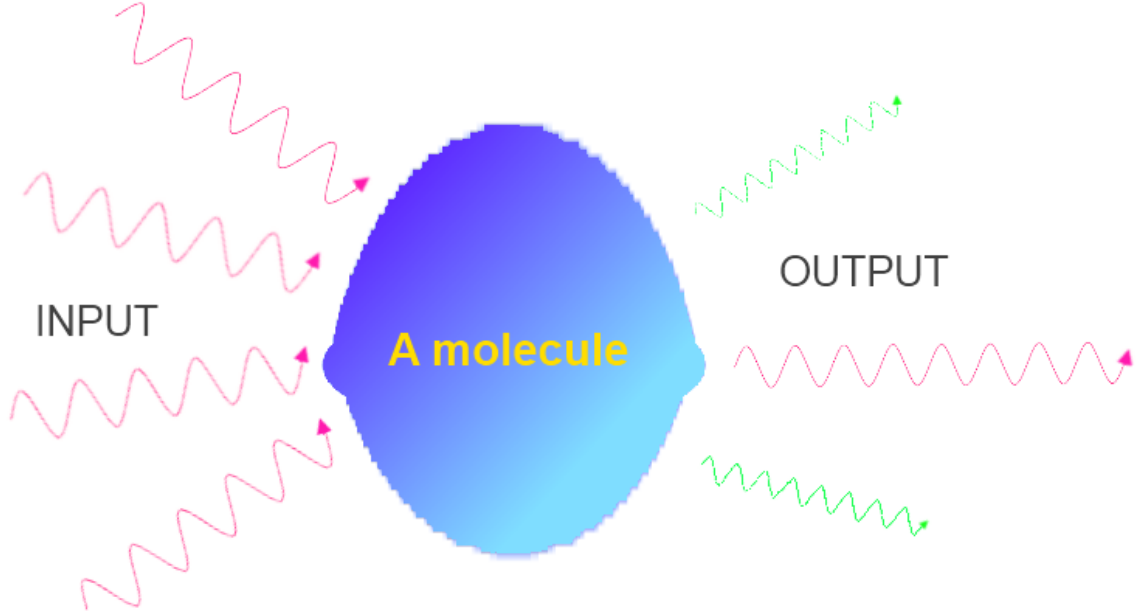


Figure 2.4.1: Schematic diagram of the nonlinear phenomenon – the input beam(s') wavelength(s) may differ from the output signal(s). This happens only in case of the strong optical signals.

$$f(z_0)' \stackrel{\text{def}}{=} \lim_{z \rightarrow z_0} \frac{f(z) - f(z_0)}{z - z_0} \quad \text{and} \quad z_0, z \in \mathbb{C}. \quad (2.3.3)$$

The Hardy space H^p defined on the upper-half plane \mathbb{H} is a class of holomorphic functions for which the norm $\|f\|_{H^p}$ is finite. The required norm satisfies the equation (2.3.4):

$$\|f\|_{H^p} = \sup_{y>0} \left[\int |f(x + iy)|^p dx \right]^{\frac{1}{p}} < \infty. \quad (2.3.4)$$

2.4 The causality principle

The causality is the important hypothesis not only in physics, but also in philosophy and statistics. Causality in physics links the cause with its effect. The first and easy example can be a force acting on a mass. The mass starts to accelerate because of the applied force. Therefore the force is here the cause and the mass acceleration is the effect.

In the field of optical research - we will be interested in both light and matter properties. When a light signal is passing through a matter, from the time-domain perspective - we can extract the input and the output signals, as presented on the Figure (2.4.1). From now on we will consistently use the **input** definition for the time-domain signal in time period **before** the interaction with the investigated matter and the **output** definition for the time-domain signal **after** the interaction with matter.

We must have in our mind, that not only in the field of optics some scientists creates the models which does not obey causality [28]. But in this thesis we will assume the causality applies to all models being investigated by us.

2.5 The Titchmarsh theorem

The central theorem in this thesis is the Titchmarsh theorem. It links the Fourier transform with the causality principle. We will focus on the output signal $a(t) : \mathbb{R} \rightarrow \mathbb{R}$ and assume that the interaction with matter happens in the $t = 0$ time, but the interaction time is negligibly short. As the causal output signal - for time $t < 0$ it's value equals zero. Our second assumption will be that the output signal is quadratically integrable. We will also assume that the Fourier transform of the output signal $\chi(\omega) = \mathcal{F}[a(t)] \in H^2(\mathbb{H})$ belongs to the Hardy space of the second order in the upper-half plane \mathbb{H} . With such assumptions the Titchmarsh theorem states for the χ function that it's real and imaginary values are Hilbert transform of each other.

We have prepared the more formal notation of the Titchmarsh theorem in the following equations:

We assume that:

$$a(t) \in L^2(\mathbb{R}), \quad (2.5.1)$$

$$\text{For all } t < 0 : a(t) = 0, \quad (2.5.2)$$

$$\chi(\omega) = \mathcal{F}[a(t)], \quad (2.5.3)$$

$$\chi(\omega) \in H^2(\mathbb{H}). \quad (2.5.4)$$

The Titchmarsh theorem states that:

$$\Re(\chi(\omega)) = \frac{1}{\pi} \int_{-\infty}^{\infty} \frac{\Im(\chi(\Omega))}{\Omega - \omega} d\Omega, \quad (2.5.5a)$$

$$\Im(\chi(\omega)) = -\frac{1}{\pi} \int_{-\infty}^{\infty} \frac{\Re(\chi(\Omega))}{\Omega - \omega} d\Omega. \quad (2.5.5b)$$

The Titchmarsh theorem states that the conditions from equations (2.5.1 with 2.5.2), (2.5.3 with 2.5.4) and (2.5.5a with 2.5.5b) are mathematically equivalent.

Proof with an exhausting review of both the Fourier and Hilbert transforms was described by Edward Charles Titchmarsh in [39] - the theory is described through all book chapters, but the theorem and its proof has been stated in chapter 5 about the conjugated integrals also Hilbert transforms.

3 Physical models to be used

3.1 The linear and the nonlinear optics

From now on we will focus on the application of the Hilbert transform in the optical research. The central interest of the optical research is the interaction of light and matter.

The light, also called the electromagnetic radiation, is a form of energy which travels between particles in a wave manner. From the microscopic point of view, light is also a beam of photons. The photon is the elementary massless particle that transport the special quantities of energy. The energy E of a single photon is inversely proportional to its wavelength λ as described in the equation (3.1.1). The $h = 4.135667516(91) \times 10^{-15} eV \cdot s$ is the Planck constant and the $c = 299792458 \frac{m}{s}$ is the speed of light:

$$E(\lambda) = \frac{h c}{\lambda}. \quad (3.1.1)$$

When the light interacts with matter the energy transfer occurs. If the light or more precisely the photon is absorbed - the matter increases its energy by the quantum of energy transported by that photon. When the light is emitted, some portion of the matter's energy is converted into a newly generated photon. In the optical research we are interested in both processes - the absorption and the generation of light. We are also interested in the theory behind these two effects - which will help us understand the nature of light in general. The good introduction into the theory of optics can be found in the McGraw-Hill encyclopedia [24], starting from the 12th volume.

Optics is divided in the main two areas - the linear and the nonlinear optics. To distinguish linear from the nonlinear phenomena, we need to remind the superposition. The superposition principle is applied to the linear system and its states the system fulfill the additivity (3.1.2) and the homogeneity (3.1.3) properties. The additivity is a term taken from algebra and it describes the function $f : \mathbb{X} \rightarrow \mathbb{Y}$ that preserves the addition operation:

$$\forall x, y \in X : f(x + y) = f(x) + f(y). \quad (3.1.2)$$

The homogeneity is an algebraic property of a function f : if the argument $x \in \mathbb{X}$ of a function $f : \mathbb{X} \rightarrow \mathbb{Y}$ is multiplied by a scalar α the result is also multiplied by this scalar. More precisely:

$$\forall \alpha \in \mathbb{R} \text{ and } \forall x \in \mathbb{X} : f(\alpha x) = \alpha f(x). \quad (3.1.3)$$

In the linear optics we state that the system satisfies the superposition principle. “The system” here is the investigated setup of light and matter. From the microscopic point of view it means - the more often photons transfers energy to and from the mass, the more the same effects take place and the only difference is the amount of energy being transferred in the set period of time. When the systems starts to “saturate”, photons cannot be processed in the same way and some new optical phenomena take place.

3.2 The response of a system

To better understand the relation between the light **input** and **output** we shall once more use the convolution. Given the input signal in the time-domain: $x(t)$ and the linear systems response function described as $h(t)$ we can easily get the output signal $y(t)$ as the convolution $x(t) * h(t)$:

$$y(t) = x(t) * h(t) \stackrel{\text{def}}{=} \int_{-\infty}^{\infty} x(t - \tau) \cdot h(\tau) d\tau. \quad (3.2.1)$$

This definition gives no new information because we now nothing about the response function $h(t)$. But from the convolution theorem [21] we know that the Fourier transform applied to the convolution of two given functions equals the simple multiplication of two Fourier transforms:

$$\mathcal{F}(a(x) * \chi(x)) = \mathcal{F}(a(x)) \cdot \mathcal{F}(\chi(x)). \quad (3.2.2)$$

The proof to the convolution theorem (3.2.2) can be found in [39].

The definition of the system's response (3.2.1) is true for the linear case. For the nonlinear systems we must provide the more complicated mathematical tool called the Volterra series model well described in the PhD thesis of Antonín Novák [29]. The output signal $y(t)$ equals the sum of components, each of which is the n^{th} order Volterra operator \mathbf{K}_n of the input signal $x(t)$:

$$y(t) = \sum_n \mathbf{K}_n[x(t)]. \quad (3.2.3)$$

The n^{th} order Volterra operator \mathbf{K}_n is defined as the multidimensional convolution:

$$\mathbf{K}_n = \int_{-\infty}^{\infty} \dots \int_{-\infty}^{\infty} k_n(\tau_1, \dots, \tau_n) \cdot x(t - \tau_1) \dots (x - \tau_n) d\tau_1 \dots d\tau_n. \quad (3.2.4)$$

The $k_n : \mathbb{X}^n \rightarrow \mathbb{Y}$ function is called the n^{th} order Volterra-kernel.

We notice the output function for the linear case (3.2.1) is equal to the nonlinear output function assuming that all the Volterra-kernels of orders higher than one are equal to zero. We say the kernel is causal if it equals zero for any negative argument.

From now on we must distinguish the light **input**, the light **output** and the matter **response** functions from each other. The matter **response** function for the interaction of the n^{th} order is the n^{th} order Volterra-kernel.

3.3 The linear system

Let imagine an input single pulse-like signal “shots” the matter. We expect the matter to respond with a short, fading response signal. The $\Theta(t) : \mathbb{R} \rightarrow \{0, 1\}$ function will state the Heaviside function defined as in the equation 3.3.1:

$$\Theta(t) = \begin{cases} 0 & \text{for } t < 0, \\ 1 & \text{otherwise.} \end{cases} \quad (3.3.1)$$

Not getting into the theory of the linear optical response, we can create our first simple response function h_{lin} as the fading sinusoidal exponent:

$$h_{\text{lin}}(t) = 1 - e^{(-t)} \sin(20t) \Theta(t). \quad (3.3.2)$$

The plot of the equation 3.3.2 is given on the Figure (3.3.1).

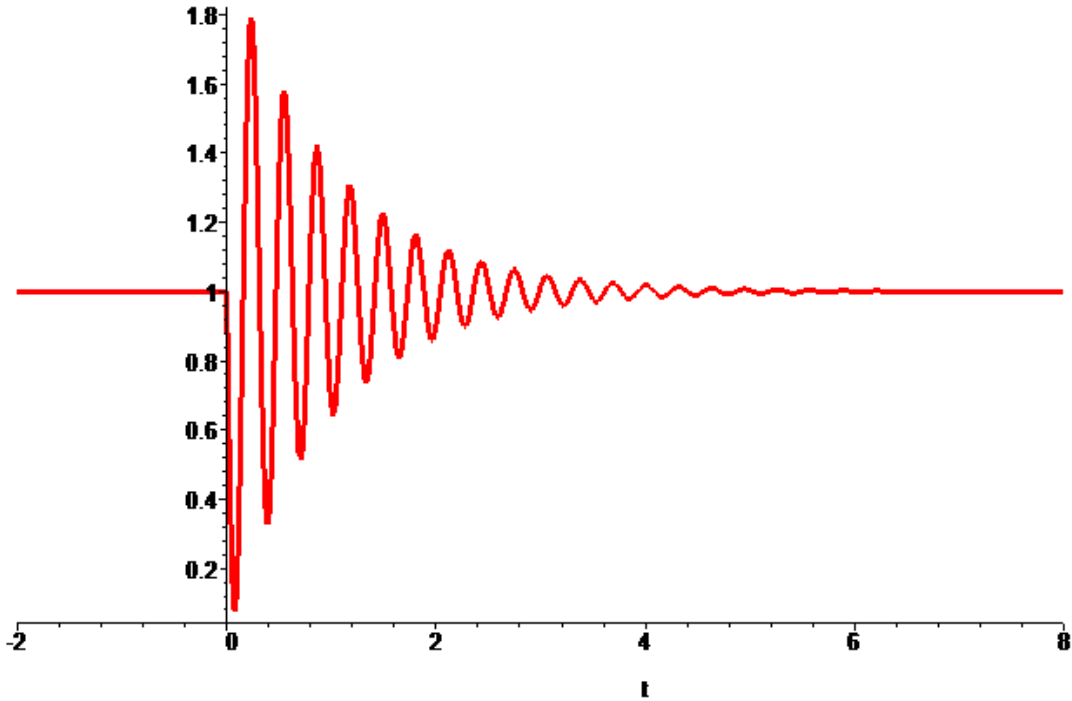


Figure 3.3.1: A typical linear response signal in time domain

If we would like to know the response signal in the frequency domain, we will apply the Fourier transform on the h_{lin} :

$$\mathcal{F}[h_{\text{lin}}] = \chi_{\text{lin}}(\omega) \approx \frac{-20}{(\omega i + 1 - 20 i)(\omega i + 1 + 20 i)}, \quad (3.3.3)$$

In the equation (3.3.3) we have omitted the Dirac delta function that will appear if we calculate the Fourier transform properly. The Dirac delta function can be omitted from the numerical point of view. The calculated χ_{lin} is called the linear optical susceptibility. We are interested in the notation of χ_{lin} as the function of frequency ω . More theoretical background about the optical susceptibility can be found in Boyd [3].

As You can see - the time domain linear response signal h_{lin} and the corresponding linear optical susceptibility χ_{lin} pass the assumptions of the Titchmarsh theorem. In the further numerical calculations we will put the χ_{lin} into tests.

3.4 Nonlinear models

In this subsection we will shortly describe the time-resolved processes which allow to determine the origin of two important nonlinear processes: the pump-and-probe and the frequency mixing process.

Pump-and-probe process

The laser is typically a source of a high-energy input signal. In a typical pump-and-probe process we use two laser beams. One of them is a strong input and we name it the 'pump'. The second input - the 'probe' - is much less intense. We try to synchronise these two

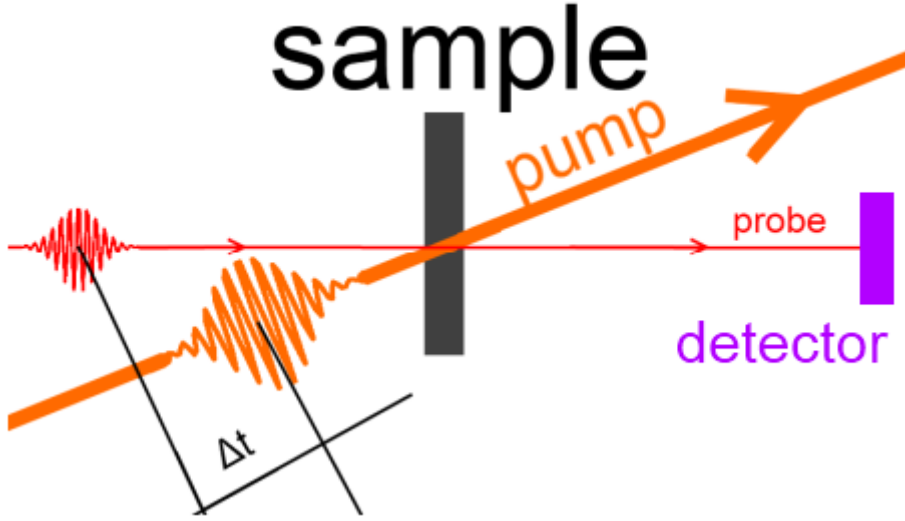


Figure 3.4.1: The pump-and-probe experiment

laser beams in the following way - firstly a pump input hits the matter sample with its strong intensity - causing modifications in the matter properties. Shortly after that - within a time period Δt - a low-intensity probe input hits the modified sample and its properties are measured through a detector. In a typical experiment the Δt time period should be adjustable. There are various types of pump-probe experiments, for example one can detect changes of the amplitude of the matter response signal. The schematic diagram of a pump-and-probe experiment is shown in Figure (3.4.1).

The key assumption in the pump-and-probe experiment is that separated and independent probe inputs cannot introduce a nonlinear response of the system alone [3]. The probe signal should be sufficiently weak. In the so-called two-level model the investigated atomic system is characterized for both the pump and the probe inputs by two different relaxation times: T_1 and T_2 respectively. A more detailed model is defined by H. N. Yum et al. [47] for the nonlinear susceptibility in case of the pump-probe process:

$$\chi_{pp}(\delta) = \frac{G n^0 \gamma_{ba}}{\Delta + \delta + i \eta} \cdot [1 - \frac{\Omega_1^2 (\Delta - \delta + i \eta) (\delta + 2 i \eta)}{(\Delta - i \eta) ((\delta + i \theta) (\Delta + \delta + i \eta) (\delta - \Delta + i \eta) - \Omega_1^2 (\delta + i \eta))^2}]. \quad (3.4.1)$$

In the equation (3.4.1) we have introduced a whole branch of new variables. The δ is the probe input frequency, the Δ means the pump input frequency. Other variables are related with the pump T_1 relaxation time:

$$\begin{aligned} \Omega_1 &= \Omega_1(T_1), \\ G &= G(T_1), \\ n^0 &= n^0(T_1), \\ \gamma_{ba} &= \gamma_{ba}(T_1), \\ \eta &= \eta(T_1), \\ \theta &= \theta(T_1), \end{aligned}$$

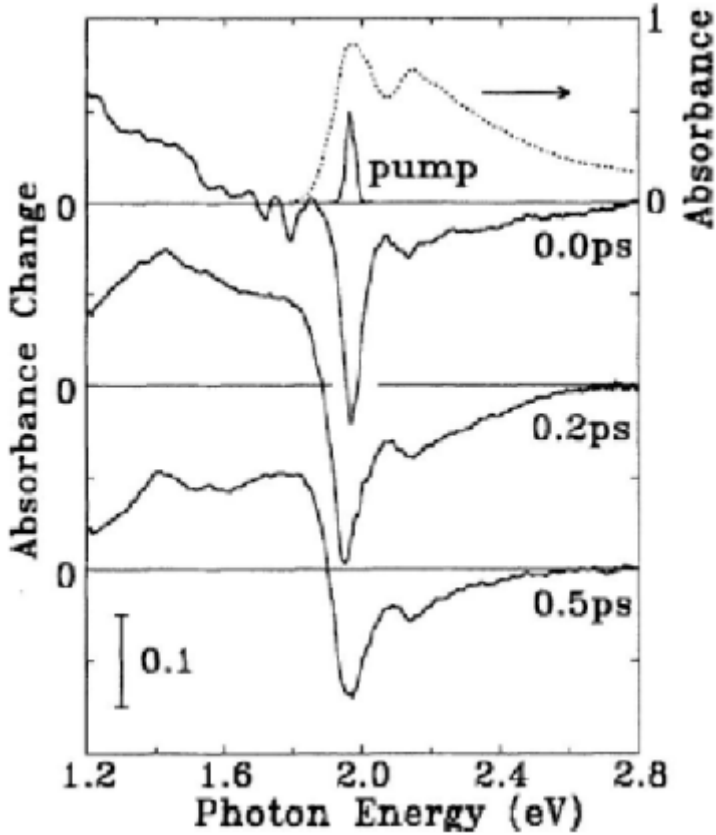


Figure 3.4.2: The pump-and-probe absorption change due to time delay between the pump and probe signal. The figure taken from [8].

The pump relaxation time depends on the time period between ($\Delta_1 t$) input pulses:

$$T_1 = T_1(\Delta_1 t). \quad (3.4.2)$$

We can now easily deduce that also the pump-and-probe nonlinear susceptibility depends on the $\Delta_1 t$ as presented in the equation (3.4.3):

$$\chi_{pp} = \chi_{pp}(\delta, \Delta_1 t). \quad (3.4.3)$$

In sense of the response theory this observation leads us to the conclusion, that the susceptibility of the nonlinear process depends not only on the input signal frequency (energy) - but also on the time delay between the moments, when two or more photons arrive at the molecule. Here we are talking about an important problem in nonlinear optics which is constructing a valid model for the pump-and-probe process - to allow us to use the Titchmarsh theorem here.

In [8] we can find results showing that the probe signal absorbance depends not only on the pump signal properties, but also on the time delay between the pump and probe - see the Figure (3.4.2).

More interesting results come when we assume that susceptibility is a complex function of two parameters, both the pump and probe signal frequency:

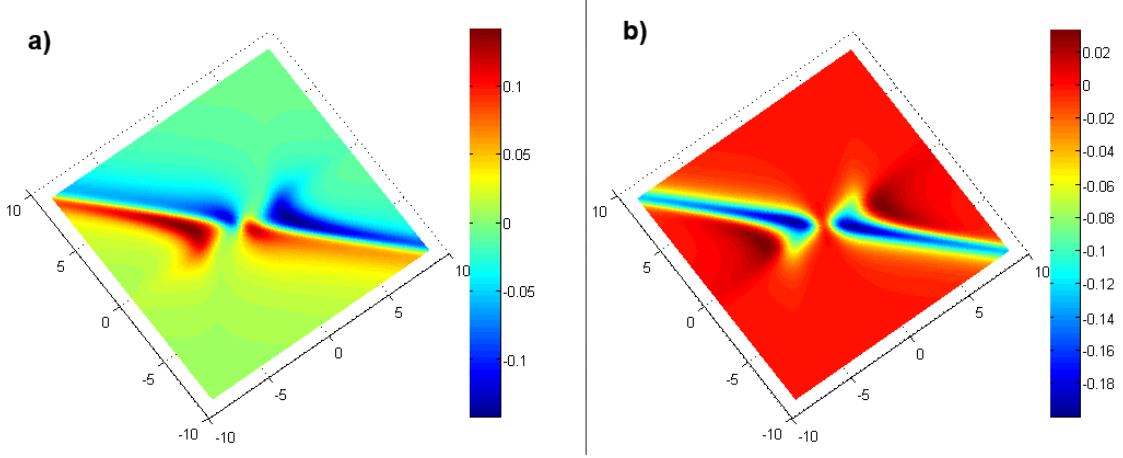


Figure 3.4.3: 2-Dimensional plots of both a) real and b) imaginary parts of the nonlinear susceptibility treated as a bi-argumental function, where the colour means the function value

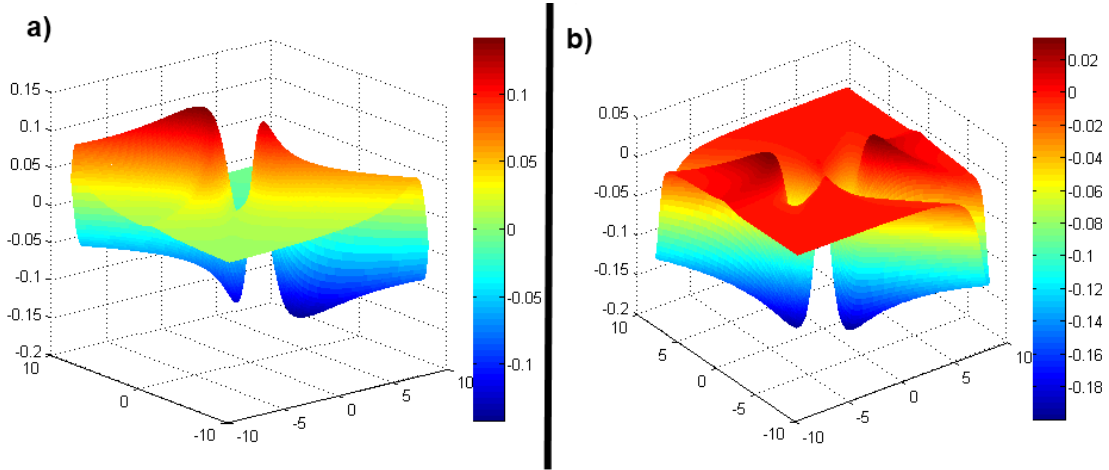


Figure 3.4.4: 3-Dimensional plots of both a) real and b) imaginary parts of nonlinear susceptibility treated as a bi-argumental function, where the colour means the function value

$$\chi_{pp} = \chi_{pp}(\delta, \Delta_1 t (\text{ const }), \Delta) \quad (3.4.4)$$

Therefore we obtain the three dimensional plots presented on the Figures (3.4.3) and (3.4.4).

Frequency Mixing Process

The frequency mixing is a general class of processes where we have two or more input photons with their frequencies: $\omega_{\text{input},1}, \omega_{\text{input},2}, \omega_{\text{input},3}, \dots$ and we receive one or more output photons with their frequencies: $\omega_{\text{output},1}, \omega_{\text{output},2}, \omega_{\text{output},3}, \dots$. In chapter 6.6 of Boyd [3] we can find the description of processes in which we use the strong signal 'pump' with frequency ω and the weak signal 'probe' with the frequency $\omega - \delta$ nearly copropagating, as it was shown in Figure (3.4.5).

For such a process the model for the linear susceptibilities has been defined by Boyd for both $\omega + \delta$ and $\omega - \delta$ frequencies, where T_1, T_2 and Δ are time-related variables,

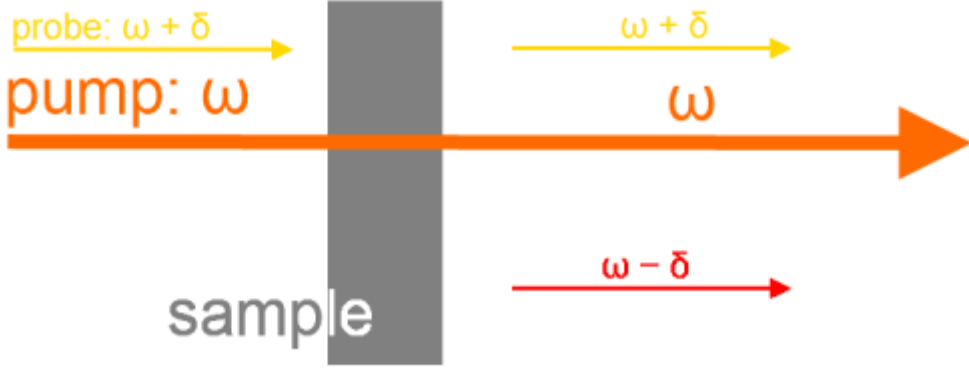


Figure 3.4.5: The pump-and-probe frequency mixing process from chapter 6.6 Boyd [3].

assumed constant in this thesis:

$$\chi_{eff,1}(\omega + \delta, T_1 = \text{const}, T_2 = \text{const}, \Delta = \text{const}) = \frac{\left(\frac{i}{T_1} + \delta\right) \text{const}}{D(\delta)} \left(\frac{i}{T_2} + \delta - \Delta - \frac{\Omega^2 \delta}{2(\Delta - \frac{i}{T_2})} \right), \quad (3.4.5a)$$

$$\chi_{eff,1}(\omega - \delta, T_1 = \text{const}, T_2 = \text{const}, \Delta = \text{const}) = \frac{\left(\frac{i}{T_1} - \delta\right) \text{const}}{D(\delta)} \left(\frac{i}{T_2} - \delta - \Delta + \frac{\Omega^2 \delta}{2(\Delta - \frac{i}{T_2})} \right). \quad (3.4.5b)$$

Boyd also derives the third-order nonlinear susceptibilities for both $\omega + \delta$ and $\omega - \delta$ frequencies (we assume T_1 , T_2 and Δ to be constant time variables).

$$\chi_{eff,3}(\omega + \delta = \omega + \omega - (\omega - \delta)) = \frac{(-\delta - \Delta - \frac{i}{T_2})(\delta + \frac{2i}{T_2}) \text{const}}{(\Delta + \frac{i}{T_2})(\Delta + \delta + \frac{i}{T_2}) D^*(\delta)}, \quad (3.4.6a)$$

$$\chi_{eff,3}(\omega - \delta = \omega + \omega - (\omega + \delta)) = \frac{(\delta - \Delta - \frac{i}{T_2})(-\delta + \frac{2i}{T_2}) \text{const}}{(\Delta + \frac{i}{T_2})(\Delta - \delta + \frac{i}{T_2}) D^*(\delta)}. \quad (3.4.6b)$$

We have used the symbol of $D^*(\delta)$ to describe the conjugate function of D . The D functions is defined as in the equation (3.4.7):

$$D(\delta) = \left(\delta + \frac{1}{T_1}\right) \left(\delta - \Delta + \frac{i}{T_2}\right) \left(\delta + \Delta + \frac{i}{T_2}\right) - \Omega^2 \left(\delta + \frac{i}{T_2}\right). \quad (3.4.7)$$

The test 3-dimensional plot is presented in the Figures (3.4.6) and (3.4.7).

We will shortly review the derivation of the Hilbert transform for nonlinear models. As proposed by Lucarini [25], we connect the imaginary and the real part of the nonlinear optical susceptibility with the higher-level Hilbert transform:

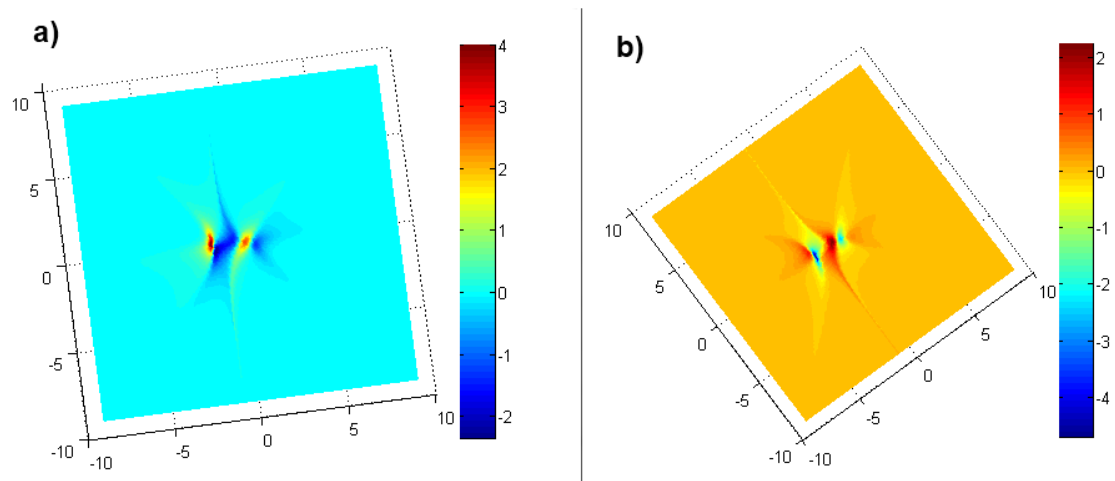


Figure 3.4.6: 2-Dimensional plots of both a) real and b) imaginary parts of nonlinear susceptibility treated as a bi-argumental function, where the colour means the function value

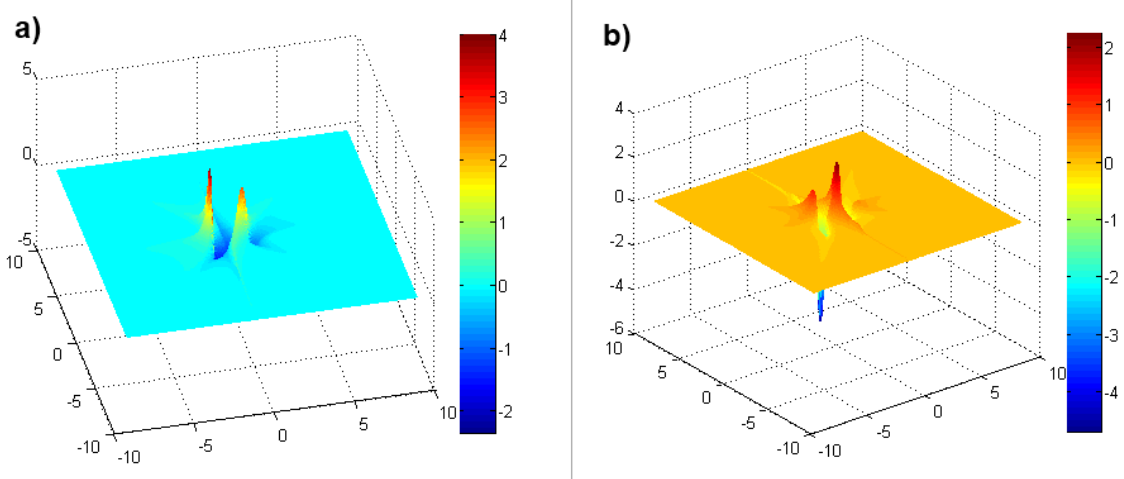


Figure 3.4.7: 3-Dimensional plots of both a) real and b) imaginary parts of nonlinear susceptibility treated as a bi-argumental function, where the colour means the function value

$$\Im(\chi_{n,i,j_1,\dots,j_n}(\sum_{l=1}^n \omega_l, \omega_1, \dots, \omega_n)) = \frac{-1}{(\pi)^n} \int_{-\infty}^{\infty} \dots \int_{-\infty}^{\infty} \frac{\Re(\chi_{n,i,j_1,\dots,j_n}(\sum_{l=1}^n \Omega_l, \Omega_1, \dots, \Omega_n))}{(\Omega_1 - \omega_1) \dots (\Omega_n - \omega_n)} d\Omega_1 \dots d\Omega_n, \quad (3.4.8a)$$

$$\Re(\chi_{n,i,j_1,\dots,j_n}(\sum_{l=1}^n \omega_l, \omega_1, \dots, \omega_n)) = \frac{1}{\pi^n} \int_{-\infty}^{\infty} \dots \int_{-\infty}^{\infty} \frac{\Im(\chi_{n,i,j_1,\dots,j_n}(\sum_{l=1}^n \Omega_l, \Omega_1, \dots, \Omega_n))}{(\Omega_1 - \omega_1) \dots (\Omega_n - \omega_n)} d\Omega_1 \dots d\Omega_n. \quad (3.4.8b)$$

These integrals are hard to solve numerically and they go beyond the subject of this thesis. Here we will assume a great simplification and we will take only one frequency ω_1 into consideration:

$$\Im(\chi_{n,i,j_1,\dots,j_n}(\sum_{l=1}^n \omega_l, \omega_1, \dots, \omega_n)) = \frac{-1}{\pi} \int_{-\infty}^{\infty} \frac{\Re(\chi_{n,i,j_1,\dots,j_n}(\sum_{l=1}^n \Omega_l, \Omega_1, \omega_2, \dots, \omega_n))}{\Omega_1 - \omega_1} d\Omega_1, \quad (3.4.9a)$$

$$\Re(\chi_{n,i,j_1,\dots,j_n}(\sum_{l=1}^n \omega_l, \omega_1, \dots, \omega_n)) = \frac{1}{\pi} \int_{-\infty}^{\infty} \frac{\Im(\chi_{n,i,j_1,\dots,j_n}(\sum_{l=1}^n \Omega_l, \Omega_1, \omega_2, \dots, \omega_n))}{\Omega_1 - \omega_1} d\Omega_1. \quad (3.4.9b)$$

But we know that the signal response does not only depend on the input frequencies $\omega_1, \dots, \omega_n$, but also on the time delays between them T_1, \dots, T_{n-1} :

$$\chi_{n,i,j_1,\dots,j_n}(\sum_{l=1}^n \omega_l, \omega_1, \dots, \omega_n) = \chi_{n,i,j_1,\dots,j_n}(\sum_{l=1}^n \omega_l, \omega_1, \dots, \omega_n, T_1, \dots, T_{n-1}). \quad (3.4.10)$$

Automatically we expand equation (3.4.9) into (3.4.11a) and (3.4.11b):

$$\Im(\chi_{n,i,j_1,j_2,\dots,j_n}(\sum_{l=1}^n \omega_l, \omega_1, \omega_2, \dots, \omega_n, T_1, T_2, \dots, T_{n-1})) = \frac{-1}{\pi} \int_{-\infty}^{\infty} \frac{\Re(\chi_{n,i,j_1,j_2,\dots,j_n}(\sum_{l=1}^n \Omega_l, \Omega_1, \omega_2, \dots, \omega_n, T_1, T_2, \dots, T_{n-1}))}{\Omega_1 - \omega_1} d\Omega_1, \quad (3.4.11a)$$

$$\Re(\chi_{n,i,j_1,j_2,\dots,j_n}(\sum_{l=1}^n \omega_l, \omega_1, \omega_2, \dots, \omega_n, T_1, T_2, \dots, T_{n-1})) = \frac{1}{\pi} \int_{-\infty}^{\infty} \frac{\Im(\chi_{n,i,j_1,j_2,\dots,j_n}(\sum_{l=1}^n \Omega_l, \Omega_1, \omega_2, \dots, \omega_n, T_1, T_2, \dots, T_{n-1}))}{\Omega_1 - \omega_1} d\Omega_1. \quad (3.4.11b)$$

The evaluation of the higher order Hilbert transforms will be a key to understand the mathematical model of the nonlinear optics. In this thesis we make only a one little step forward.

3.5 The quantum-perturbation models

The quantum mechanics is a part of physics where the microscopic particles and energies are described. We can call the quantum mechanics also the quantum physics or the quantum theory. The main focus of the quantum physics is on the vectors describing the properties of indicated physical system at a given time. These vectors are the sets of properties and physical values which are time and space dependent. Such vectors are also named the complex wave functions. The values of such vectors are not unrestricted due to the main assumption that any physical action must be a multiple of a small physical quantity - called the Planck constant: $h = 6.62606957(29) \times 10^{-34}$ Joule times second .

The maths used to describe the quantum world is far more complicated than one used in the classical physics and we will not get into the details in this thesis. We will shortly introduce the two physical models of the quantum linear and nonlinear susceptibility described by Kuzyk [27] and Boyd [3]. The calculations used in both cited works are based on the time-dependent perturbation. The introduced concept of the perturbation is an interesting mathematical idea to solve difficult, differential equations.

The sum-over-states model

The first model is named the sum-over-states. In this model we will sum all possible excited states and transitions between such states for a single atom. In the linear case we assume that the atom can only be in m excited states with no other option for atom than transition from the ground state to one of the m exited states and forth. The reason for such a prohibition is simple - we will assume only one photon is interacting with the atom. You may associate the excited state with a situation when a single photon is absorbed by the atom and its energy is added to the energy of the whole system.

In the nonlinear cases - we will assume that the number of possible atom states and inner-states transitions is increasing. To describe the second-order nonlinear susceptibility we will assume there are m possible troikas - so the combination of three possible states with an option for transition between each state in a troika. To describe the third-order nonlinear susceptibility - we will assume that there are m possible fours of states.

We name this model the sum-over-states, because we will perform summation over all possible excited states for the theoretical model of an atom. We have already introduced the Planck constant h . We will also used the N constant to describe the number density of atoms - which describe the concentration of any countable objects in a given, three-dimensional volume. We shall also introduce the vacuum permittivity constant $\epsilon_0 \approx 8.854187817620 \times 10^{-12}$ Farad per meter .

There are two more physical values to be discussed. First of the is $\mu_{i,ab}$ and the second is ω_{cd} . $\mu_{i,ab}$ will be a matrix-like value, and the ω_{cd} will be a vector-like value. There are many situations in physics, when a value is described by the vector, two-dimensional matrix or a matrices of higher order. Such values are called **tensors**. μ_{ab} tensor is described as the electric dipole moment with the Coulomb-meter SI unit. The electric dipole

moment in physics describes the separation of the negative and the positive charges in a systems consisting of charges. It is also called the system's polarity. It describes the polarity of a system between a state "a" and the state "b". The order of indices also matters, so $\mu_{i,ab}$ is a different value from $\mu_{i,ba}$. In our calculations this value will be a two-dimensional tensor - so a matrix - because one dimension will be related with the "ab" or "ba" direction and the second dimension will be related with i - the indicated spatial property of an atom. The atom "shotted" with a photon in the direction of the axis OX may behave different than "shotted" from the OY axis. This is also a simplification and in general case the more photons are we taking into consideration, the higher order of a tensor need to be introduced.

The last value is an amount of energy related with a frequency ω_{cd} required for an atom to make a transition between state "c" and state "d". We will use a one-dimensional tensor to describe this value. P_I is the intrinsic permutation operator, in general it is used not to repeat the very same summands again and again just with slight modification of + and - signs - but please see details in [3].

The ω_p is the frequency of the input photon and it will be a variable in our equations. The final equations are taken from Boyd [3]. They describe the linear (first order) optical susceptibility and the nonlinear (second and third order) optical susceptibilities as a functions of ω_p :

$$\chi_{1,i,j}(\omega_p) = \frac{N}{\varepsilon_0 h} \sum_m \left(\frac{\mu_{i,gn} \mu_{j,mg}}{\omega_{mg} - \omega_p} + \frac{\mu_{j,gn} \mu_{i,mg}}{\omega_{mg} + \omega_p} \right), \quad (3.5.1a)$$

$$\begin{aligned} \chi_{2,i,j,k}(\omega_p + \omega_q, \omega_q, \omega_p) &= \frac{N}{\varepsilon_0 h^2} P_I \sum_{mn} \left(\frac{\mu_{i,gn} \mu_{j,nm} \mu_{k,mg}}{(\omega_{ng} - \omega_p - \omega_q)(\omega_{mg} - \omega_p)} + \right. \\ &\quad \left. + \frac{\mu_{j,gn} \mu_{i,nm} \mu_{k,mg}}{(\omega_{ng} + \omega_q)(\omega_{mg} - \omega_p)} + \frac{\mu_{i,gn} \mu_{k,nm} \mu_{i,mg}}{(\omega_{ng} + \omega_q)(\omega_{mg} + \omega_p + \omega_q)} \right), \end{aligned} \quad (3.5.1b)$$

where ,

$$\chi_{3,k,j,i,h}(\omega_\sigma, \omega_r, \omega_q, \omega_p) = \quad (3.5.1c)$$

$$\begin{aligned} &\frac{N}{\varepsilon_0 h^3} P_I \sum_{mnv} \left(\frac{\mu_{k,gv} \mu_{j,vn} \mu_{i,nm} \mu_{h,mg}}{(\omega_{vg} - \omega_r - \omega_q - \omega_p)(\omega_{ng} - \omega_q - \omega_p)(\omega_{mg} - \omega_p)} \right. \\ &\quad + \frac{\mu_{j,gv} \mu_{k,vn} \mu_{i,nm} \mu_{h,mg}}{(\omega_{vg} + \omega_r)(\omega_{ng} - \omega_q - \omega_p)(\omega_{mg} - \omega_p)} + \frac{\mu_{j,gv} \mu_{i,vn} \mu_{k,nm} \mu_{h,mg}}{(\omega_{vg} + \omega_r)(\omega_{ng} + \omega_r + \omega_q)(\omega_{mg} - \omega_p)} \\ &\quad \left. + \frac{\mu_{j,gv} \mu_{i,vn} \mu_{h,nm} \mu_{k,mg}}{(\omega_{vg} + \omega_r)(\omega_{ng} + \omega_r + \omega_q)(\omega_{mg} + \omega_r + \omega_q + \omega_p)} \right). \end{aligned}$$

The density matrix model

Starting from the models described in the (3.5.1a), (3.5.1b) and (3.5.1c) equations we can easily jump to the density matrix operator models. Not getting into the theoretical background - we will introduce a new term γ_{ab} which will be the imaginary tensor describing the so called dumping rate, which is an element of the density matrix, describing the coherence between states a and b . The models have been described in the following equations:

$$\chi_1(\omega_p) = \frac{N}{\varepsilon_0 h} \sum_n \left(\frac{\mu_{i,an} \mu_{j,na}}{\omega_{na} - \omega_p - i \gamma_{na}} + \frac{\mu_{i,na} \mu_{j,an}}{\omega_{na} - \omega_p + i \gamma_{na}} \right), \quad (3.5.2a)$$

$$\chi_{2,i,j,k}(\omega_p + \omega_q, \omega_q, \omega_p) = \frac{N}{2 \varepsilon_0 h^2} \sum_{lmn} \rho_{0,ll} \left(\frac{\mu_{i,l,n} \mu_{j,nm} \mu_{k,ml}}{(\omega_{nl} - \omega_p - \omega_q - i \gamma_{nl})(\omega_{ml} - \omega_p - i \gamma_{ml})} + \right. \\ \left. + \frac{\mu_{i,l,n} \mu_{k,nm} \mu_{j,ml}}{(\omega_{nl} - \omega_p - \omega_q - i \gamma_{nl})(\omega_{ml} - \omega_q - i \gamma_{ml})} + \right. \\ \left. + \frac{\mu_{k,l,n} \mu_{i,nm} \mu_{j,ml}}{(\omega_{mn} - \omega_p - \omega_q - i \gamma_{mn})(\omega_{nl} + \omega_q + i \gamma_{nl})} + \right. \\ \left. + \frac{\mu_{j,l,n} \mu_{i,nm} \mu_{k,ml}}{(\omega_{mn} - \omega_p - \omega_q - i \gamma_{mn})(\omega_{nl} + \omega_q + i \gamma_{nl})} + \right. \\ \left. + \frac{\mu_{j,l,n} \mu_{i,nm} \mu_{k,ml}}{(\omega_{nm} + \omega_p + \omega_q + i \gamma_{nm})(\omega_{ml} - \omega_p - i \gamma_{ml})} + \right. \\ \left. + \frac{\mu_{k,l,n} \mu_{j,nm} \mu_{i,ml}}{(\omega_{nm} + \omega_p + \omega_q + i \gamma_{nm})(\omega_{ml} - \omega_p - i \gamma_{ml})} + \right. \\ \left. + \frac{\mu_{k,l,n} \mu_{j,nm} \mu_{i,ml}}{(\omega_{ml} + \omega_p + \omega_q + i \gamma_{ml})(\omega_{nl} + \omega_p + i \gamma_{nl})} + \right. \\ \left. + \frac{\mu_{j,l,n} \mu_{k,nm} \mu_{i,ml}}{(\omega_{ml} + \omega_p + \omega_q + i \gamma_{ml})(\omega_{nl} + \omega_q + i \gamma_{nl})} \right), \quad (3.5.2b)$$

$$+ \frac{\mu_{k,l,v} \mu_{j,vn} \mu_{i,nm} \mu_{h,ml}}{(\omega_{vl} - \omega_p - \omega_q - \omega_r - i \gamma_{vl})(\omega_{nl} - \omega_p - \omega_q - i \gamma_{nl})(\omega_{ml} - \omega_p - i \gamma_{ml})} + \\ + \frac{\mu_{h,l,v} \mu_{k,vn} \mu_{j,nm} \mu_{i,ml}}{(\omega_{nv} - \omega_p - \omega_q - \omega_r - i nv)(\omega_{mv} - \omega_p - \omega_q - i \gamma_{mv})(\omega_{vl} + \omega_p + i \gamma_{vl})} + \\ + \frac{\mu_{i,l,v} \mu_{k,vn} \mu_{j,nm} \mu_{h,ml}}{(\omega_{nv} - \omega_p - \omega_q - \omega_r - i \gamma_{nv})(\omega_{vm} + \omega_p + \omega_q + i \gamma_{vm})(\omega_{ml} - \omega_p - i \gamma_{ml})} + \\ + \frac{\mu_{h,l,v} \mu_{i,vn} \mu_{k,nm} \mu_{j,ml}}{(\omega_{mn} - \omega_p - \omega_q - \omega_r - i \gamma_{mn})(\omega_{nl} - \omega_p - \omega_q + i \gamma_{nl})(\omega_{vl} + \omega_p + i \gamma_{vl})} + \\ + \frac{\mu_{j,l,v} \mu_{k,vn} \mu_{i,nm} \mu_{h,ml}}{(\omega_{vn} - \omega_p - \omega_q - \omega_r + i \gamma_{vn})(\omega_{nl} - \omega_p - \omega_q - i \gamma_{nl})(\omega_{ml} - \omega_p - i \gamma_{ml})} + \\ + \frac{\mu_{h,l,v} \mu_{j,vn} \mu_{k,nm} \mu_{i,ml}}{(\omega_{nm} + \omega_p + \omega_q + \omega_r + i \gamma_{nm})(\omega_{mv} - \omega_p - \omega_q - i \gamma_{mv})(\omega_{vl} + \omega_p + i \gamma_{vl})} + \\ + \frac{\mu_{i,l,v} \mu_{j,vn} \mu_{k,nm} \mu_{h,ml}}{(\omega_{vm} + \omega_p + \omega_q + \omega_r + i \gamma_{nm})(\omega_{vm} + \omega_p + \omega_q + i \gamma_{mv})(\omega_{ml} - \omega_p - i \gamma_{ml})} + \\ + \frac{\mu_{h,l,v} \mu_{i,vn} \mu_{j,mn} \mu_{k,ml}}{(\omega_{ml} + \omega_p + \omega_q + \omega_r + i \gamma_{ml})(\omega_{nl} + \omega_p + \omega_q + i \gamma_{nl})(\omega_{vl} + \omega_p + i \gamma_{vl})}. \quad (3.5.2c)$$

$$\cdot \sum_{vnml} \rho_{0,ll} \left(\frac{\mu_{k,l,v} \mu_{j,vn} \mu_{i,nm} \mu_{h,ml}}{(\omega_{vl} - \omega_p - \omega_q - \omega_r - i \gamma_{vl})(\omega_{nl} - \omega_p - \omega_q - i \gamma_{nl})(\omega_{ml} - \omega_p - i \gamma_{ml})} + \right. \\ \left. + \frac{\mu_{h,l,v} \mu_{k,vn} \mu_{j,nm} \mu_{i,ml}}{(\omega_{nv} - \omega_p - \omega_q - \omega_r - i nv)(\omega_{mv} - \omega_p - \omega_q - i \gamma_{mv})(\omega_{vl} + \omega_p + i \gamma_{vl})} + \right. \\ \left. + \frac{\mu_{i,l,v} \mu_{k,vn} \mu_{j,nm} \mu_{h,ml}}{(\omega_{nv} - \omega_p - \omega_q - \omega_r - i \gamma_{nv})(\omega_{vm} + \omega_p + \omega_q + i \gamma_{vm})(\omega_{ml} - \omega_p - i \gamma_{ml})} + \right. \\ \left. + \frac{\mu_{h,l,v} \mu_{i,vn} \mu_{k,nm} \mu_{j,ml}}{(\omega_{mn} - \omega_p - \omega_q - \omega_r - i \gamma_{mn})(\omega_{nl} - \omega_p - \omega_q + i \gamma_{nl})(\omega_{vl} + \omega_p + i \gamma_{vl})} + \right. \\ \left. + \frac{\mu_{j,l,v} \mu_{k,vn} \mu_{i,nm} \mu_{h,ml}}{(\omega_{vn} - \omega_p - \omega_q - \omega_r + i \gamma_{vn})(\omega_{nl} - \omega_p - \omega_q - i \gamma_{nl})(\omega_{ml} - \omega_p - i \gamma_{ml})} + \right. \\ \left. + \frac{\mu_{h,l,v} \mu_{j,vn} \mu_{k,nm} \mu_{i,ml}}{(\omega_{nm} + \omega_p + \omega_q + \omega_r + i \gamma_{nm})(\omega_{mv} - \omega_p - \omega_q - i \gamma_{mv})(\omega_{vl} + \omega_p + i \gamma_{vl})} + \right. \\ \left. + \frac{\mu_{i,l,v} \mu_{j,vn} \mu_{k,nm} \mu_{h,ml}}{(\omega_{vm} + \omega_p + \omega_q + \omega_r + i \gamma_{nm})(\omega_{vm} + \omega_p + \omega_q + i \gamma_{mv})(\omega_{ml} - \omega_p - i \gamma_{ml})} + \right. \\ \left. + \frac{\mu_{h,l,v} \mu_{i,vn} \mu_{j,mn} \mu_{k,ml}}{(\omega_{ml} + \omega_p + \omega_q + \omega_r + i \gamma_{ml})(\omega_{nl} + \omega_p + \omega_q + i \gamma_{nl})(\omega_{vl} + \omega_p + i \gamma_{vl})} \right).$$

What is interesting, after expanding all the permutations in 3.5.2 we will get the 48 different summands - which show how the quantum mechanical approach is hard to apply.

In further calculations we will use both the 3.5.1 and 3.5.2 equations in simplified version - with just a few summands. the visualization of the results for a typical quantum-perturbative model obtained with equations 3.5.2 are shown in the figure 3.5.1:

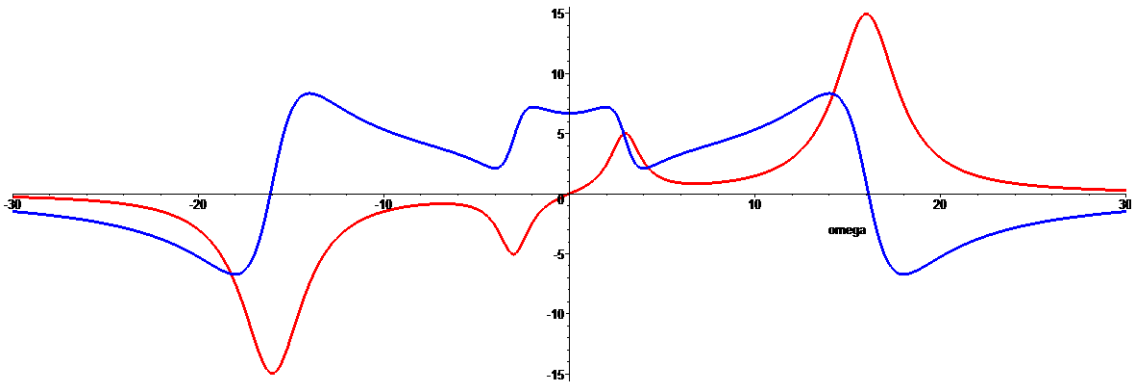


Figure 3.5.1: Quantum-perturbative plot for 3-level model of with arbitrary (non-physical) parameters. Red plot is for the imaginary and the blue plot is for the real part of the linear susceptibility.

4 Simpson and trapezoidal quadrature based Hilbert transform - HTRAN

4.1 Overview of the HTRAN

In this chapter we present the simplest possible but still nice working numerical calculation of the Hilbert transform based on the report by I. J. Weinberg [45]. It uses the Simpson and trapezoidal quadrature. We have slightly modified author's algorithm and it no longer requires the input to be an even function.

The algorithm is presented in two parts. In the first part, we present how the Hilbert transform equation can be modified with one strict assumption from the singular integral to the non-singular one. In the second part, we will use the new set of input function values based on the interpolation method.

We assume that the input function R is defined for a discrete set of arguments:

$$F = \{F_1, F_2, \dots, F_N\} \quad (F_i < F_j \text{ for } i < j). \quad (4.1.1)$$

We will calculate the Hilbert transform of R for the same discrete set of arguments F . An example has been presented on the Figure (4.1.1), where the blue plot represents the input function R and the green plot represents the output function HT .

We start from the modification of the main Hilbert transform equation from the basic representation (second term) into a limit of two integrals (third term):

$$HT(\omega) = \frac{1}{\pi} \int_{-\infty}^{\infty} \frac{R(\Omega)}{\Omega - \omega} d\Omega = \lim_{\varepsilon \rightarrow 0} \left(\int_{-\infty}^{\omega - \varepsilon} \frac{R(\Omega)}{\Omega - \omega} d\Omega + \int_{\omega + \varepsilon}^{\infty} \frac{R(\Omega)}{\Omega - \omega} d\Omega \right). \quad (4.1.2)$$

Now for each frequency ω we observe the following property:

$$\int_{-\infty}^{\infty} \frac{1}{\Omega - \omega} d\Omega = 0. \quad (4.1.3)$$

We use the observation (4.1.3) and modify the equation (4.1.2):

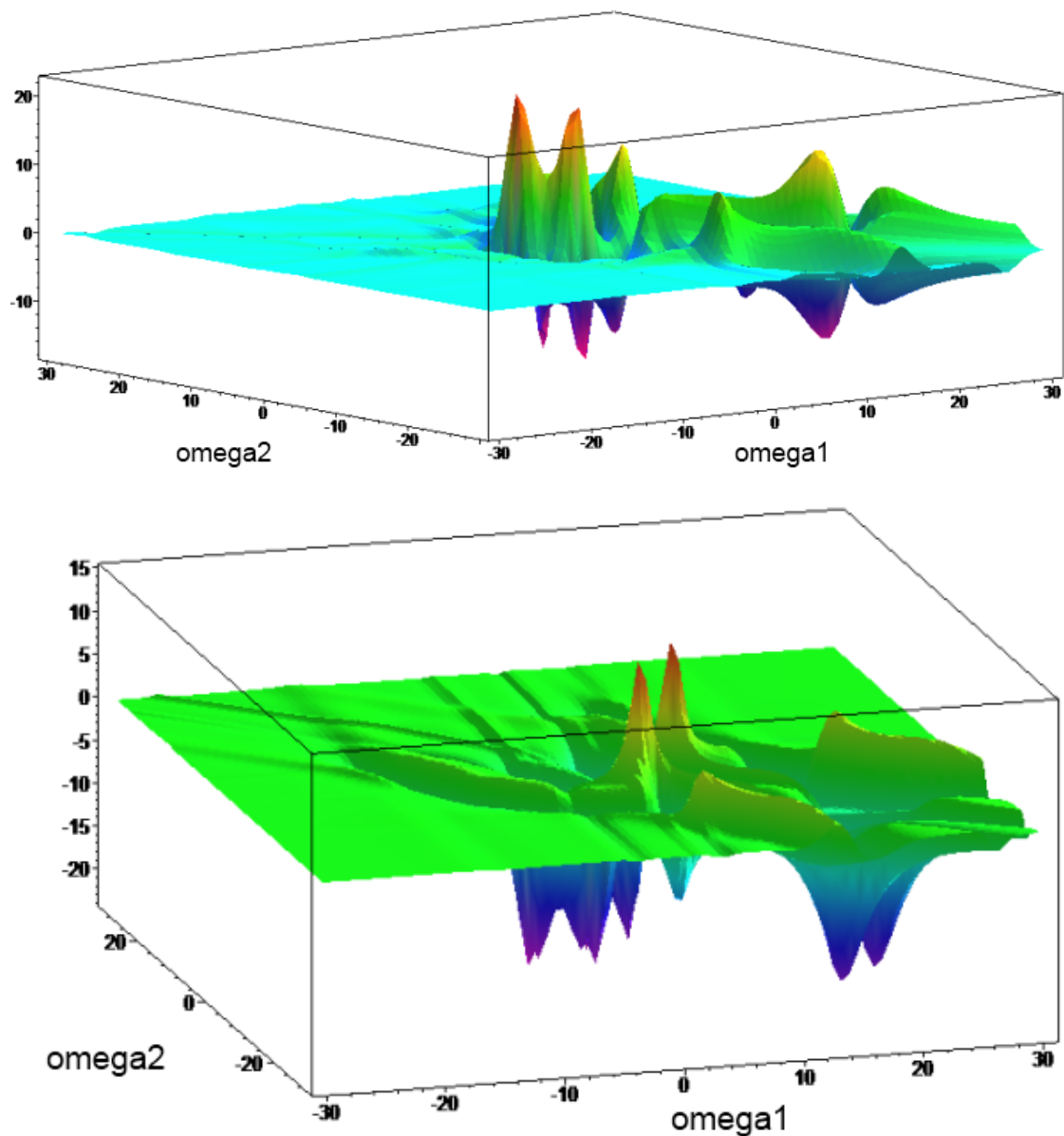


Figure 3.5.2: Quantum-perturbative plot for 3-level model of with arbitrary (non-physical) parameters. Red plot is for the imaginary and the blue plot is for the real part of the second-order susceptibility.

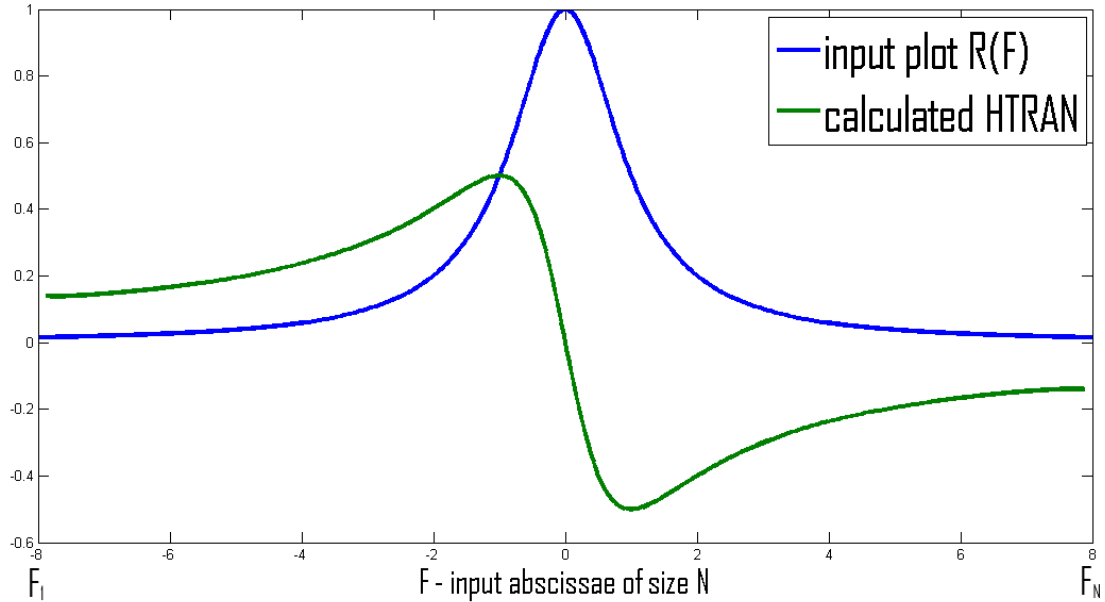


Figure 4.1.1: A sample input plot (ordered pairs of OX abscissae - F - and the OY ordinates - R) with the sample output plot HT for the HTRAN algorithm.

$$HT(\omega) = \frac{1}{\pi} \int_{-\infty}^{\infty} \frac{R(\Omega) - R(\omega)}{\Omega - \omega} d\Omega + \frac{1}{\pi} \int_{-\infty}^{\infty} \frac{R(\Omega)}{\Omega - \omega} d\Omega = \frac{1}{\pi} \int_{-\infty}^{\infty} \frac{R(\Omega) - R(\omega)}{\Omega - \omega} d\Omega. \quad (4.1.4)$$

We can easily transform the result of the (4.1.4) as follows:

$$HT(\omega) = \frac{1}{\pi} \left[\int_{-\infty}^{F_1} \frac{R(\Omega) - R(\omega)}{\Omega - \omega} d\Omega + \int_{F_1}^{F_N} \frac{R(\Omega) - R(\omega)}{\Omega - \omega} d\Omega + \int_{F_N}^{\infty} \frac{R(\Omega) - R(\omega)}{\Omega - \omega} d\Omega \right]. \quad (4.1.5)$$

As the input function R is assumed to be square-integrable, we will put even more strict assumption:

$$R(\omega) = 0 \text{ for } \omega < F_1 \text{ or } \omega > F_N. \quad (4.1.6)$$

With the strict-vanishing assumption (4.1.6) for $R(\omega)$, we can simplify the equation (4.1.5) as follows:

$$HT(\omega) = \frac{1}{\pi} \left[\int_{-\infty}^{F_1} -\frac{R(\omega)}{\Omega - \omega} d\Omega + \int_{F_1}^{F_N} \frac{R(\Omega) - R(\omega)}{\Omega - \omega} d\Omega + \int_{F_N}^{\infty} -\frac{R(\omega)}{\Omega - \omega} d\Omega \right]. \quad (4.1.7)$$

As $\omega \in [F_1, F_N]$ we will now consider two cases - that takes into account the position of ω in relation to F_1 and F_N . We have two possibilities:

$$\omega - F_1 < F_N - \omega \text{ and } F_N - \omega \leq \omega - F_1 \quad (4.1.8)$$

We shall also notice the symmetry property of the function $\frac{1}{\Omega - \omega}$ for any $M > 0$:

$$\int_{-\infty}^{\omega-M} \frac{1}{\Omega - \omega} d\Omega + \int_{\omega+M}^{\infty} \frac{1}{\Omega - \omega} d\Omega = 0 \quad (4.1.9)$$

Together with the observation (4.1.9) each of two cases from (4.1.8) leads to results obtained in equations (4.1.10a) and (4.1.10b) respectively:

$$\begin{aligned} \text{HT}(\omega) &= \frac{1}{\pi} \left[\int_{2\omega-F_N}^{F_1} -\frac{R(\omega)}{\Omega - \omega} d\Omega + \int_{F_1}^{F_N} \frac{R(\Omega) - R(\omega)}{\Omega - \omega} d\Omega \right] \\ &= \frac{1}{\pi} \left[-R(\omega) \ln\left(\frac{F_1 - \omega}{\omega - F_N}\right) + \int_{F_1}^{F_N} \frac{R(\Omega) - R(\omega)}{\Omega - \omega} d\Omega \right], \end{aligned} \quad (4.1.10a)$$

$$\begin{aligned} \text{HT}(\omega) &= \frac{1}{\pi} \left[\int_{F_1}^{F_N} \frac{R(\Omega) - R(\omega)}{\Omega - \omega} d\Omega + \int_{F_N}^{2\omega-F_1} \frac{-R(\omega)}{\Omega - \omega} d\Omega \right] \\ &= \frac{1}{\pi} \left[\int_{F_1}^{F_N} \frac{R(\Omega) - R(\omega)}{\Omega - \omega} d\Omega - R(\omega) \ln\left(\frac{\omega - F_1}{F_N - \omega}\right) \right]. \end{aligned} \quad (4.1.10b)$$

And we can see that both the 4.1.10 derivations lead to the same result:

$$\text{HT}(\omega) = \frac{1}{\pi} \left[-R(\omega) \ln\left(\frac{\omega - F_1}{F_N - \omega}\right) + \int_{F_1}^{F_N} \frac{R(\Omega) - R(\omega)}{\Omega - \omega} d\Omega \right] \quad (4.1.11)$$

We also observe that for any ω inside the range $[F_1, F_N]$ both values $\omega - F_1$ and $F_N - \omega$ are non-negative. That leads to a simple observation that condition $0 < \frac{\omega - F_1}{F_N - \omega}$ is satisfied and therefore the logarithm argument is well defined. What now interests us the most, is the integral:

$$Y(\omega) = \int_{F_1}^{F_N} \frac{R(\Omega) - R(\omega)}{\Omega - \omega} d\Omega \quad (4.1.12)$$

We would like the denominator in the (4.1.12) equation never equals zero, so we can calculate the whole integral numerically. For this reason we are preparing a new set of values, which are just a simple midways of F :

$$\widehat{F}_k = \frac{F_k + F_{k+1}}{2} \quad \text{for } k = 1 \dots N - 1 \quad (4.1.13)$$

We will also need to approximate the values of a new \widehat{R} at \widehat{F}_j ($j = 1 \dots N - 1$) points. We will do this by a simple cubic interpolation:

$$R(\widehat{F}_1) = \widehat{R}_1 = \frac{3R_1 + 6R_2 - R_3}{8} \quad (4.1.14a)$$

$$\widehat{R}_k = \frac{-R_{k-1} + 9R_k + 9R_{k+1} - R_{k+2}}{16} \quad \text{for } k = 2 \dots N - 2 \quad (4.1.14b)$$

$$\widehat{R}_{N-1} = \frac{-R_{N-2} + 6R_{N-1} + 3R_N}{8} \quad (4.1.14c)$$

By now, the calculation of the Y function from the (4.1.12) equation will be performed by a simple quadrature integration. The introduced \hat{Y}_i symbol describes the numerical approximation of the Y function calculated with the following equation:

$$\hat{Y}_i = \sum_{j=1}^N \frac{h_j(R_j - \hat{R}_i)}{F_j - \hat{F}_i} \text{ for } i = 1 \dots N-1. \quad (4.1.15)$$

To do such an integration we will hire the Simpson's rule. If N is odd, we have:

$$h_1 = h_N = \frac{F_2 - F_1}{3} = \frac{\Delta F}{3} \quad (4.1.16a)$$

$$h_j = \frac{4 \Delta F}{3} \text{ for } j = 2, 4 \dots N-1 \quad (4.1.16b)$$

$$h_j = \frac{2 \Delta F}{3} \text{ for } j = 3, 5 \dots N-2 \quad (4.1.16c)$$

If N is even, the last interval should be obtained using the trapezoidal rule:

$$h_1 = \frac{\Delta F}{3} = \frac{F_2 - F_1}{3} \quad (4.1.17a)$$

$$h_j = \frac{4 \Delta F}{3} \text{ for } j = 2, 4 \dots N-2 \quad (4.1.17b)$$

$$h_j = \frac{2 \Delta F}{3} \text{ for } j = 3, 5 \dots N-3 \quad (4.1.17c)$$

$$h_{N-1} = \frac{5 \Delta F}{6} \quad (4.1.17d)$$

$$h_N = \frac{\Delta F}{2} \quad (4.1.17e)$$

In the next step, we calculate the Hilbert transform at points $\widehat{F}_j (j = 1, \dots, N-1)$:

$$\widehat{HT}_i = \frac{1}{\pi} \left[-\widehat{R}_i \ln\left(\frac{\widehat{F}_i - F_1}{F_N - \widehat{F}_i}\right) + \widehat{Y}_i \right]. \quad (4.1.18)$$

Finally we need to undo the cubic interpolation. To do so, we perform the following calculations:

$$HF(F_1) = HT_1 = \frac{15 \widehat{HT}_1 - 10 \widehat{HT}_2 + 3 \widehat{HT}_3}{8} \quad (4.1.19a)$$

$$HT_2 = \frac{3 \widehat{HT}_1 + 6 \widehat{HT}_2 - 1 \widehat{HT}_3}{8} \quad (4.1.19b)$$

$$HT_i = \frac{-\widehat{HT}_{i-1} + 9 \widehat{HT}_i + 9 \widehat{HT}_{i+1} - \widehat{HT}_{i+1}}{16} \text{ for } i = 3, 4, \dots N-2 \quad (4.1.19c)$$

$$HT_{N-1} = \frac{-\widehat{HT}_{N-3} + 6 \widehat{HT}_{N-2} + 3 \widehat{HT}_{N-1}}{8} \quad (4.1.19d)$$

$$HT_N = \frac{3 \widehat{HT}_{N-3} - 10 \widehat{HT}_{N-2} + 15 \widehat{HT}_{N-1}}{8} \quad (4.1.19e)$$

In following chapters we will show the results obtained with this method.

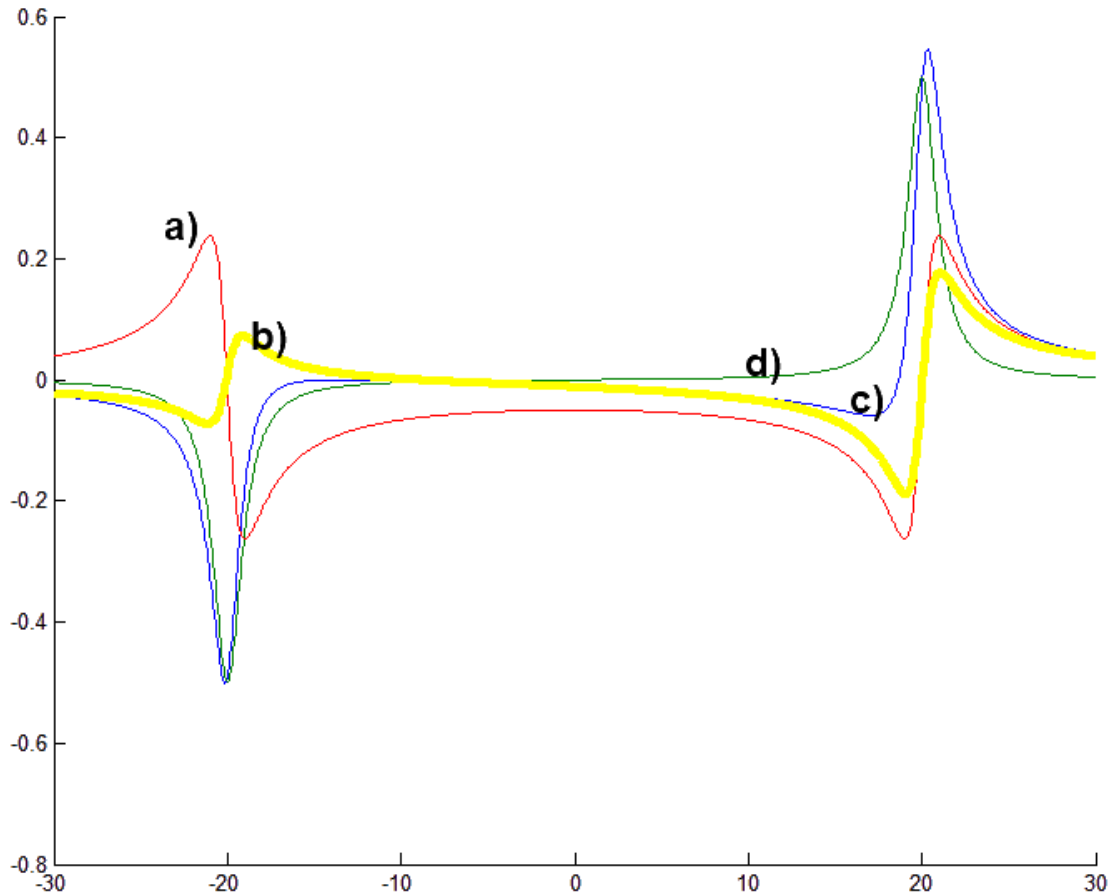


Figure 4.2.1: The Figure presents the results of the HTRAN method applied for the simple linear model. Results are plotted together a) The plot of the real part of $\chi(\omega)$ b) absolute error plot (c -plot minus d -plot) c) imaginary part of $\chi(\omega)$ obtained with the Hilbert transform of a -plot d) part of $\chi(\omega)$ imaginary calculated analytically.

4.2 HTRAN for simple linear model - results

We shall remind the model presented in Chapter (3) in the equation 3.3.3:

$$\mathcal{F}[h_{\text{lin}}] = \chi_{\text{lin}}(\omega) \approx \frac{-20}{(\omega i + 1 - 20i)(\omega i + 1 + 20i)}. \quad (4.2.1)$$

The real part of χ_{lin} will be used as the input R function in the equation (4.1.2). The output HT function calculated with the HTRAN algorithm is compared to the imaginary part of the χ_{lin} . We have presented the results in the Figure 4.2.1. In this and in the following chapters we would like the error function represented with the yellow colour to be as close to zero as possible. We also would like the numerical results to be close to the values calculated analytically.

4.3 HTRAN for simple nonlinear model - results

We remind the equation for the pump-and-probe susceptibility model (3.4.1):

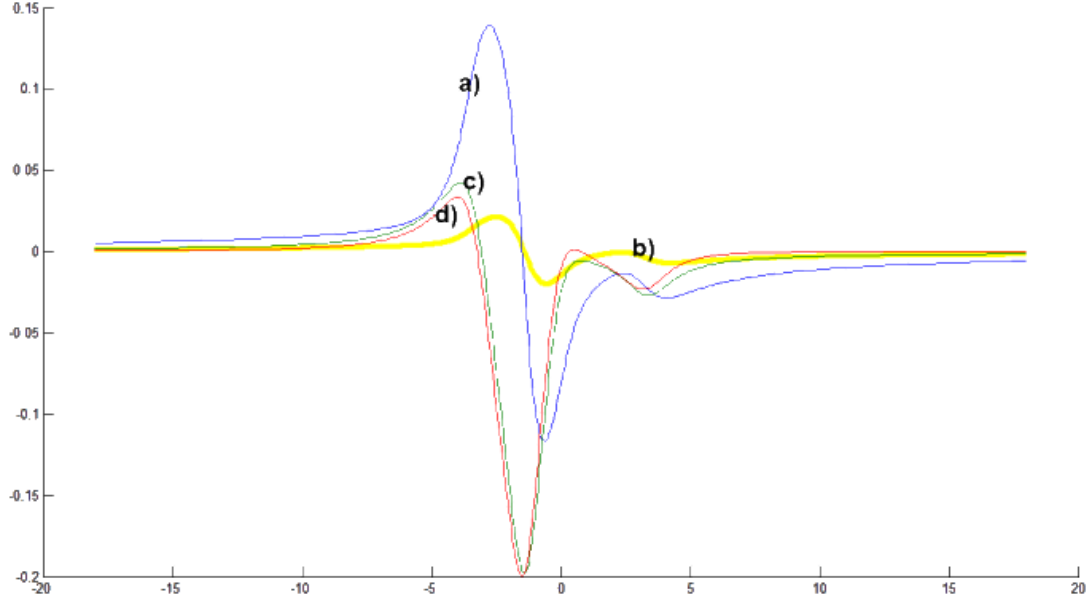


Figure 4.3.1: The Figure presents the results of the HTRAN method applied for the pump-and-probe model. Results are lotted together a) The plot of the real part of $\chi_{pp}(\omega)$ b) absolute error plot (c-plot minus d-plot) c) imaginary part of $\chi_{pp}(\omega)$ d) imaginary part of $\chi_{pp}(\omega)$ calculated analytically.

$$\begin{aligned} \chi_{pp}(\delta) = & \frac{G n_0 \gamma_{ba}}{\Delta + \delta + I \eta} \\ & \left(1 - \frac{\Omega_1^2 (\Delta - \delta + I \eta) (\delta + 2 I \eta)}{(\Delta - I \eta) ((\delta + I \theta) (\Delta + \delta + I \eta) (\delta - \Delta + I \eta) - \Omega_1^2 (\delta + I \eta)) 2} \right) \quad (4.3.1) \end{aligned}$$

$$G = 1,$$

$$\gamma_{ba} = 1,$$

$$n_0 = 1,$$

and we have assign the values for the constants: $\Delta = 1.3$,

$$\eta = 1,$$

$$\theta = 1.4,$$

$$\Omega_1 = 4.3.$$

The results for such set of arbitrary parameters are shown on the Figure 4.3.1.

The resulted b-plot seems to be a not-so-bad introduction into the Hilbert transform evaluation, as we have only employed the simple Simpson's rule. We would also like to perform the three-dimensional analysis of the assumed pump-probe susceptibility, so we employ the (3.4.9a) and (3.4.9b) equations for each frequency, which require performing two integrations (one, for each frequency-domain argument). Unfortunately, only the obtained three-dimensional shapes are similar to the original ones, but we have received a huge relative error as presented in the Figure 4.3.2.

Let's now perform the evaluation for the wave-mixing model as stated in the model described by 3.4.5a. We expand this equation to resolve the complex conjugate of D function and the resulting function is:

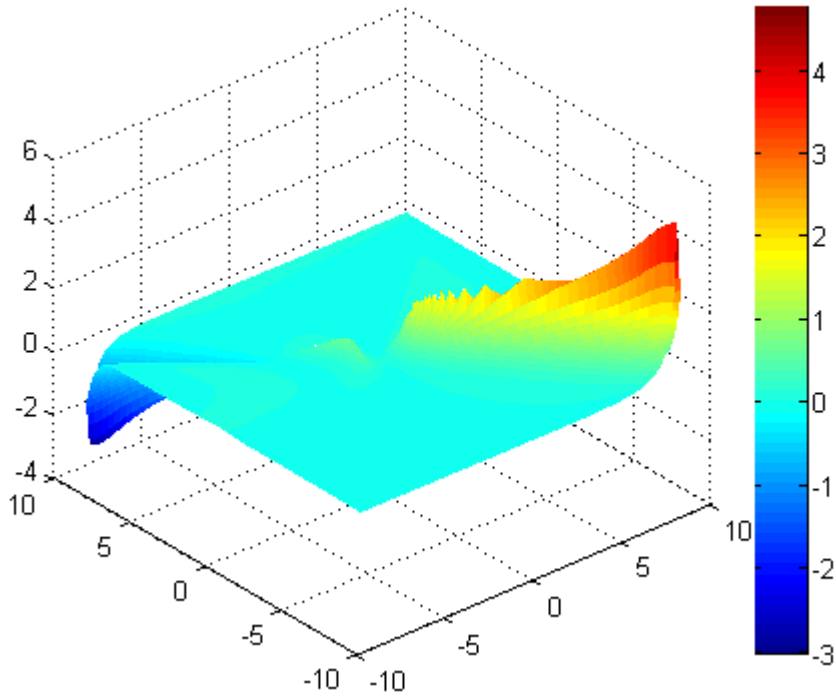


Figure 4.3.2: The Figure presents the combined relative error for the results of the HTRAN method applied for the two-dimensional pump-and-probe model. The light-cyan colour shows the area of error below 100.

$$\chi_{mix}(\delta) = \frac{2 N w_0 \mu_{ba}^4}{3 \varepsilon_0 h^3} \left(-\delta - \Delta - \frac{i}{T_2} \right) \left(\delta + \frac{2i}{T_2} \right) \left((\Delta + \frac{i}{T_2}) (\Delta + \delta + \frac{i}{T_2}) \right) \quad (4.3.2)$$

$$\left(\delta^3 - \frac{2i\delta^2}{T_2} - \delta\Delta^2 - \frac{2i\delta}{T_1 T_2} - \frac{\delta}{T_2^2} + \frac{\delta^2}{T_1} - \frac{\Delta^2}{T_1} - \frac{1}{T_1 T_2^2} - \Omega_2 \delta + \frac{\Omega_2 i}{T_2} \right)$$

With such a complex function we obtain the following two and three dimensional results on Figure 4.3.3.

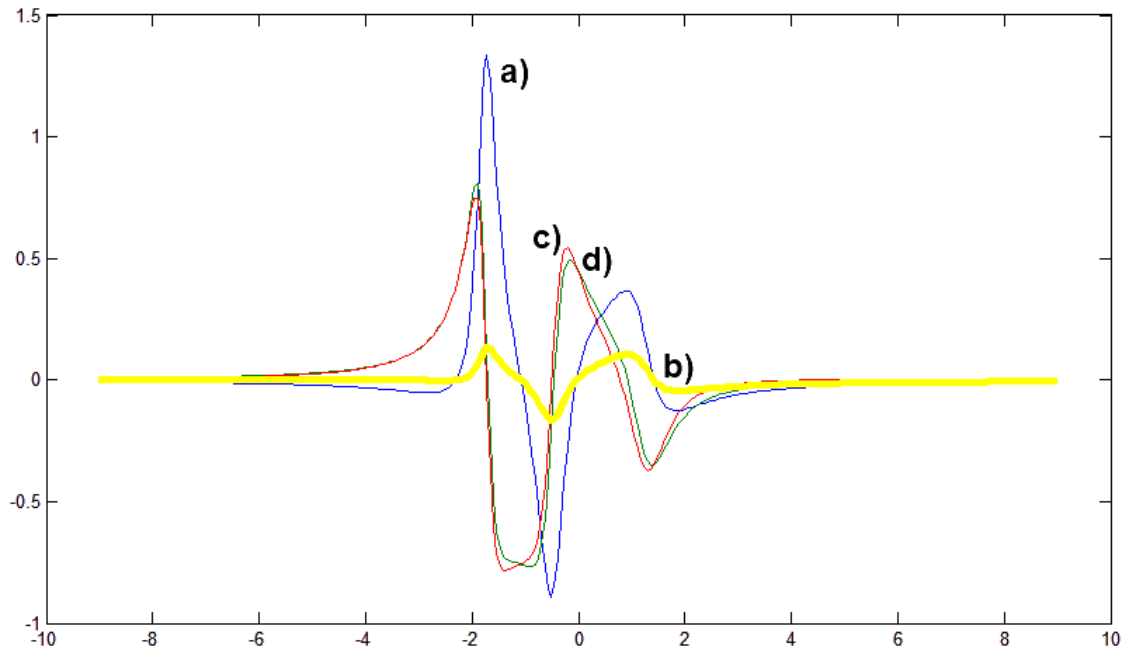
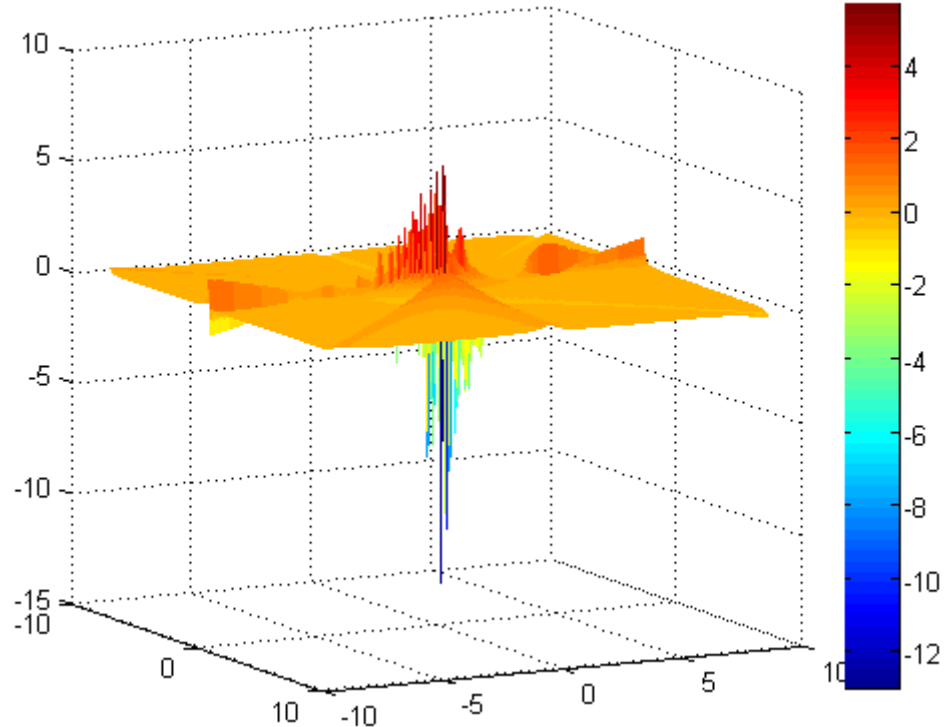


Figure 4.3.3: The Figure presents the combined relative error for the results of the HTRAN method applied for the two-dimensional wave-mixing model. a) The plot of the real part of $\chi_{mix}(\omega)$ b) absolute error plot (c-plot minus d-plot) c) (red) imaginary part of $\chi_{mix}(\omega)$ d) (grey) imaginary part of $\chi_{mix}(\omega)$ calculated analytically.

As the obtained three-dimensional shape looks very similar to those obtained analytically, the relative error still remains huge for some areas (Figure 4.3.4):



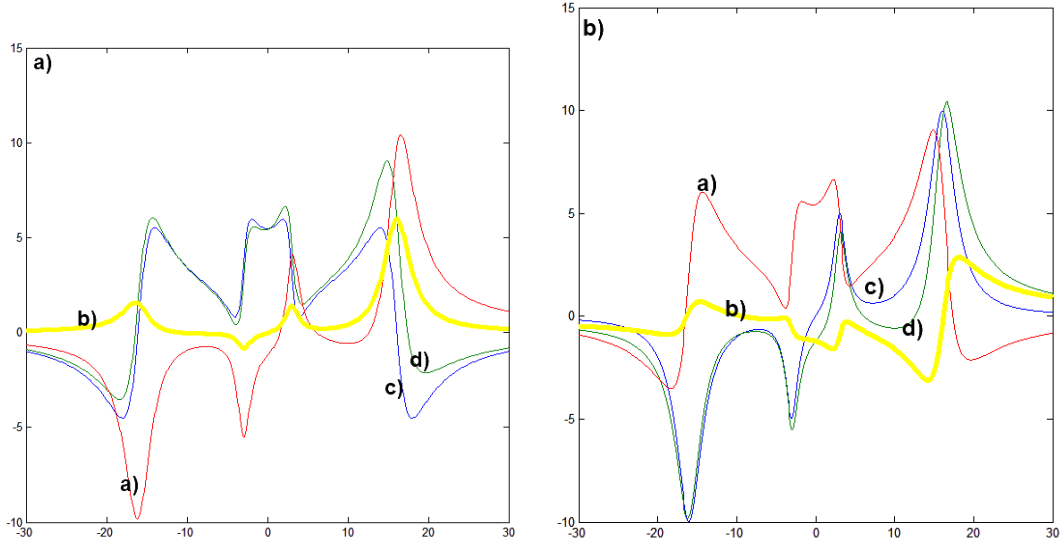


Figure 4.4.1: The Figure presents the results of the HTRAN method applied for the linear quantum-perturbative model. The results for both real and imaginary values are plotted together on Figures a and b: a.a) The plot of the imaginary part of $\chi_{1,qp}(\omega)$ a.b) absolute error plot (a.d-plot minus a.c-plot) a.c) real part of $\chi_{1,qp}(\omega)$ calculated analytically a.d) real part of $\chi_{1,qp}(\omega)$ obtained with the Hilbert transform of a-plot b.a) The plot of the real part of $\chi_{1,qp}(\omega)$ b.b) absolute error plot (b.d-plot minus b.c-plot) b.c) imaginary part of $\chi_{1,qp}(\omega)$ calculated analytically b.d) imaginary part of $\chi_{1,qp}(\omega)$ obtained with the Hilbert transform of a-plot

Figure 4.3.4: The Figure presents the combined relative error for the real part of nonlinear susceptibility $\chi_{mix}(\delta)$ describing the wave-mixing process.

4.4 HTRAN for simple quantum-perturbative model - results

We will use the models already prepared for both linear and second-order nonlinear susceptibilities defined in the Chapter 3.5.

$$\chi_{1,qp}(\omega) = \frac{N}{\varepsilon_0 \hbar} \sum_{n=1}^2 \left(\frac{\mu_{1,n} \mu_{2,n}}{\Omega_n - \omega - i \gamma_n} + \frac{\mu_{2,n} \mu_{1,n}}{\Omega_n + \omega + i \gamma_n} \right), \quad (4.4.1)$$

where we have used the following values of the constants:

$$\mu = [[1, 3], [-1, -2]],$$

$$\Omega = [3, 16],$$

$$\gamma = [1, 2],$$

$$N = 5,$$

$$\varepsilon_0 = 1,$$

$$\hbar = -1$$

Results are gathered on the Figure 4.4.1.

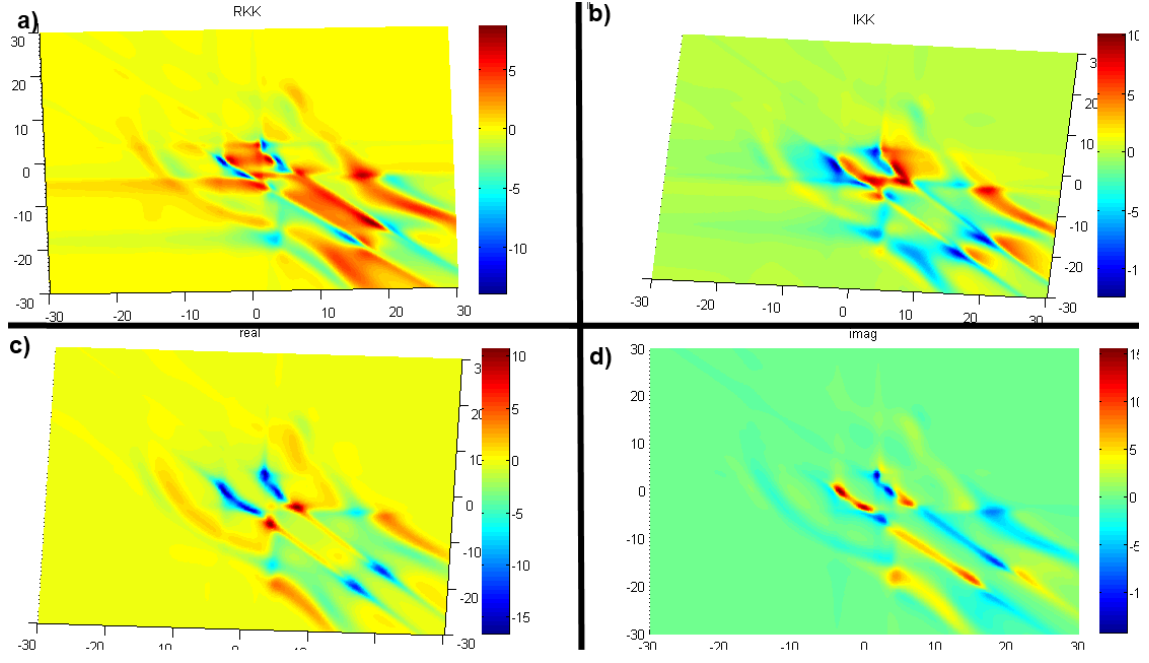


Figure 4.4.2: The Figure presents the results of the HTRAN method applied for the second-order non-linear quantum-perturbative model. Results in the three-dimensional-like plot are plotted together. a) - The calculated real part of $\chi_{2,qp}$ b) The calculated imaginary part of $\chi_{2,qp}$ c) The real part of nonlinear susceptibility $\chi_{2,qp}$ calculated analytically d) The imaginary part of the nonlinear susceptibility $\chi_{2,qp}$

$$\begin{aligned}
\chi_{2,qp}(\omega_1, \omega_2) = 2 N \varepsilon_0 h^2 & \sum_{n=1}^2 \sum_{m=1}^2 \sum_{l=1}^2 \left(\right. \\
& \frac{\mu_{l,n} \mu_{nm} \mu_{ml}}{(\Omega_{nl} - \omega_1 - \omega_2 - i \gamma_{nl})(\Omega_{ml} - \omega_1 - i \gamma_{ml})} + \\
& + \frac{\mu_{l,n} \mu_{nm} \mu_{ml}}{(\Omega_{nl} - \omega_1 - \omega_1 - i \gamma_{nl})(\Omega_{ml} - \omega_2 - i \gamma_{ml})} + \\
& + \frac{\mu_{l,n} \mu_{nm} \mu_{ml}}{(\Omega_{mn} - \omega_1 - \omega_2 - i \gamma_{mn})(\Omega_{nl} + \omega_2 + i \gamma_{nl})} + \\
& + \frac{\mu_{l,n} \mu_{nm} \mu_{ml}}{(\Omega_{mn} - \omega_1 - \omega_2 - i \gamma_{mn})(\Omega_{nl} + \omega_2 + i \gamma_{nl})} + \\
& + \frac{\mu_{l,n} \mu_{nm} \mu_{ml}}{(\Omega_{nm} + \omega_1 + \omega_2 + i \gamma_{nm})(\Omega_{ml} - \omega_1 - i \gamma_{ml})} + \\
& + \frac{\mu_{l,n} \mu_{nm} \mu_{ml}}{(\Omega_{nm} + \omega_1 + \omega_2 + i \gamma_{nm})(\Omega_{ml} - \omega_1 - i \gamma_{ml})} + \\
& + \frac{\mu_{l,n} \mu_{nm} \mu_{ml}}{(\Omega_{ml} + \omega_1 + \omega_2 + i \gamma_{ml})(\Omega_{nl} + \omega_1 + i \gamma_{nl})} + \\
& \left. + \frac{\mu_{l,n} \mu_{nm} \mu_{ml}}{(\Omega_{ml} + \omega_1 + \omega_2 + i \gamma_{ml})(\Omega_{nl} + \omega_2 + i \gamma_{nl})} \right). \quad (4.4.2)
\end{aligned}$$

In the 4.4.2 we are using the following constants' values: $\mu = [[1, 3], [-1, -2]]$, $\Omega = [[3, 16], [4, 12]]$, $\gamma = [[1, 2], [-1, 3]]$, $N = 5$, $\varepsilon_0 = 1$, $h = -1$.

In the Figure 4.4.2 we can see that there is a similarity in obtained plots, but both the

relative and absolute error do not satisfy us at all. Results obtained with 2-Dimensional model were more satisfying.

We have implemented the HTRAN method in the MATLAB[®] environment, and its source code is available in the Appendix A.1.

5 Newton-Cotes Hilbert transform

5.1 Overview of the NC quadrature of arbitrary degree

Newton-Cotes formula for numerical integration is taken into consideration. We compare formula for an arbitrary degree - having in our mind that the choice between formulas of high and low degree must be undertaken with the awareness of numerical errors which may arise. Newton-Cotes quadrature is a method for numerical integration with equispaced vertices. As we would like to integrate function $f = f(x)$ within the range $[a, b]$ we introduce the following calculations.

$$x_{n,k} = a + \frac{(b-a)}{n} k \text{ for } k = 0, 1, \dots, n \quad (5.1.1a)$$

$$\omega_n(x) = (x - x_{n,0})(x - x_{n,1}), \dots, (x - x_{n,n}) \quad (5.1.1b)$$

$$\lambda_{n,k}(x) = \frac{\omega_n(x)}{\left(\frac{\partial}{\partial x} \omega_n(x_{n,k})\right)(x - x_{n,k})} \text{ for } k = 0, 1, \dots, n \quad (5.1.1c)$$

$$A_{n,k} = \int_a^b \lambda_{n,k}(x) dx = \frac{(b-a)(-1)^{(n-k)}}{n k! (n-k)!} \int_0^n \prod_{j=0, j \neq k}^n (t-j) dt \text{ for } k = 0, 1, \dots, n \quad (5.1.1d)$$

With parameters defined in this way, the quadrature in sense of Newton-Cotes is defined as following:

$$NC_n(f) = A_{n,k} \sum_{k=0}^n \left(a + \frac{(b-a)}{n} k \right). \quad (5.1.2)$$

Let's remind the Hilbert transform from the equation (2.1.2):

$$\mathcal{H}[f(x)] = \frac{1}{\pi} \int_{-\infty}^{\infty} \frac{f(\omega)}{(x-\omega)} d\omega. \quad (5.1.3)$$

We would like to apply the Newton-Cotes quadrature to calculate the Hilbert transform. While the NC quadrature is not perfect, we need perform the integration without including a short region $[x-cs, x+cs]$ near the singularity. We will also omit the infinities and instead of them we will integrate from a starting point a to the ending point b :

$$\mathcal{H}_{NC}[f(x)] \approx \frac{1}{\pi} \int_a^{x-cs} \frac{f(\omega)}{(x-\omega)} d\omega + \frac{1}{\pi} \int_{x+cs}^b \frac{f(\omega)}{(x-\omega)} d\omega. \quad (5.1.4)$$

Parameters such as a , b and cs are widely described the Appendix A.2 with the whole source code and additional comments.

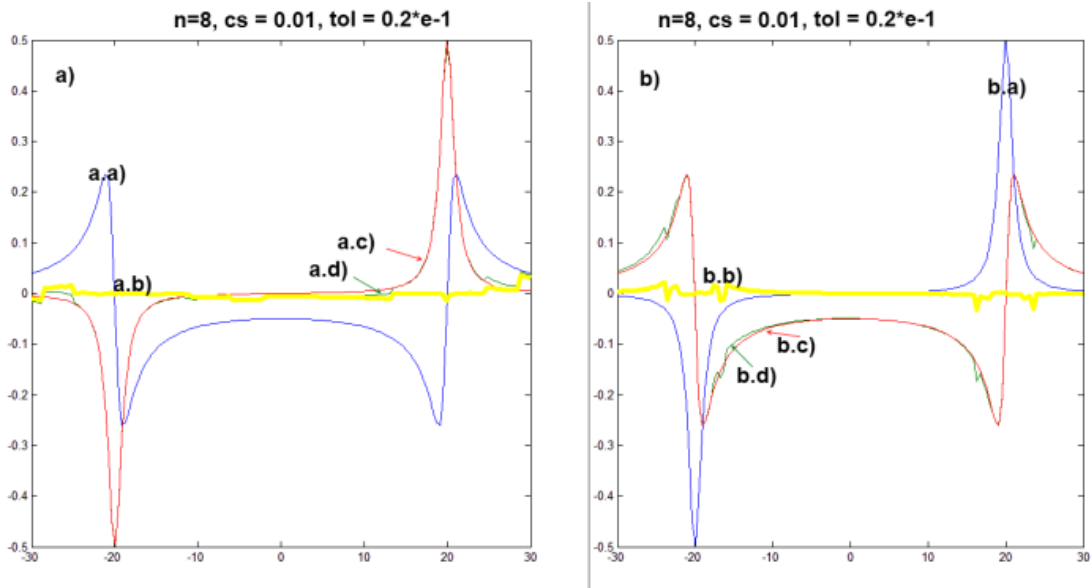


Figure 5.2.1: The Figure presents the first of four results of the NC Hilbert Transform method applied for the simple linear model. Results are plotted together. Calculations were performed with the parameters ($n = 8$, $cs = .1e-1$, $tol = .2e-1$)
 a.a) The plot of the real part of $\chi(\omega)$
 a.b) absolute error plot
 a.c) imaginary part of $\chi(\omega)$ calculated analytically
 a.d) imaginary part of $\chi(\omega)$ obtained with the NC Hilbert transform of a.a-plot,
 b.a) The plot of the imaginary part of $\chi(\omega)$
 b.b) absolute error plot
 b.c) real part of $\chi(\omega)$ calculated analytically
 b.d) real part of $\chi(\omega)$ obtained with the NC Hilbert transform of b.a-plot

5.2 NC for simple linear model - results

As the prepared numeric method depends on many input parameter arguments, we have tried to perform the evaluation in many different cases, some of those results are stated below. We have used the same model as in chapter 4.2.

$$\chi(\omega) \approx \frac{-20}{(\omega i + 1 - 20i)(\omega i + 1 + 20i)} \quad (5.2.1)$$

Some results has been presented on the Figures 5.2.1, 5.2.2, 5.2.3 and 5.2.4

We cannot tell with a hundred percent confidence which set of parameters will fit the best any given function and the user will need to try many combinations before obtaining the final plot, but what we gave is the opportunity to set each one parameter manually, which may lead to better results in the particular cases.

5.3 NC for simple nonlinear model - results

We have performed calculations for the same both nonlinear pump-probe and wave-mixing model as in the chapter 4.2. We have assigned some randomly picked values to the constants:

$$G = 1, \gamma_{ba} = -0.1, n_0 = 1, \Delta = 1.3, eta = 1, \theta = 1.4, \Omega_1 = 4.3, \Omega_1 = 1, w_0 = 1, h = 1, \mu_{ba} = 1, T_1 = 1, \varepsilon_0 = 1,$$

and we will used them in the pump-and-probe (5.3.1) and the frequency mixing 5.3.2 model equations:

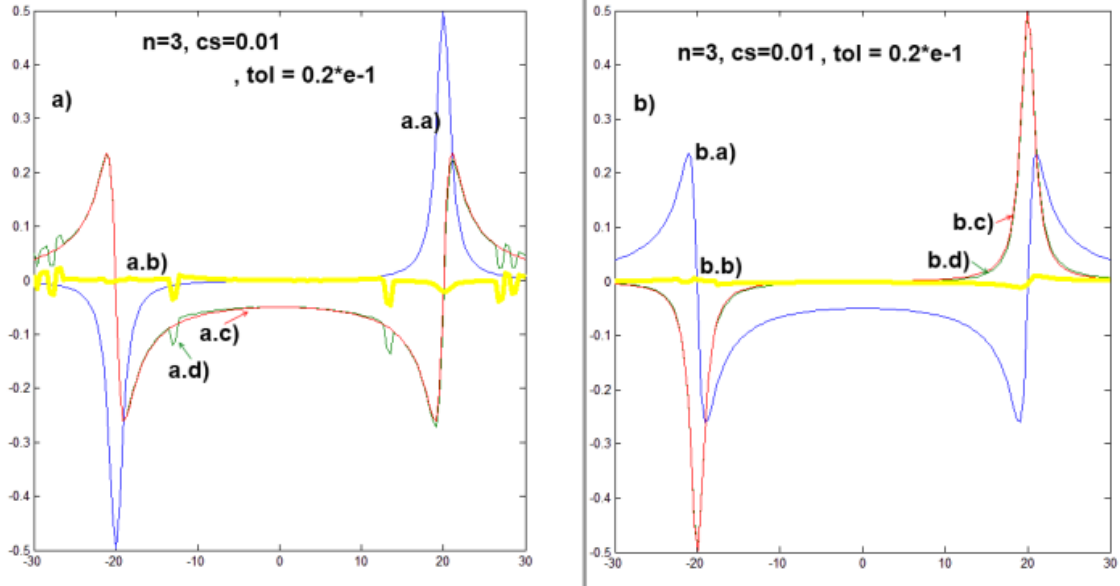


Figure 5.2.2: The Figure presents the second of four results of the NC Hilbert Transform method applied for the simple linear model. Results are plotted together. Calculations were performed with the parameters ($n = 3$, $cs = .1e-1$, $tol = .2e-1$)
a.a) The plot of the imaginary part of $\chi(\omega)$ a.b) absolute error plot (a.d-plot minus a.c-plot)
a.c) real part of $\chi(\omega)$ calculated analytically a.d) real part of $\chi(\omega)$ obtained with the NC Hilbert transform of a.a-plot
b.a) The plot of the real part of $\chi(\omega)$ b.b) absolute error plot (b.d-plot minus b.c-plot)
b.c) imaginary part of $\chi(\omega)$ calculated analytically b.d) imaginary part of $\chi(\omega)$ obtained with the NC Hilbert transform of b.a-plot

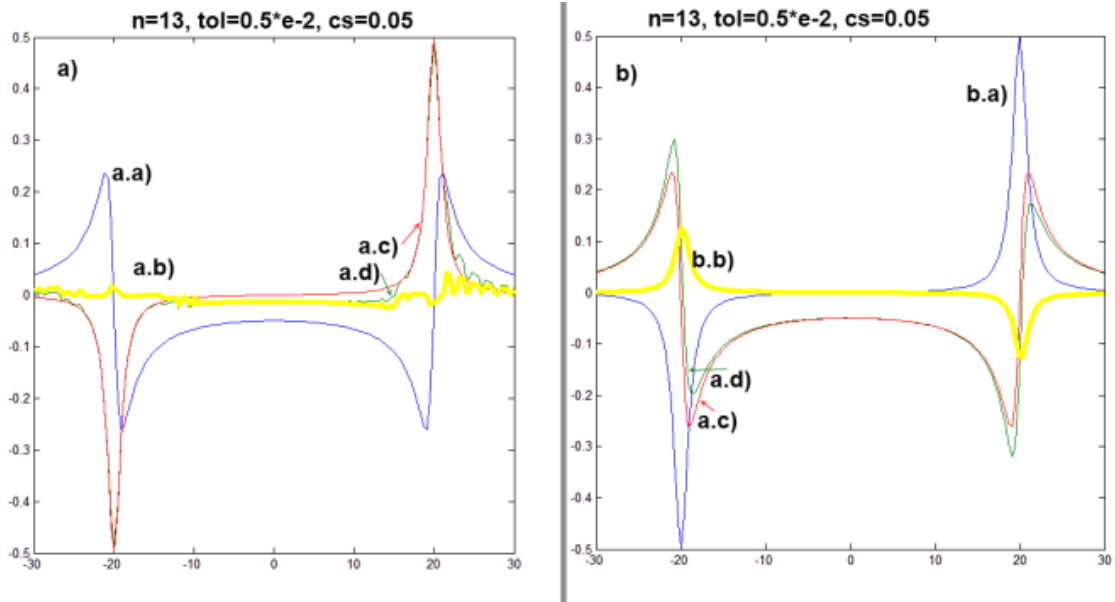


Figure 5.2.3: The Figure presents the third of four results of the NC Hilbert Transform method applied for the simple linear model. Results are plotted together. Calculations were performed with the parameters ($n = 13$, $tol = .5e-2$, $cs = .5e-1$)
a.a) The plot of the real part of $\chi(\omega)$ a.b) absolute error plot (a.d-plot minus a.c-plot)
a.c) imaginary part of $\chi(\omega)$ calculated analytically a.d) imaginary part of $\chi(\omega)$ obtained with the NC Hilbert transform of a.a-plot
b.a) The plot of the imaginary part of $\chi(\omega)$ b.b) absolute error plot (b.d-plot minus b.c-plot)
b.c) real part of $\chi(\omega)$ calculated analytically b.d) real part of $\chi(\omega)$ obtained with the NC Hilbert transform of b.a-plot

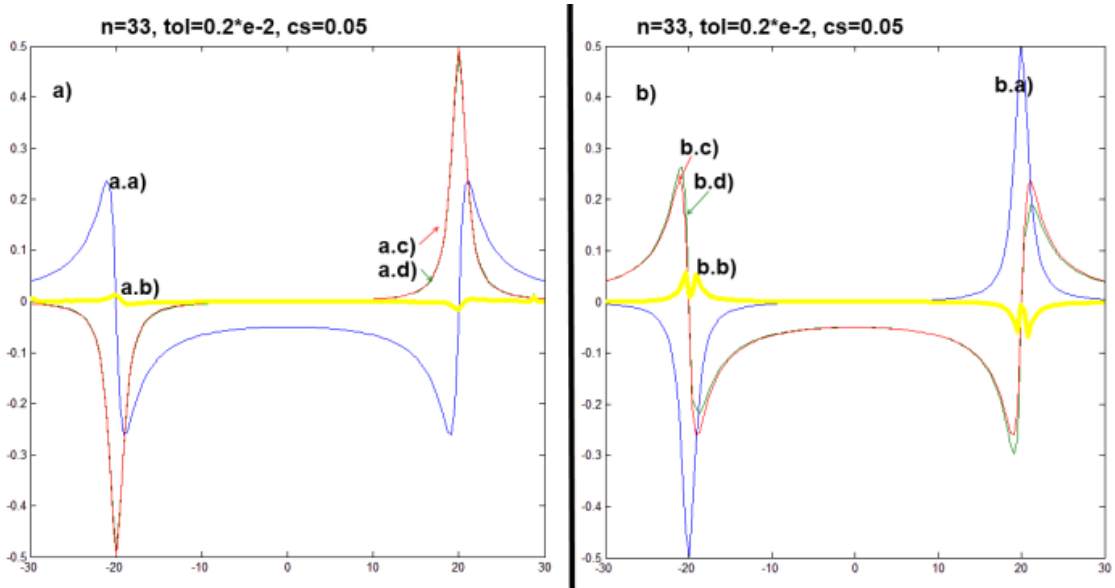


Figure 5.2.4: The Figure presents the fourth of four results of the NC Hilbert Transform method applied for the simple linear model. Results are plotted together. Calculations were performed with the parameters ($n = 33$, $\text{tol} = .2e-2$, $\text{cs} = .5e-1$)
 a.a) The plot of the real part of $\chi(\omega)$ a.b) absolute error plot (a.d-plot minus a.c-plot)
 a.c) imaginary part of $\chi(\omega)$ calculated analytically a.d) imaginary part of $\chi(\omega)$ obtained with the NC Hilbert transform of a.a-plot, b.a) The plot of the imaginary part of $\chi(\omega)$ b.b) absolute error plot (b.d-plot minus b.c-plot) b.c) real part of $\chi(\omega)$ b.d) real part of $\chi(\omega)$ obtained with the NC Hilbert transform of b.a-plot

$$\begin{aligned} \chi_{pp}(\delta) &= \frac{G n_0 \gamma_{ba}}{\Delta + \delta + I \eta} \\ &\left(1 - \frac{\Omega_1^2 (\Delta - \delta + I \eta) (\delta + 2 I \eta)}{2 (\Delta - I \eta) ((\delta + I \theta) (\Delta + \delta + I \eta) (\delta - \Delta + I \eta) - \Omega_1^2 (\delta + I \eta))} \right), \quad (5.3.1) \end{aligned}$$

$$\begin{aligned} \chi_{mix}(\delta) &= 6 N w_0 \varepsilon_0 h^3 \mu_{ba}^4 (-\delta - \Delta - \frac{i}{T_2}) (\delta + \frac{2i}{T_2}) (\Delta + \frac{i}{T_2}) (\Delta + \delta + \frac{i}{T_2}) \cdot \quad (5.3.2) \\ &\cdot (\delta^3 - \frac{2i\delta^2}{T_2} - \delta \Delta^2 - \frac{2i\delta}{T_1 T_2} - \frac{\delta}{T_2^2} + \frac{\delta^2}{T_1} - \frac{\Delta^2}{T_1} - \frac{1}{T_1 T_2^2} - \Omega_2 \delta + \frac{\Omega_2 i}{T_2}). \end{aligned}$$

Results for pump-and-probe model has been presented in the Figure 5.3.1. Results for the frequency mixing model has been presented in the Figure 5.3.2.

5.4 NC for simple quantum-perturbative model - results

Linear model - results:

For the linear susceptibility we have used the model from the 3.5:

$$\chi_{1,qp}(\omega) = \frac{N}{\varepsilon_0 h} \sum_{n=1}^2 \left(\frac{\mu_{1,n} \mu_{2,n}}{\Omega_n - \omega - i \gamma_n} + \frac{\mu_{2,n} \mu_{1,n}}{\Omega_n + \omega + i \gamma_n} \right) \quad (5.4.1)$$

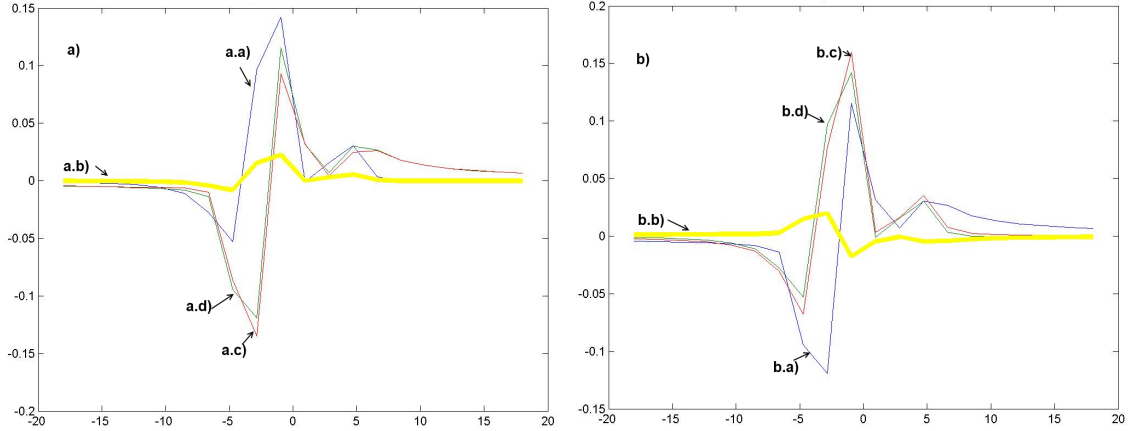


Figure 5.3.1: The Figure presents results of the NC Hilbert Transform method applied for the pump-and-probe model. Results are plotted together. Calculations were performed with the parameters ($n = 4$, $cs = .1e-1$, $tol = .1e-1$) a.a) The plot of the real part of $\chi_{pp}(\omega)$ a.b) absolute error plot (a.d-plot minus a.c-plot) a.c) imaginary part of $\chi_{pp}(\omega)$ calculated analytically a.d) imaginary part of $\chi_{pp}(\omega)$ obtained with the NC Hilbert transform of a.a-plot, b.a) The plot of the imaginary part of $\chi_{pp}(\omega)$ b.b) absolute error plot (b.d-plot minus b.c-plot) b.c) real part of $\chi_{pp}(\omega)$ calculated analytically b.d) real part of $\chi_{pp}(\omega)$ obtained with the NC Hilbert transform of b.a-plot

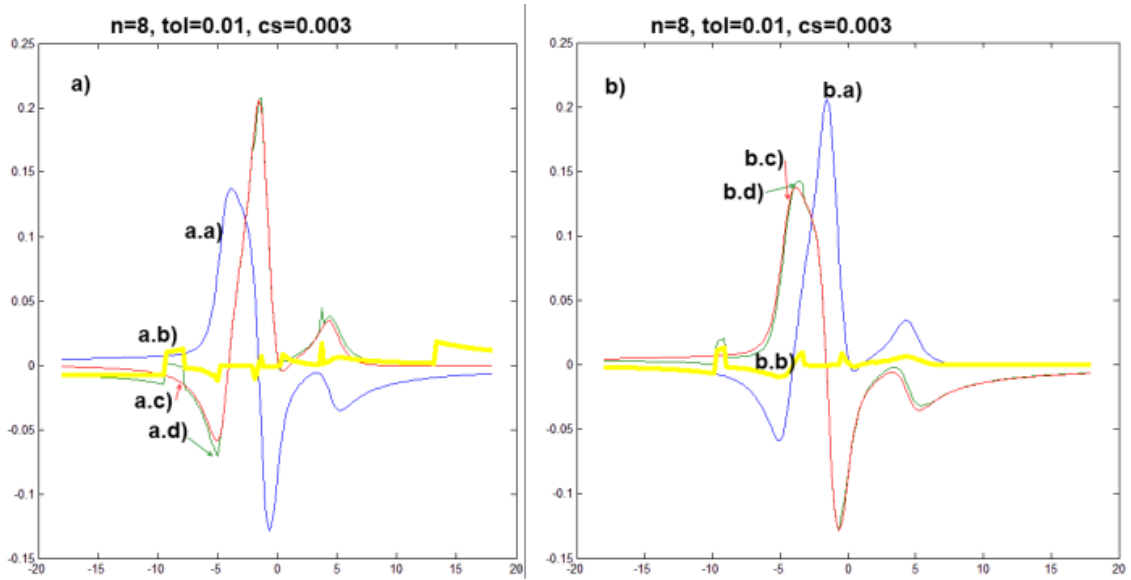


Figure 5.3.2: The Figure presents results of the NC Hilbert Transform method applied for the frequency mixing model. Results are plotted together. Calculations were performed with the parameters ($n = 8$, $cs = .3e-2$, $tol = .1e-1$) a.a) The plot of the real part of $\chi_{mix}(\omega)$ a.b) absolute error plot (a.d-plot minus a.c-plot) a.c) imaginary part of $\chi_{mix}(\omega)$ calculated analytically a.d) imaginary part of $\chi_{mix}(\omega)$ obtained with the Hilbert transform of a.a-plot, b.a) The plot of the imaginary part of $\chi_{mix}(\omega)$ b.b) absolute error plot (b.d-plot minus b.c-plot) b.c) real part of $\chi_{mix}(\omega)$ calculated analytically b.d) real part of $\chi_{mix}(\omega)$ obtained with the Hilbert transform of b.a-plot

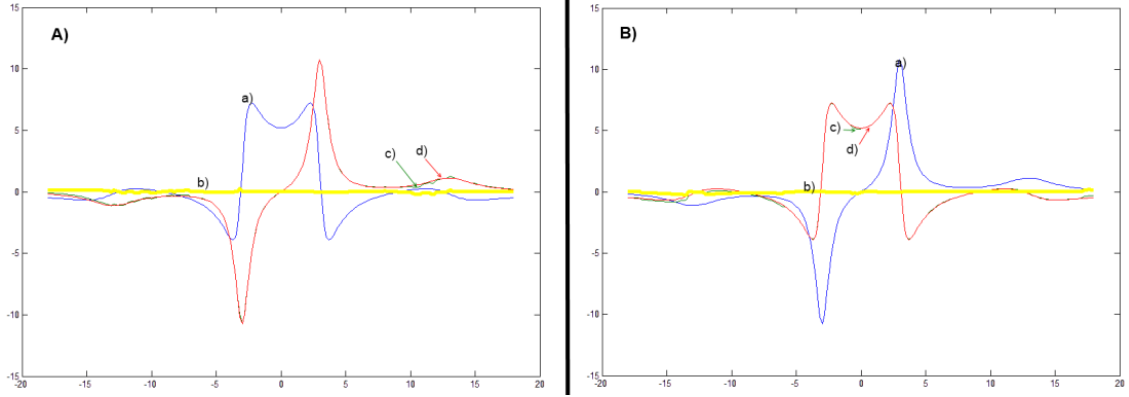


Figure 5.4.1: The Figure presents results of the NC Hilbert Transform method applied for the simple quantum-perturbative model. Results are plotted together. a.a) The plot of the imaginary part of $\chi_{1,qp}(\omega)$ a.b) absolute error plot (d-plot minus c-plot) a.c) real part of $\chi_{1,qp}(\omega)$ obtained with the NC Hilbert transform of a-plot a.d) real part of $\chi_{1,qp}(\omega)$ calculated analytically b.b) The plot of the real part of $\chi_{1,qp}(\omega)$ b.b) absolute error plot (d-plot minus c-plot) b.c) imaginary part of $\chi_{1,qp}(\omega)$ obtained with the NC Hilbert transform of a-plot b.d) imaginary part of $\chi_{1,qp}(\omega)$ calculated analytically

This time we used the following parameters: $\mu = [[3, -0.5], [1.2, 2.4]]$, $\Omega = [-3, 13]$, $\gamma = [0.7, 2.3]$, $N = 8$, $\varepsilon_0 = 1.4$, $h = -2.7$.

Evaluation time of two plots given in the 5.4.1 was 615 seconds.

Second-order model - results:

For the second-order susceptibility we used the model from the 3.5:

$$\begin{aligned} \chi_{2,qp}(\omega_1, \omega_2) = & 2 N \varepsilon_0 h^2 \sum_{n=1}^2 \sum_{m=1}^2 \sum_{l=1}^2 \left(\right. \\ & \frac{\mu_{l,n} \mu_{nm} \mu_{ml}}{(\Omega_{nl} - \omega_1 - \omega_2 - i \gamma_{nl}) (\Omega_{ml} - \omega_1 - i \gamma_{ml})} + \\ & + \frac{\mu_{l,n} \mu_{nm} \mu_{ml}}{(\Omega_{nl} - \omega_1 - \omega_1 - i \gamma_{nl}) (\Omega_{ml} - \omega_2 - i \gamma_{ml})} + \\ & + \frac{\mu_{l,n} \mu_{nm} \mu_{ml}}{(\Omega_{mn} - \omega_1 - \omega_2 - i \gamma_{mn}) (\Omega_{nl} + \omega_2 + i \gamma_{nl})} + \\ & + \frac{\mu_{l,n} \mu_{nm} \mu_{ml}}{(\Omega_{mn} - \omega_1 - \omega_2 - i \gamma_{mn}) (\Omega_{nl} + \omega_2 + i \gamma_{nl})} + \\ & + \frac{\mu_{l,n} \mu_{nm} \mu_{ml}}{(\Omega_{nm} + \omega_1 + \omega_2 + i \gamma_{nm}) (\Omega_{ml} - \omega_1 - i \gamma_{ml})} + \\ & + \frac{\mu_{l,n} \mu_{nm} \mu_{ml}}{(\Omega_{nm} + \omega_1 + \omega_2 + i \gamma_{nm}) (\Omega_{ml} - \omega_1 - i \gamma_{ml})} + \\ & + \frac{\mu_{l,n} \mu_{nm} \mu_{ml}}{(\Omega_{ml} + \omega_1 + \omega_2 + i \gamma_{ml}) (\Omega_{nl} + \omega_1 + i \gamma_{nl})} + \\ & \left. + \frac{\mu_{l,n} \mu_{nm} \mu_{ml}}{(\Omega_{ml} + \omega_1 + \omega_2 + i \gamma_{ml}) (\Omega_{nl} + \omega_2 + i \gamma_{nl})} \right) \quad (5.4.2) \end{aligned}$$

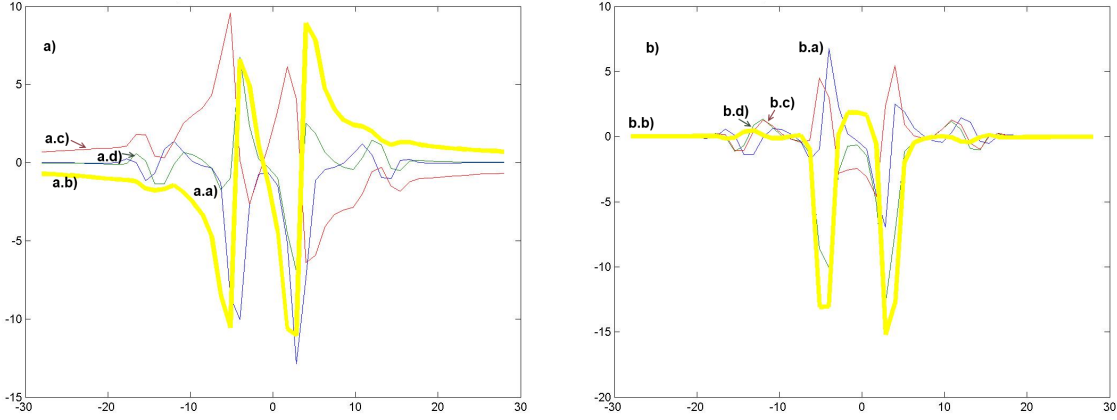


Figure 5.4.2: The Figure presents the results of the NC Hilbert Transform method applied for the second-order quantum-perturbative model. Results are plotted together. Calculations were performed with the parameters ($n = 4$, $cs = .1e-1$, $tol = .1e-1$). a.a) The plot of the real part of $\chi_{2,qp}(\omega)$. a.b) absolute error plot (a.d-plot minus a.c-plot). a.c) imaginary part of $\chi_{2,qp}(\omega)$ calculated analytically. a.d) imaginary part of $\chi_{2,qp}(\omega)$ obtained with the NC Hilbert transform of a.a-plot. b.a) The plot of the imaginary part of $\chi_{2,qp}(\omega)$. b.b) absolute error plot (b.d-plot minus b.c-plot). b.c) real part of $\chi_{2,qp}(\omega)$ calculated analytically. b.d) real part of $\chi_{2,qp}(\omega)$ obtained with the NC Hilbert transform of b.a-plot.

with the constant values already chosen:

$$\mu = \begin{vmatrix} 1 & 3 \\ -1 & -2 \end{vmatrix}, \Omega = \begin{vmatrix} 3 & 16 \\ 4 & 12 \end{vmatrix}, \gamma = \begin{vmatrix} 1 & 2 \\ -1 & 3 \end{vmatrix}, N = 5, \varepsilon_0 = 1, h = -1.$$

Results are presented in the Figure 5.4.2. We can see a very large relative error reaching up to the 100%. We can also see that this model seems to be invalid. This will be checked with another methods in next chapters.

6 Hilbert Clenshaw-Curtis Implementation

6.1 Overview of the Hilbert Clenshaw-Curtis Implementation

The algorithm for the Hilbert transform using the modified Clenshaw-Curtis quadrature is presented.

Closhaw Curtis quadrature:

The heart of the calculation has been presented by T. Hasegawa and T. Torri in [15]. First we will need to calculate the Cauchy principal value integral on the interval $[-1, 1]$:

$$\int_{-1}^1 \frac{f(x)}{(x-c)} dx \text{ for } c \in (-1, 1). \quad (6.1.1)$$

The first step suggested by the authors is to remove the singularity from the integral (Eq. 6.1.2) :

$$\int_{-1}^1 \frac{f(x)}{(x-c)} dx = \int_{-1}^1 \frac{f(x) - f(c)}{(x-c)} + f(c) \log\left(\frac{1-c}{1+c}\right) \quad (6.1.2)$$

After some transformation authors finally obtain the iterative formula presented in the equations 6.1.3a and 6.1.3b. The formula 6.1.3a depends on the parameter N, which will be used in the adaptive algorithm. The recursive equation 6.1.3b should be solved with the starting values: $d_N = d_{N+1} = 0$

$$\int_{-1}^1 \frac{f(x)}{(x-c)} dx \approx 2 \sum_{k=0}^{N/2-1} \frac{d_{2k}}{1-4k^2} + f(c) \log\left(\frac{1-c}{1+c}\right) \quad (6.1.3a)$$

$$d_{k+1} - 2cd + k + d_{k-1} = 2a_k^N \text{ for } k = N, N-1, \dots, 1. \quad (6.1.3b)$$

The remaining issue is to calculate the a_k^N coefficients, which has been described in the equation 6.1.4. It is also known as the discrete cosine transform of the first type (DCT-I):

$$a_k^N = \frac{2}{N} \sum_{j=0}^N f \left(\cos\left(\frac{\pi j}{N}\right) \right) \cos\left(\frac{\pi kj}{N}\right), 0 \leq k \leq N \quad (6.1.4)$$

Hilbert transform using the Clenshaw-Curtis quadrature:

While the Clenshaw-Curtis quadrature is defined for finite range $[-1, 1]$, the Hilbert transform uses the definite and improper integral over the range $[-\infty, \infty]$. Here we must remind the law of conservation of energy, from which we can easily deduce that the susceptibility - as the investigated physical quantity - for low frequencies and thus for low energies has low values. From this it follows that function $f = f(x)$ tends to zero when closing to infinities. Thereby the value of integrated function from equation 6.1.5 decreases rapidly and for relatively large values of x this integrand will be omitted.

$$\frac{f(x)}{x-c} dx \quad (6.1.5)$$

Therefore, we will not be changing the integration range from interval to real line. What must be taken into consideration right now - is that the well-chosen, finite interval for integration stated in 6.1.6 or an integral with a period few times bigger.

$$[A, B] = [a - 2|b-a|, b + 2|b-a|] \quad (6.1.6)$$

The specific choice of integration interval should be done during the numerical calculations. As default in our algorithm, we have set the integration interval to be based on the 6.1.6, but with period simply 5 times longer. For all investigated models it gave us satisfactory results.

Our implementation of the Hilbert Clenshaw-Curtis iterations:

So far we have presented the overview of procedures responsible for evaluation of the Clenshaw-Curtis quadrature and the Hilbert transform using the Clenshaw-Curtis quadrature at one point. But in the typical situation we have the whole vector of function values for a given range of abscissas - so what is left - we perform the single-point Hilbert transform based on the Clenshaw-Curtis quadrature for each given point. But to omit the problems with singularities, we will add some post- and precalculations - using the cubic interpolation. The whole procedure is now:

INPUT:

X, Y - given N -length abscissas and related ordinates
 A, B - extended ranges of the interval (based on Y)

PRE-CALCULATIONS:

$$T = B - A \quad (6.1.7)$$

$$C = \frac{B + A}{2} \quad (6.1.8)$$

From N points of Y we calculate the cubic interpolation having $N - 1$ inner points:

$$Yp_1 = \frac{3Y_1 + 6Y_2 - Y_3}{8} \quad (6.1.9a)$$

$$Yp_k = \frac{-Y_{k-1} + 9Y_k + 9Y_{k+1} - Y_{k+2}}{16} \quad (6.1.9b)$$

$$Yp_N = \frac{-Y_{N-2} + 6Y_{N-1} + 3Y_N}{8} \quad (6.1.9c)$$

MAIN CALCULATIONS: As the central part, we calculate the $N - 1$ values for each one of inner points:

$$d_k = \frac{2(Yp_k - C)}{T}, \text{ for } k = 1, \dots, N - 1 \quad (6.1.10)$$

$$Hh_k \approx \frac{1}{\pi} \int_A^B \frac{f(\frac{x-T}{2} + C)}{x - d_k} dx, \text{ for } k = 1, \dots, N - 1 \quad (6.1.11)$$

POST-CALCULATIONS:

From $N - 1$ points of Hh we calculate N points using the reverse cubic interpolation:

$$H_1 = \frac{15Hh_1 - 10Hh_2 + 3Hh_3}{8} \quad (6.1.12a)$$

$$H_2 = \frac{3Hh_1 + 6Hh_2 - Hh_3}{8} \quad (6.1.12b)$$

$$H_k = \frac{-Hh_{k-1} + 9Hh_k + 9Hh_{k+1} - Hh_{k+2}}{16} \quad (6.1.12c)$$

$$H_{N-1} = \frac{-Hh_{N-3} + 6Hh_2 - Hh_3}{8} \quad (6.1.12d)$$

$$H_N = \frac{3Hh_{N-3} - 10Hh_{N-2} + 15Hh_{N-1}}{8} \quad (6.1.12e)$$

OUTPUT:

H - N -length Hilbert transform for given function values at X abscissas

The algorithm source has been presented in the Appendix A.3.

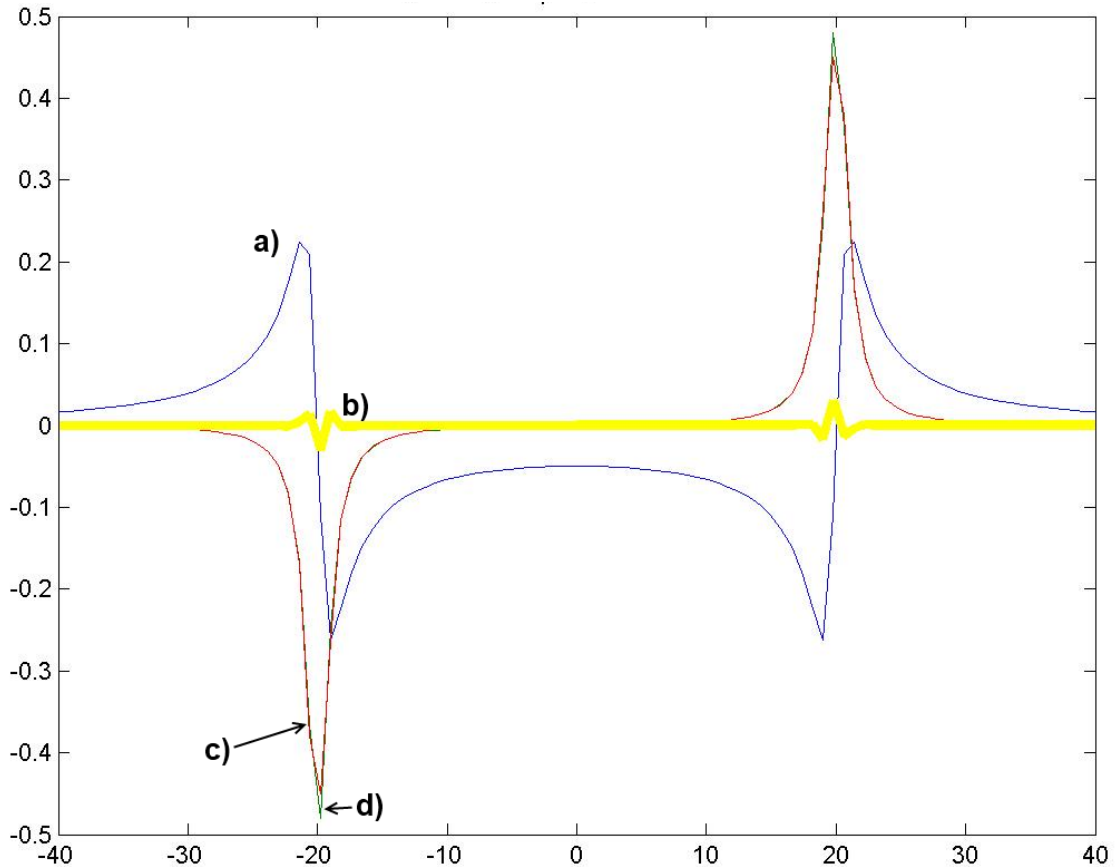


Figure 6.2.1: The Figure presents the results of the Hilbert Clenshaw-Curtis iterations method applied to the real part of the simple linear model. Results are plotted together. a) The plot of the real part of $\chi(\omega)$ b) absolute error plot (c-plot minus d-plot) c) imaginary part of $\chi(\omega)$ obtained with the Hilbert transform of a-plot d) imaginary part of $\chi(\omega)$ calculated analytically.

6.2 HCCI for simple linear model

The Figures 6.2.1 and 6.2.2 presents the results obtained with the method for the model defined in model 3.3.3. As we can see - the Hilbert Clenshaw-Curtis iterations gives us much better accuracy than HTRAN or Newton-Cotes quadrature. In next chapters we will check what happens for another models.

6.3 HCCI for simple nonlinear model

For the pump-probe and frequency mixing models we have used the same parameters as in chapter 5.3. The results obtained with the Hilbert Clenshaw-Curtis iterations has been presented in Figures 6.3.1 and 6.3.2 respectively.

As we can see here - once again the results come with quite well accuracy.

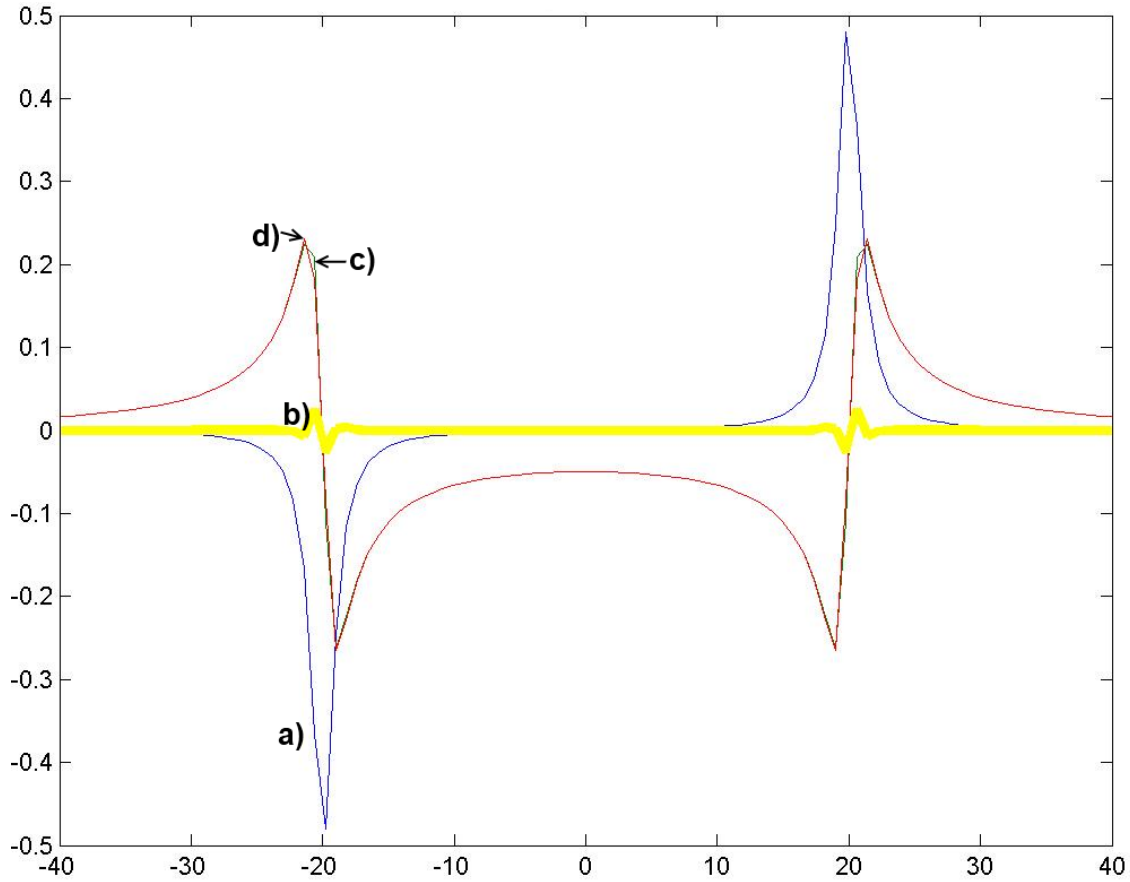


Figure 6.2.2: The Figure presents the results of the Hilbert Clenshaw-Curtis iterations method applied to the imaginary part of the simple linear model. Results are plotted together. a) The plot of the imaginary part of $\chi(\omega)$ b) absolute error plot (c-plot minus d-plot) c) real part of $\chi(\omega)$ obtained with the Hilbert transform of a-plot d) real part of $\chi(\omega)$ calculated analytically.

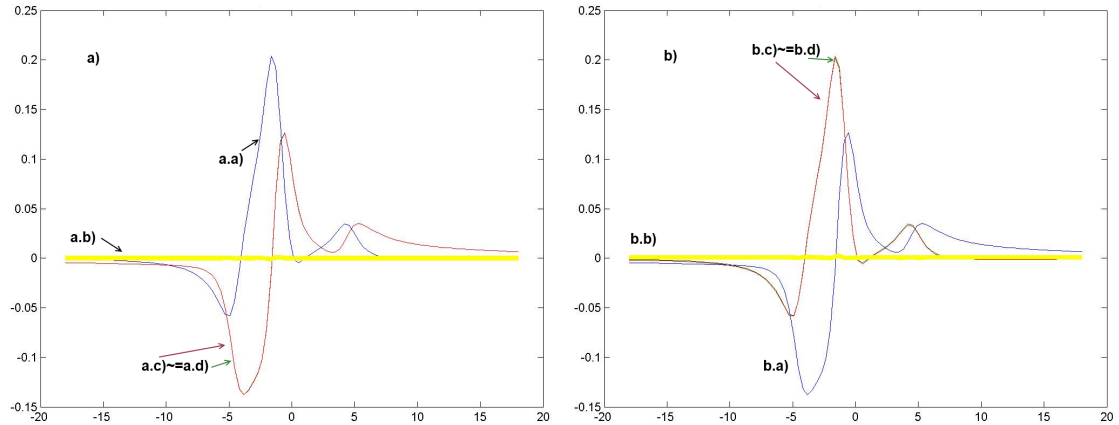


Figure 6.3.1: Results for the pump-probe model using the Hilbert Clenshaw-Curtis iterations a.a) The plot of the real part of $\chi_{pp}(\delta)$ a.b) absolute error plot (a.d-plot minus a.c-plot) a.c) imaginary part of $\chi_{pp}(\delta)$ calculated analytically a.d) imaginary part of $\chi_{pp}(\delta)$ obtained with the Hilbert transform of a.a-plot, b.a) The plot of the imaginary part of $\chi_{pp}(\delta)$ b.b) absolute error plot (b.d-plot minus b.c-plot) b.c) real part of $\chi_{pp}(\omega)$ calculated analytically b.d) real part of $\chi_{pp}(\delta)$ obtained with the Hilbert transform of b.a-plot

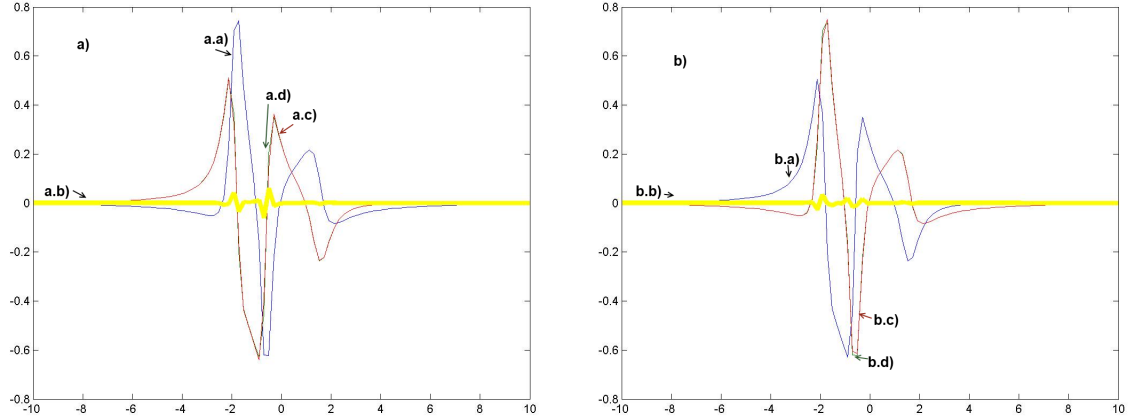


Figure 6.3.2: Results for the frequency mixing model using the Hilbert Clenshaw-Curtis iterations a.a) The plot of the real part of $\chi_{mix}(\delta)$ a.b) absolute error plot (a.d-plot minus a.c-plot) a.c) imaginary part of $\chi_{mix}(\delta)$ calculated analytically a.d) imaginary part of $\chi_{mix}(\delta)$ obtained with the Hilbert transform of a.a-plot, b.a) The plot of the imaginary part of $\chi_{mix}(\delta)$ b.b) absolute error plot (b.d-plot minus b.c-plot) b.c) real part of $\chi_{mix}(\omega)$ calculated analytically b.d) real part of $\chi_{mix}(\delta)$ obtained with the Hilbert transform of b.a-plot

6.4 HCCI for simple quantum-perturbative model

Linear model - results:

As in the Chapter 5.3, we have used the same model to describe the simple linear quantum-perturbative model:

$$\chi_{1,qp}(\omega) = \frac{N}{\varepsilon_0 h} \sum_{n=1}^2 \left(\frac{\mu_{1,n} \mu_{2,n}}{\Omega_n - \omega - i \gamma_n} + \frac{\mu_{2,n} \mu_{1,n}}{\Omega_n + \omega + i \gamma_n} \right) \quad (6.4.1)$$

This time we used the following parameters:

$$\mu = [[3, -0.5], [1.2, 2.4]], \Omega = [-3, 13], \gamma = [0.7, 2.3], N = 8, \varepsilon_0 = 1.4, h = -2.7 .$$

Results are presented in the Figure 6.4.1. We can see a perfect match here!

Second-order model - results:

We have also used the same model as in 5.3 to describe the second-order susceptibility model:

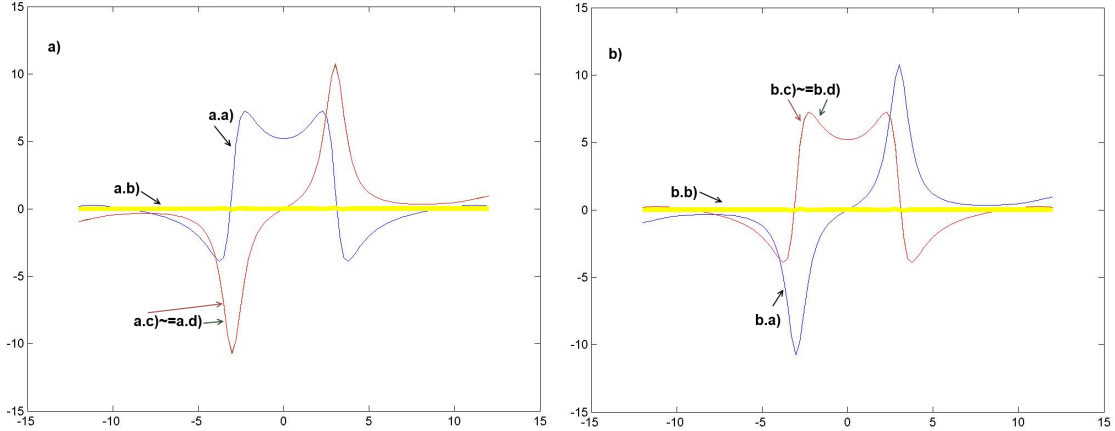


Figure 6.4.1: Results for the linear quantum perturbative model for HCCI quadrature a.a) The plot of the imaginary part of $\chi_{1,qp}(\omega)$ a.b) absolute error plot (d-plot minus c-plot) a.c) real part of $\chi_{1,qp}(\omega)$ obtained with the Hilbert transform of a-plot a.d) real part of $\chi_{1,qp}(\omega)$ calculated analytically b.b) The plot of the real part of $\chi_{1,qp}(\omega)$ b.b) absolute error plot (d-plot minus c-plot) b.c) imaginary part of $\chi_{1,qp}(\omega)$ obtained with the Hilbert transform of a-plot b.d) imaginary part of $\chi_{1,qp}(\omega)$ calculated analytically

$$\begin{aligned}
\chi_{2,qp}(\omega_1, \omega_2) = & 2 N \varepsilon_0 h^2 \sum_{n=1}^2 \sum_{m=1}^2 \sum_{l=1}^2 \left(\frac{\mu_{l,n} \mu_{nm} \mu_{ml}}{(\Omega_{nl} - \omega_1 - \omega_2 - i \gamma_{nl})(\Omega_{ml} - \omega_1 - i \gamma_{ml})} + \right. \\
& + \frac{\mu_{l,n} \mu_{nm} \mu_{ml}}{(\Omega_{nl} - \omega_1 - \omega_1 - i \gamma_{nl})(\Omega_{ml} - \omega_2 - i \gamma_{ml})} + \\
& + \frac{\mu_{l,n} \mu_{nm} \mu_{ml}}{(\Omega_{mn} - \omega_1 - \omega_2 - i \gamma_{mn})(\Omega_{nl} + \omega_2 + i \gamma_{nl})} + \\
& + \frac{\mu_{l,n} \mu_{nm} \mu_{ml}}{(\Omega_{mn} - \omega_1 - \omega_2 - i \gamma_{mn})(\Omega_{nl} + \omega_2 + i \gamma_{nl})} + \\
& + \frac{\mu_{l,n} \mu_{nm} \mu_{ml}}{(\Omega_{nm} + \omega_1 + \omega_2 + i \gamma_{nm})(\Omega_{ml} - \omega_1 - i \gamma_{ml})} + \\
& + \frac{\mu_{l,n} \mu_{nm} \mu_{ml}}{(\Omega_{nm} + \omega_1 + \omega_2 + i \gamma_{nm})(\Omega_{ml} - \omega_1 - i \gamma_{ml})} + \\
& + \frac{\mu_{l,n} \mu_{nm} \mu_{ml}}{(\Omega_{ml} + \omega_1 + \omega_2 + i \gamma_{ml})(\Omega_{nl} + \omega_1 + i \gamma_{nl})} + \\
& \left. + \frac{\mu_{l,n} \mu_{nm} \mu_{ml}}{(\Omega_{ml} + \omega_1 + \omega_2 + i \gamma_{ml})(\Omega_{nl} + \omega_2 + i \gamma_{nl})} \right) \quad (6.4.2)
\end{aligned}$$

for the defined set of parameters:

$$\mu = \begin{vmatrix} 1 & 3 \\ -1 & -2 \end{vmatrix}, \Omega = \begin{vmatrix} 3 & 16 \\ 4 & 12 \end{vmatrix}, \gamma = \begin{vmatrix} 1 & 2 \\ -1 & 3 \end{vmatrix}, N = 5, \varepsilon_0 = 1, h = -1$$

Results are presented in the Figure 6.4.2. As for the Newton-Cotes calculations in Chapter 5.4 we can see the model could be invalid because the arisen errors reach up to 100%.

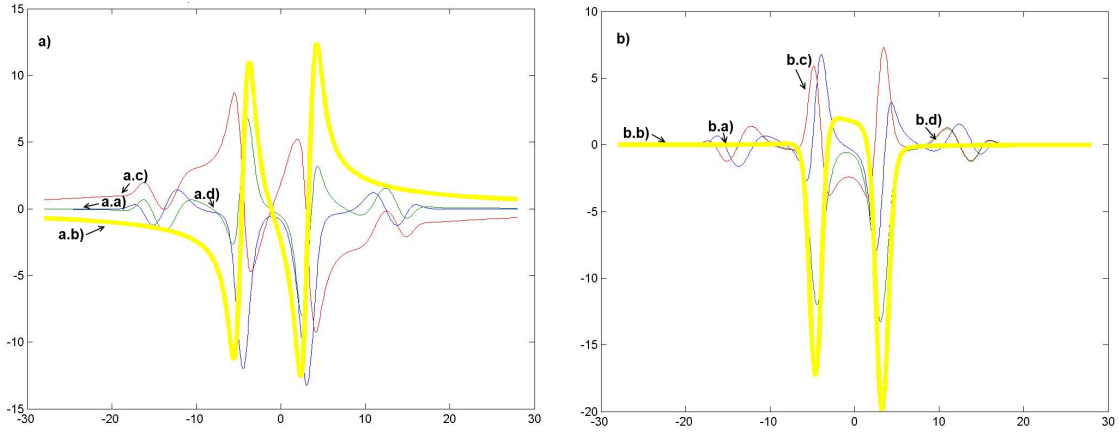


Figure 6.4.2: Results for the second-order quantum perturbative model for HCCI quadrature a.a) The plot of the real part of $\chi_{2,qp}(\omega)$ a.b) absolute error plot (a.d-plot minus a.c-plot) a.c) imaginary part of $\chi_{2,qp}(\omega)$ calculated analytically a.d) imaginary part of $\chi_{2,qp}(\omega)$ obtained with the Hilbert transform of a.a-plot, b.a) The plot of the imaginary part of $\chi_{2,qp}(\omega)$ b.b) absolute error plot (b.d-plot minus b.c-plot) b.c) real part of $\chi_{2,qp}(\omega)$ calculated analytically b.d) real part of $\chi_{2,qp}(\omega)$ obtained with the Hilbert transform of b.a-plot

7 Fast Hartley transform approach

7.1 Overview of the FTHA

The Fast Hartley Transform approach for the Hilbert transform is based on two efficient $O(n \log n)$ discrete Hartley transforms and was well described by Soo-Chang Pei in [38]. This approach is faster than another discrete Hilbert transform based on two Fourier transforms, because the whole computation are carried using only real numbers, which is faster than Fourier computation carried using time consuming complex numbers.

Discrete Hartley Transform

For a given N -length vector X both the discrete Hartley transform and inverse discrete Hartley transform are defined as follows:

$$\text{DHT}(X_k) = \sum_{n=0}^{N-1} X_n \left(\cos\left(\frac{2\pi k n}{N}\right) + \sin\left(\frac{2\pi k n}{N}\right) \right) \quad (7.1.1a)$$

$$\text{IDHT}(H_k) = \frac{1}{N} \sum_{k=0}^{N-1} H_k \left(\cos\left(\frac{2\pi k n}{N}\right) + \sin\left(\frac{2\pi k n}{N}\right) \right) \quad (7.1.1b)$$

Hartley transform convolution theorem

Now we will introduce the Hartley transform convolution theorem. We define the N -length vector x as convolution of two N -length vectors x_1, x_2 as follows:

$$x_n = x_{1,n} * x_{2,n} = \sum_{k=0}^{N-1} x_{1,k} x_{2,n-k} \quad (7.1.2)$$

For a given convolution, the following theorem is stated:

$$\text{DHT}(x_n) = \text{DHT}(x_{1,k}) \text{ even}(\text{DHT}(x_{2,k})) + \text{DHT}(x_{1,-k}) \text{ odd}(\text{DHT}(h_{2,k})), \quad (7.1.3)$$

with: $\text{DHT}(x_{2,k}) = \text{even}(\text{DHT}(x_{2,k})) + \text{odd}(\text{DHT}(x_{2,k}))$

The proof of the Hartley transform convolution theorem can be found in [38].

Relation between discrete Fourier and discrete Hilbert transform

To better understand the relation between the discrete Fourier and discrete Hilbert transform we will introduce the discrete Hilbert kernel:

$$h_k = \frac{1}{\pi k} \text{ discrete Hilbert kernel}. \quad (7.1.4)$$

The discrete Fourier transform of the discrete Hilbert kernel will be marked with the symbol $H(k)$:

$$H(k) = \text{DFT}(h_k), \quad (7.1.5)$$

and the H has the following properties:

$$H(k) = i \text{ for } k = 1, 2, \dots, \frac{N}{2} - 1, \quad (7.1.6a)$$

$$H(k) = 0 \text{ for } k = 0, \frac{N}{2}, \quad (7.1.6b)$$

$$H(k) = -i \text{ for } k = \frac{N}{2} + 1, \frac{N}{2} + 2, \dots, N - 1 \quad (7.1.6c)$$

We derive the discrete Fourier transform of the Hilbert transform for a given N -length vector x :

$$\text{DFT}(\text{DISCRETE_HILBERT}(x_k)) = H(k) \text{DFT}(x_k) = (-i) \text{sgn}(k) \text{DFT}(x_k). \quad (7.1.7)$$

Application of the discrete Hartley transform to calculate the discrete Hilbert transform:

Using the Hartley transform convolution theorem 7.1.6 for a given N -length vector x we obtain:

$$\begin{aligned} \text{DHT}(\text{DISCRETE_HILBERT}(x_k)) &= \\ &= \text{DHT}(x_k) \text{even}(\text{DHT}(h_k)) + \text{DHT}(x_{-k}) \text{odd}(\text{DHT}(h_k)), \end{aligned} \quad (7.1.8)$$

where we have use the time reversal notation: $x_{-k} = x_{(N-k) \bmod N}$.

Now we should notice, that the discrete Hilbert transform kernel defined in 7.1.4 is an odd function, so its even part equals zero. So 7.1.8 simplifies now into a product of two separate Hartley transforms:

$$\text{DHT}(\text{DISCRETE_HILBERT}(x_k)) = \text{DHT}(x_{-k}) \text{odd}(\text{DHT}(h_k)) = \text{DHT}(x_{-k}) \text{DHT}(h_k) \quad (7.1.9)$$

By [38] the second transform is defined:

$$\text{DHT}(h_k) = 1 \text{ for } k = 1, 2, \dots, \frac{N}{2} - 1 \quad (7.1.10a)$$

$$\text{DHT}(h_k) = 0 \text{ for } k = 0, \frac{N}{2} \quad (7.1.10b)$$

$$\text{DHT}(h_k) = -1 \text{ for } k = \frac{N}{2} + 1, \frac{N}{2} + 2..N - 1 \quad (7.1.10c)$$

In order to calculate the Hilbert of a given N-length vector x the last thing to do is to apply the inverse discrete Hartley transform on the very right side of 7.1.9 equation.

Fast Hartley Transform algorithm

Ronald F. Ullmann has showed the fast algorithm for the discrete Hartley transform in [44]. The important assumption is that - as for the fast Fourier transform algorithm, the fast Hartley transform algorithm is defined for a K-length vector x , where K is the power-of-two:

$$\exists p \in \mathbb{N} : K = 2^p \quad (7.1.11)$$

The 7.1.11 condition for the algorithm and the further possibilities to modify it are discussed further. We will start with the very same thing as in the fast Fourier algorithm - we split the x vector into two smaller vectors:

$$x_{1, \frac{m}{2}} = x_m \text{ for } m = 0, 2, \dots, N - 1 \quad (7.1.12a)$$

$$x_{2, \frac{m-1}{2}} = x_m \text{ for } m = 1, 3, \dots, N - 2 \quad (7.1.12b)$$

Taking into account the initial definition of the discrete Hartley transform 7.1.1a, we obtain:

$$\begin{aligned} \text{DHT}(x_k) = & \left(\sum_{n=0}^{\frac{N}{2}-1} x(2n) (\cos\left(\frac{2\pi k 2n}{N}\right) + \sin\left(\frac{2\pi k 2n}{N}\right)) \right) + \\ & \left(\sum_{n=0}^{\frac{N}{2}-1} x(2n+1) (\cos\left(\frac{2\pi k (2n+1)}{N}\right) + \sin\left(\frac{2\pi k (2n+1)}{N}\right)) \right) \end{aligned} \quad (7.1.13)$$

In [44] the following "shift rule" for the discrete Hartley transform is stated :

$$\text{DHT}(x_{k+c}) = \text{DHT}(x_k) \cos(c) + \text{DHT}(x_{-k}) \sin(c) \quad (7.1.14)$$

If we apply the Hartley shift rule 7.1.14 to the split equation in 7.1.13 we obtain:

$$\begin{aligned} \text{DHT}(x_k) &= \text{DHT}(x_{1,k}) + \cos\left(\frac{2\pi k}{N}\right) \text{DHT}(x_{2,k}) + \sin\left(\frac{2\pi k}{N}\right) \text{DHT}(x_{2,-k}) \\ &\quad \text{for } k = 0, 1, 3, \dots, \frac{N}{2} - 1 \end{aligned} \quad (7.1.15)$$

The rule 7.1.15 can be applied only for the half of the possible k values ($k < \frac{N}{2}$). Now we will use the periodic properties of the discrete Hartley transform kernel:

$$\cos\left(\frac{2\pi k(n+N)}{N}\right) + \sin\left(\frac{2\pi k 2(n+N)}{N}\right) = \cos\left(\frac{2\pi k n}{N}\right) + \sin\left(\frac{2\pi k 2n}{N}\right) \quad (7.1.16a)$$

$$\cos\left(\frac{2\pi k(n+\frac{N}{2})}{N}\right) + \sin\left(\frac{2\pi k 2(n+\frac{N}{2})}{N}\right) = -\left(\cos\left(\frac{2\pi k n}{N}\right) + \sin\left(\frac{2\pi k 2n}{N}\right)\right) \quad (7.1.16b)$$

The rule 7.1.15 using the periodicity property from 7.1.16 can be now used for all k indices:

$$\text{DHT}(x_k) = \text{DHT}(x_{1,k}) + \cos\left(\frac{2\pi k}{N}\right) \text{DHT}(x_{2,k}) + \sin\left(\frac{2\pi k}{N}\right) \text{DHT}(x_{2,-k}) \quad (7.1.17a)$$

$$\text{for } k = 0, 1, \dots, \frac{N}{2} - 1$$

$$\begin{aligned} \text{DHT}(x_k) &= \\ \text{DHT}(x_{1,k-\frac{N}{2}}) &- \cos\left(\frac{2\pi(k-\frac{N}{2})}{N}\right) \text{DHT}(x_{2,k-\frac{N}{2}}) - \sin\left(\frac{2\pi(k-\frac{N}{2})}{N}\right) \text{DHT}(x_{2,-k+\frac{N}{2}}) \end{aligned} \quad (7.1.17b)$$

$$\text{for } k = \frac{N}{2}, \frac{N}{2} + 2, \dots, N - 1$$

The remaining definition for the negative index, need to be explained:

$$\text{DHT}(v_{-k}) = \text{DHT}(v_{(N-k) \bmod N}) \quad (7.1.18)$$

Of course this is a typical divide-and-conquer approach, where the complexity is reduced from $O(n^2)$ to $O(n \log(n))$, very similar to the approach used in the Cooley-Tukey FFT algorithm [11].

Non-power-of-two case

There are several approaches when calculating the fast Fourier transform for a non-power-of-two case length of the input x vector. One approach PFA is the Good-Thomas [13] / prime-factor algorithm for a vector length K defined:

$$K = K_1 K_2, \quad (7.1.19)$$

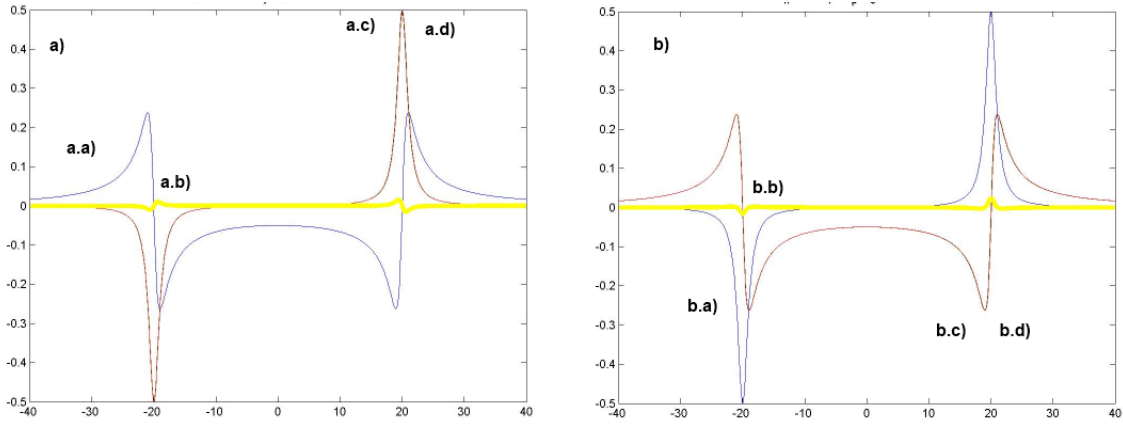


Figure 7.2.1: The Figure presents the results of the Fast Hartley Hilbert Transform method applied to the simple linear model. Results are plotted together. a.a) The plot of the real part of $\chi(\omega)$ a.b) absolute error plot (c-plot minus d-plot) a.c) imaginary part of $\chi(\omega)$ obtained with the Hilbert transform of a-plot a.d) imaginary part of $\chi(\omega)$ calculated analytically. b.a) The plot of the imaginary part of $\chi(\omega)$ b.b) absolute error plot (c-plot minus d-plot) b.c) real part of $\chi(\omega)$ obtained with the Hilbert transform of a-plot b.d) real part of $\chi(\omega)$ calculated analytically.

Where K_1 and K_2 are relatively prime numbers. Another approach was presented by Leo Bluestein, called also the chirp z-transform algorithm is presented in [2]. Another author, George Bruun, has invented the approach based on the recursive polynomial-factorization in [6]. Rader has prepared the special FFT algorithm especially for vectors of prime size in [33]. But we will use the simplest possible approach - called the zero-padding. So in case of input vector with the size of non-power-of-two, we add the suffix vector filled with vectors to fit the next possible power-of-two size. In the worst case, the input vector size will be doubled, which has no influence on the asymptotic complexity, which remains $O(n \log n)$. While the discrete signal analysis is the domain of scientists, we will end with conclusion stated by M. Lamb in [22] that he is uncertain, if zero padding has an influence on the spectral resolution, but in most cases it has a little influence on the results obtained in the discrete transforms.

The source code of the discrete Hilbert transform using both the fast Hartley transform and inverse fast Hartley transform has been presented in Appendix A.4.

7.2 FTHA for simple linear model

In the Figure 7.2.1 we have presented the results obtained with the Fast Hartley Hilbert Transform for the simple linear model defined in model 3.3.3. As we can see - the Fast Hartley Hilbert Transform gives us quite well accuracy, similar to HCCI and much better than HTRAN or Newton-Cotes quadrature.

7.3 FTHA for simple nonlinear model

For the pump-probe and frequency mixing models we have used the same parameters as in chapter 5.3. The results obtained with the Fast Hartley Hilbert Transform has been presented in Figures 7.3.1 and 7.3.2 respectively.

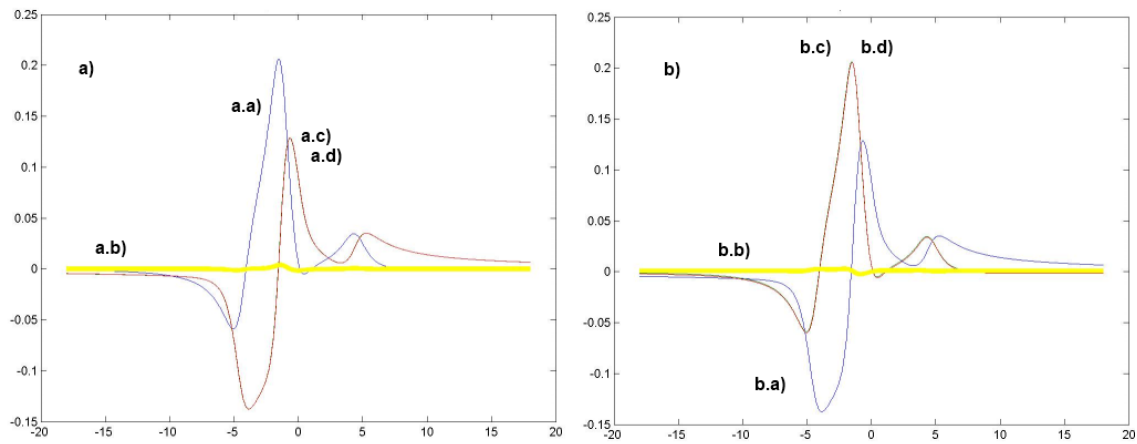


Figure 7.3.1: The Figure presents the results of the Fast Hartley Hilbert Transform method applied to the pump-and-probe model. Results are plotted together. a.a) The plot of the real part of $\chi_{pp}(\omega)$ a.b) absolute error plot (a.d-plot minus a.c-plot) a.c) imaginary part of $\chi_{pp}(\omega)$ calculated analytically a.d) imaginary part of $\chi_{pp}(\omega)$ obtained with the Hilbert transform of a.a-plot, b.a) The plot of the imaginary part of $\chi_{pp}(\omega)$ b.b) absolute error plot (b.d-plot minus b.c-plot) b.c) real part of $\chi_{pp}(\omega)$ calculated analytically b.d) real part of $\chi_{pp}(\omega)$ obtained with the Hilbert transform of b.a-plot

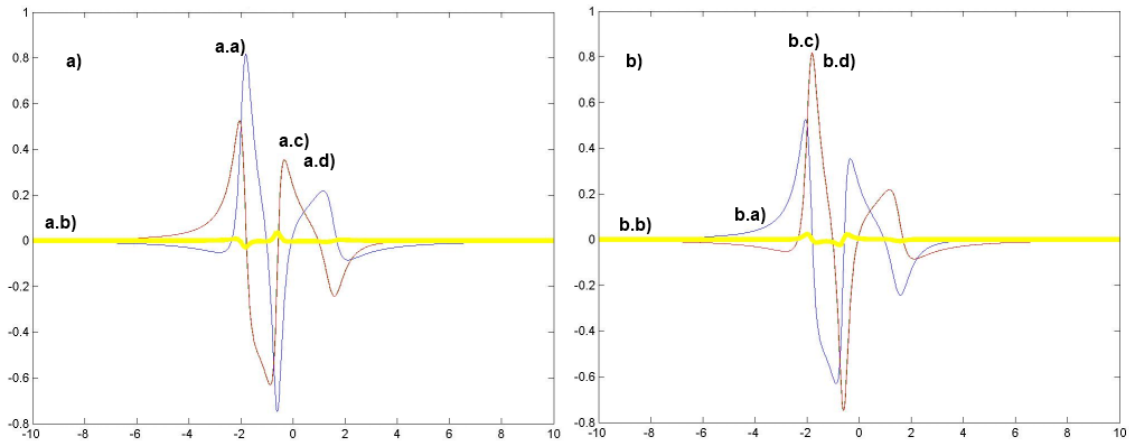


Figure 7.3.2: The Figure presents the results of the Fast Hartley Hilbert Transform method applied to the frequency mixing model. Results are plotted together. a.a) The plot of the real part of $\chi_{mix}(\delta)$ a.b) absolute error plot (a.d-plot minus a.c-plot) a.c) imaginary part of $\chi_{mix}(\omega)$ calculated analytically a.d) imaginary part of $\chi_{mix}(\omega)$ obtained with the Hilbert transform of a.a-plot, b.a) The plot of the imaginary part of $\chi_{mix}(\omega)$ b.b) absolute error plot (b.d-plot minus b.c-plot) b.c) real part of $\chi_{mix}(\omega)$ calculated analytically b.d) real part of $\chi_{mix}(\omega)$ obtained with the Hilbert transform of b.a-plot

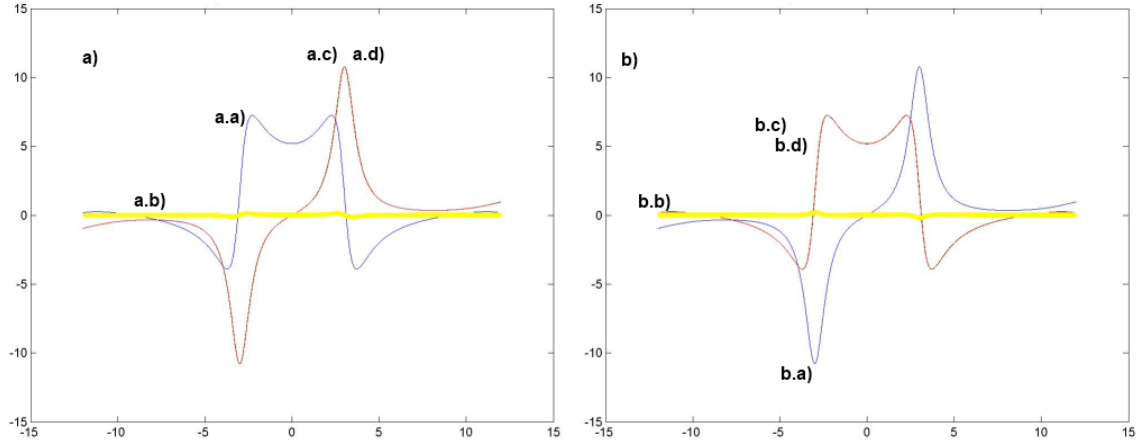


Figure 7.4.1: Results for the linear quantum perturbative model for FHT Hilbert transform a.a) The plot of the imaginary part of $\chi_{1,qp}(\omega)$ a.b) absolute error plot (d-plot minus c-plot) a.c) real part of $\chi_{1,qp}(\omega)$ obtained with the Hilbert transform of a-plot a.d) real part of $\chi_{1,qp}(\omega)$ calculated analytically b.b) The plot of the real part of $\chi_{1,qp}(\omega)$ b.b) absolute error plot (d-plot minus c-plot) b.c) imaginary part of $\chi_{1,qp}(\omega)$ obtained with the Hilbert transform of a-plot b.d) imaginary part of $\chi_{1,qp}(\omega)$ calculated analytically

Once again we can see a very good accuracy, better than for HTRAN or Newton-Cotes, and similar to HCCI.

7.4 FTHA for simple quantum-perturbative model

Linear model - results:

As in the Chapter 5.3, we have used the same model to describe the simple linear quantum-perturbative model:

$$\chi_{1,qp}(\omega) = \frac{N}{\varepsilon_0 h} \sum_{n=1}^2 \left(\frac{\mu_{1,n} \mu_{2,n}}{\Omega_n - \omega - i \gamma_n} + \frac{\mu_{2,n} \mu_{1,n}}{\Omega_n + \omega + i \gamma_n} \right) \quad (7.4.1)$$

This time we used the following parameters:

$$\mu = [[3, -0.5], [1.2, 2.4]], \Omega = [-3, 13], \gamma = [0.7, 2.3], N = 8, \varepsilon_0 = 1.4, h = -2.7$$

Results are presented in the Figure 7.4.1. We can see a perfect match here!

Second-order model - results:

We have also used the same model as in 5.3 to describe the second-order susceptibility model:

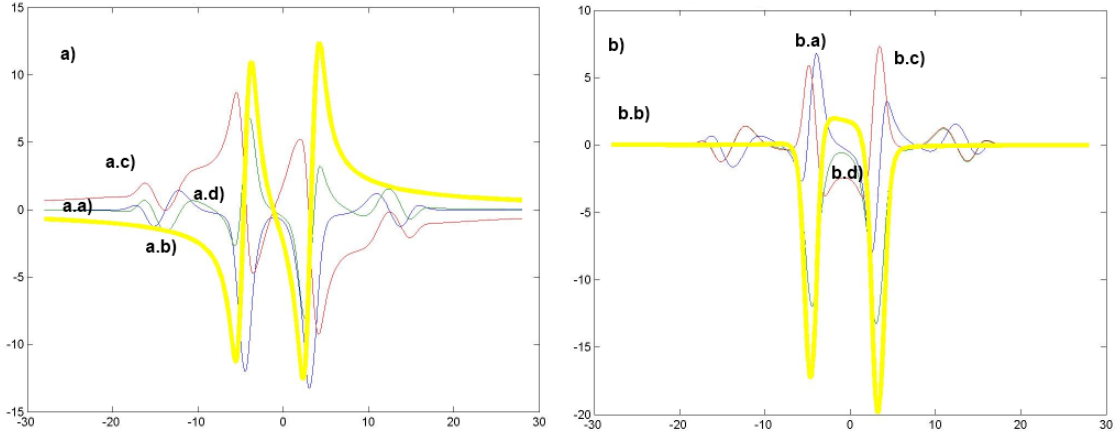


Figure 7.4.2: Results for the second-order quantum perturbative model for FHT Hilbert transform a.) The plot of the real part of $\chi_{2,qp}(\omega)$ a.b) absolute error plot (a.d-plot minus a.c-plot) a.c) imaginary part of $\chi_{2,qp}(\omega)$ calculated analytically a.d) imaginary part of $\chi_{2,qp}(\omega)$ obtained with the Hilbert transform of a.a-plot, b.a) The plot of the imaginary part of $\chi_{2,qp}(\omega)$ b.b) absolute error plot (b.d-plot minus b.c-plot) b.c) real part of $\chi_{2,qp}(\omega)$ calculated analytically b.d) real part of $\chi_{2,qp}(\omega)$ obtained with the Hilbert transform of b.a-plot

$$\begin{aligned}
\chi_{2,qp}(\omega_1, \omega_2) = & 2 N \varepsilon_0 h^2 \sum_{n=1}^2 \sum_{m=1}^2 \sum_{l=1}^2 \left(\frac{\mu_{l,n} \mu_{nm} \mu_{ml}}{(\Omega_{nl} - \omega_1 - \omega_2 - i\gamma_{nl})(\Omega_{ml} - \omega_1 - i\gamma_{ml})} + \right. \\
& + \frac{\mu_{l,n} \mu_{nm} \mu_{ml}}{(\Omega_{nl} - \omega_1 - \omega_1 - i\gamma_{nl})(\Omega_{ml} - \omega_2 - i\gamma_{ml})} + \\
& + \frac{\mu_{l,n} \mu_{nm} \mu_{ml}}{(\Omega_{mn} - \omega_1 - \omega_2 - i\gamma_{mn})(\Omega_{nl} + \omega_2 + i\gamma_{nl})} + \\
& + \frac{\mu_{l,n} \mu_{nm} \mu_{ml}}{(\Omega_{mn} - \omega_1 - \omega_2 - i\gamma_{mn})(\Omega_{nl} + \omega_2 + i\gamma_{nl})} + \\
& + \frac{\mu_{l,n} \mu_{nm} \mu_{ml}}{(\Omega_{nm} + \omega_1 + \omega_2 + i\gamma_{nm})(\Omega_{ml} - \omega_1 - i\gamma_{ml})} + \\
& + \frac{\mu_{l,n} \mu_{nm} \mu_{ml}}{(\Omega_{nm} + \omega_1 + \omega_2 + i\gamma_{nm})(\Omega_{ml} - \omega_1 - i\gamma_{ml})} + \\
& + \frac{\mu_{l,n} \mu_{nm} \mu_{ml}}{(\Omega_{ml} + \omega_1 + \omega_2 + i\gamma_{ml})(\Omega_{nl} + \omega_1 + i\gamma_{nl})} + \\
& \left. + \frac{\mu_{l,n} \mu_{nm} \mu_{ml}}{(\Omega_{ml} + \omega_1 + \omega_2 + i\gamma_{ml})(\Omega_{nl} + \omega_2 + i\gamma_{nl})} \right), \quad (7.4.2)
\end{aligned}$$

and we have used the following values of the constants:

$$\mu = \begin{vmatrix} 1 & 3 \\ -1 & -2 \end{vmatrix}, \quad \Omega = \begin{vmatrix} 3 & 16 \\ 4 & 12 \end{vmatrix}, \quad \gamma = \begin{vmatrix} 1 & 2 \\ -1 & 3 \end{vmatrix}, \quad N = 5, \quad \varepsilon_0 = 1, \quad h = -1$$

Results are presented in the Figure 7.4.2. As for the previous calculations, we can see the model could be invalid because of the raised errors reach up to 100%.

8 Hermite-Hilbert transform

8.1 Overview of the HHT

Hermite-Hilbert transform approach is based on the precalculation of already-known Hermite polynomials and Hermite base of orthogonal functions. The algorithm is based on the master thesis of Mathias Johansson [18].

Hermite polynomials and Hermite functions:

Hermite polynomial of an arbitrary n degree is defined as follows:

$$H_n(x) = \frac{(-1)^n e^{(x^2)} d^n e^{(-x^2)}}{dt^n} \quad (8.1.1)$$

There is also an recursive equation for Hermite polynomials:

$$H_n(x) = 2x H_{n-1}(x) + 2(n-1) H_{n-2}(x) \quad (8.1.2a)$$

$$H_0(x) = 1 \quad (8.1.2b)$$

Using the Hermite polynomial we would like to derive a set of orthogonal polynomials in L^2 . Therefore we introduce the weight function and the norm function:

$$w(x) = e^{(-\frac{x^2}{2})} \quad (8.1.3a)$$

$$N_n(x) = \sqrt{2^n n! \sqrt{\pi}} \quad (8.1.3b)$$

If we multiply the n-th Hermite polynomial with the weight function $w(x)$ and divide it by the n-th norm function N_n we obtain a n-th orthogonal Hermite function:

$$\phi_n(x) = \frac{w(x) H_n(x)}{N_n(x)} = \frac{e^{(-\frac{x^2}{2})} H_n(x)}{\sqrt{2^n n! \sqrt{\pi}}} \quad (8.1.4)$$

Based on the recursive equation in 8.1.2 we also obtain:

$$\phi_n(x) = \sqrt{\frac{2x \phi_{n-1}(x)}{n}} - (n-1) \sqrt{\frac{\phi_{n-2}(x)}{(n-1)n}} \quad (8.1.5a)$$

$$\phi_0(x) = \frac{e^{(-\frac{x^2}{2})}}{\pi^{(\frac{1}{4})}} \quad (8.1.5b)$$

Hilbert transform of Hermite functions:

Johansson after polish mathematician Stefan L. Hahn [14] states that for any $f(x)$ and $\text{HILBERT}(f(x))$ belonging to L_1 we have:

$$\text{HILBERT}(x f(x)) = x \text{HILBERT}(F(x)) - \frac{1}{\pi} \int_{-\infty}^{\infty} f(\tau) d\tau \quad (8.1.6)$$

The proof of the Theorem stated in 8.1.6 is short:

$$\text{HILBERT}(x f(x)) = \frac{1}{\pi} \int_{-\infty}^{\infty} \frac{\tau f(\tau)}{x - \tau} d\tau = \frac{1}{\pi} \int_{-\infty}^{\infty} \frac{(x - s) f(x - s)}{s} ds, \quad (8.1.7)$$

$$\begin{aligned} \text{where } s &= x - \tau = \frac{1}{\pi} \int_{-\infty}^{\infty} \frac{x f(x - s)}{s} ds - \frac{1}{\pi} \int_{-\infty}^{\infty} f(x - s) ds = \\ &= x \text{HILBERT}(f(x)) - \frac{1}{\pi} \int_{-\infty}^{\infty} f(\tau) d\tau \end{aligned}$$

From both equations 8.1.6 and 8.1.5 we now obtain the important result:

$$\text{HILBERT}(\phi_n(x)) = \sqrt{\frac{2}{n}} \left(x \phi_{n-1}(x) - \frac{1}{\pi} \int_{-\infty}^{\infty} \phi_{n-1}(\eta) d\eta \right) - (n-1) \sqrt{\frac{1}{n(n-1)}} \phi_{n-2}(x) \quad (8.1.8a)$$

$$\text{HILBERT}(\phi_0(x)) = 2 \sqrt{2} \pi^{(\frac{1}{4})} \int_0^{\infty} e^{(-\frac{\omega^2}{2})} \sin(\omega x) d\omega \quad (8.1.8b)$$

Hilbert transform based on the Hermite functions:

Now we can derive the Hilbert transform of an arbitrary function. We start with expanding $f = f(x)$ into a series sum:

$$f(x) = \sum_{n=0}^{\infty} a_n \phi_n(x) \quad (8.1.9a)$$

$$a_n(x) = \int_{-\infty}^{\infty} f(x) \phi_n(x) dx \quad (8.1.9b)$$

For each function that has a limited series expansion at infinity we can provide an estimation used in further numerical algorithm:

$$f(x) \approx \sum_{n=0}^N a_n \phi_n(x) \quad (8.1.10a)$$

$$\text{HILBERT}(f(x)) \approx \sum_{n=0}^N a_n \text{HILBERT}(\phi_n(x)) \quad (8.1.10b)$$

Short description of the numerical algorithm:

Taking a look on the 8.1.10 we can see that the only difficulty is to calculate the a_n coefficients, while both the $\phi_n(x)$ and $\text{HILBERT}(\phi_n(x))$ can be precalculated once. The integral in 8.1.9 is now much easier because there is no singularity. The algorithm is given in Appendix A.5 and it consists of three main parts:

1. PRECALCULATION of the Hermite function coefficients with Maple Toolbox
- MAIN LOOP:
2. ESTIMATION OF a_n COEFFICIENTS
3. CALCULATION OF THE HILBERT TRANSFORM (8.1.10b)

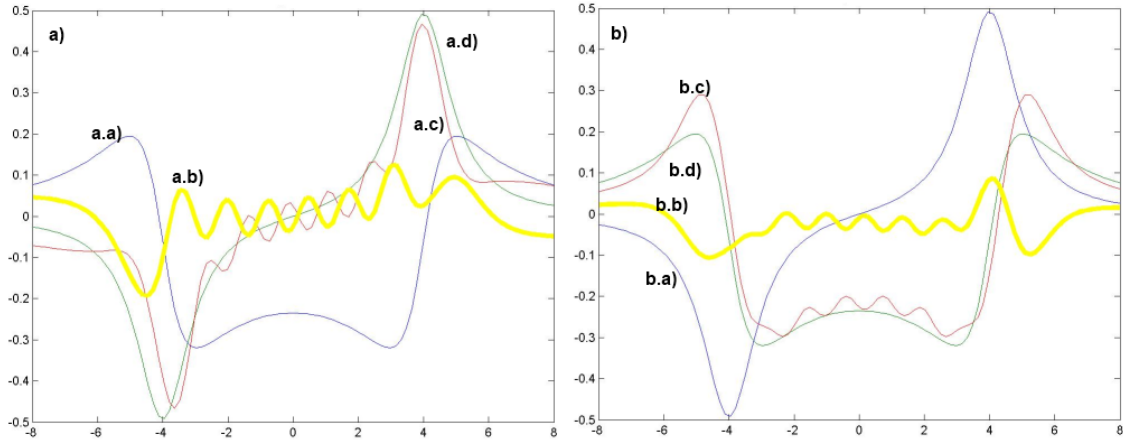


Figure 8.2.1: The Figure presents the results of the Hermite-Hilbert transform method applied to the simple linear model. Results are plotted together: a.a) The plot of the real part of $\chi(\omega)$ a.b) absolute error plot (c-plot minus d-plot) a.c) imaginary part of $\chi(\omega)$ obtained with the Hilbert transform of a-plot a.d) imaginary part of $\chi(\omega)$ calculated analytically. b.a) The plot of the imaginary part of $\chi(\omega)$ b.b) absolute error plot (c-plot minus d-plot) b.c) real part of $\chi(\omega)$ obtained with the Hilbert transform of a-plot b.d) real part of $\chi(\omega)$ calculated analytically.

8.2 HHT for simple linear model

In the Figure 8.2.1 we have presented the results obtained with the Hermite-Hilbert transform for the simple linear model defined in model 3.3.3. As we can see - the Hermite-Hilbert transform comes with poor accuracy, but we would like to put this method into examination with defined models.

8.3 HHT for simple nonlinear model

For the pump-probe and frequency mixing models we have used the same parameters as in chapter 5.3. The results obtained with the Hermite-Hilbert transform has been presented in Figures 8.3.1 and 8.3.2 respectively.

In these results we can draw two conclusions. The method based on the periodical polynomials as Hilbert polynomials will give us “zig-zag” like results. The other conclusion is that results obtained seems to be close, but much worst that those obtained with HCCI or FHT.

8.4 HHT for simple quantum-perturbative model

Linear model - results:

As in the Chapter 5.3, we have used the same model to describe the simple linear quantum-perturbative model:

$$\chi_{1,qp}(\omega) = \frac{N}{\varepsilon_0 h} \sum_{n=1}^2 \left(\frac{\mu_{1,n} \mu_{2,n}}{\Omega_n - \omega - i \gamma_n} + \frac{\mu_{2,n} \mu_{1,n}}{\Omega_n + \omega + i \gamma_n} \right) \quad (8.4.1)$$

This time we used the following parameters:

$$\mu = [[3, -0.5], [1.2, 2.4]], \Omega = [-3, 13], \gamma = [0.7, 2.3], N = 8, \varepsilon_0 = 1.4, h = -2.7$$

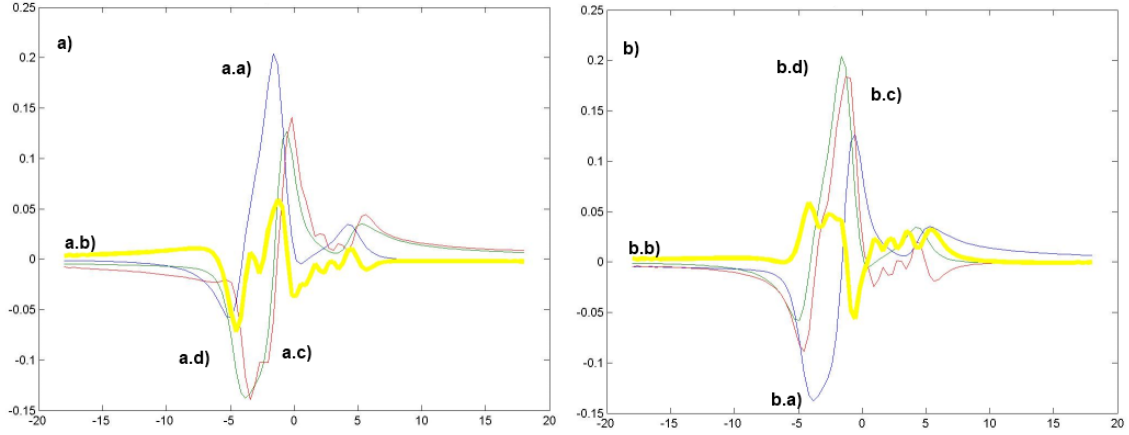


Figure 8.3.1: The Figure presents the results of the Hermite-Hilbert transform method applied to the pump-and-probe model. Results are plotted together: a.a) The plot of the real part of $\chi_{pp}(\omega)$ a.b) absolute error plot (a.d-plot minus a.c-plot) a.c) imaginary part of $\chi_{pp}(\omega)$ obtained with the Hermite-Hilbert transform of a.a-plot, a.d) imaginary part of $\chi_{pp}(\omega)$ calculated analytically b.a) The plot of the imaginary part of $\chi_{pp}(\omega)$ b.b) absolute error plot (b.d-plot minus b.c-plot) b.c) real part of $\chi_{pp}(\omega)$ obtained with the Hermite-Hilbert transform of b.a-plot b.d) real part of $\chi_{pp}(\omega)$ calculated analytically

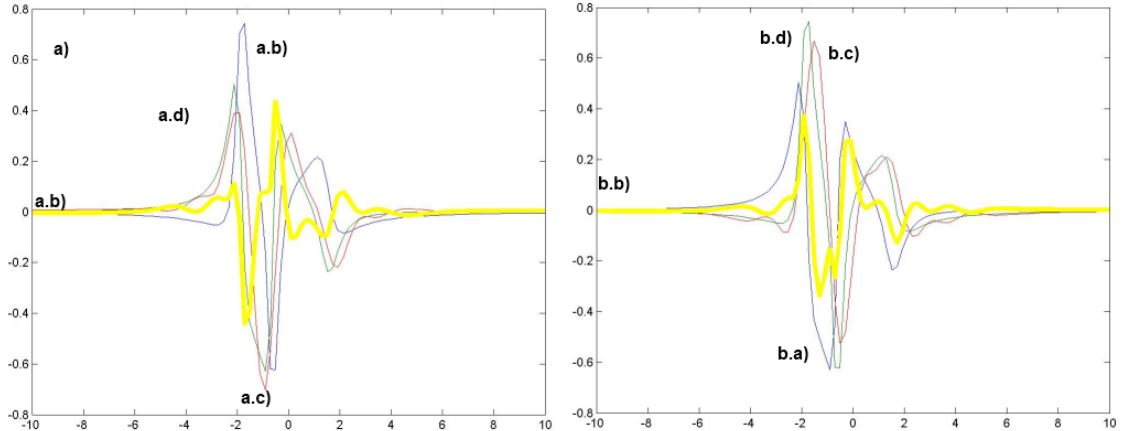


Figure 8.3.2: The Figure presents the results of the Hermite-Hilbert transform method applied to the frequency mixing model. Results are plotted together: a.a) The plot of the real part of $\chi_{mix}(\omega)$ a.b) absolute error plot (a.d-plot minus a.c-plot) a.c) imaginary part of $\chi_{mix}(\omega)$ obtained with the Hermite-Hilbert transform of a.a-plot, a.d) imaginary part of $\chi_{mix}(\omega)$ calculated analytically b.a) The plot of the imaginary part of $\chi_{mix}(\omega)$ b.b) absolute error plot (b.d-plot minus b.c-plot) b.c) real part of $\chi_{mix}(\omega)$ obtained with the Hermite-Hilbert transform of b.a-plot b.d) real part of $\chi_{mix}(\omega)$ calculated analytically

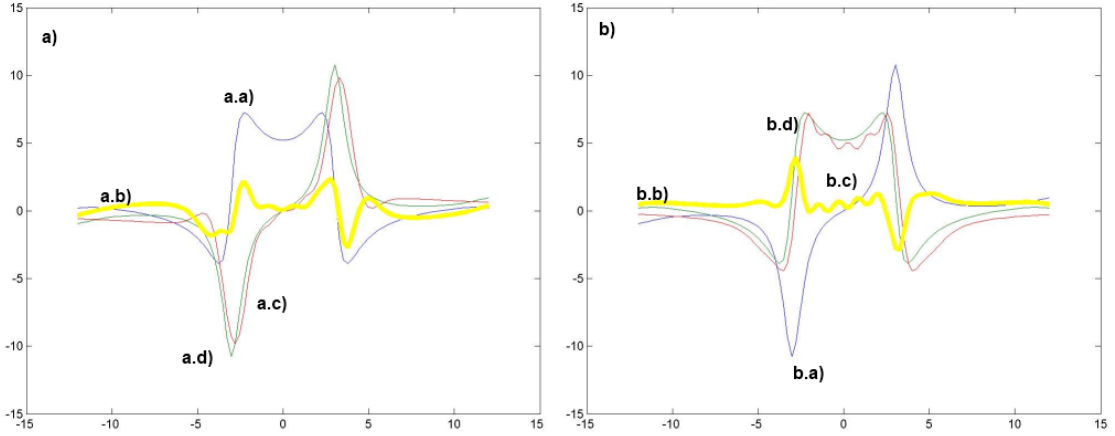


Figure 8.4.1: Results for the linear quantum perturbative model for Hermite-Hilbert transform a.a) The plot of the imaginary part of $\chi_{1,qp}(\omega)$ a.b) absolute error plot (d-plot minus c-plot) a.c) real part of $\chi_{1,qp}(\omega)$ obtained with the Hermite-Hilbert transform of a-plot a.d) real part of $\chi_{1,qp}(\omega)$ calculated analytically b.b) The plot of the real part of $\chi_{1,qp}(\omega)$ b.b) absolute error plot (d-plot minus c-plot) b.c) imaginary part of $\chi_{1,qp}(\omega)$ obtained with the Hermite-Hilbert transform of a-plot b.d) imaginary part of $\chi_{1,qp}(\omega)$ calculated analytically

Results are presented in the Figure 8.4.1.

Second-order model - results:

We have also used the same model as in 5.3 to describe the second-order susceptibility model:

$$\begin{aligned} \chi_{2,qp}(\omega_1, \omega_2) = & 2 N \varepsilon_0 h^2 \sum_{n=1}^2 \sum_{m=1}^2 \sum_{l=1}^2 \left(\frac{\mu_{l,n} \mu_{nm} \mu_{ml}}{(\Omega_{nl} - \omega_1 - \omega_2 - i \gamma_{nl})(\Omega_{ml} - \omega_1 - i \gamma_{ml})} + \right. \\ & + \frac{\mu_{l,n} \mu_{nm} \mu_{ml}}{(\Omega_{nl} - \omega_1 - \omega_1 - i \gamma_{nl})(\Omega_{ml} - \omega_2 - i \gamma_{ml})} + \\ & + \frac{\mu_{l,n} \mu_{nm} \mu_{ml}}{(\Omega_{mn} - \omega_1 - \omega_2 - i \gamma_{mn})(\Omega_{nl} + \omega_2 + i \gamma_{nl})} + \\ & + \frac{\mu_{l,n} \mu_{nm} \mu_{ml}}{(\Omega_{mn} - \omega_1 - \omega_2 - i \gamma_{mn})(\Omega_{nl} + \omega_2 + i \gamma_{nl})} + \\ & + \frac{\mu_{l,n} \mu_{nm} \mu_{ml}}{(\Omega_{nm} + \omega_1 + \omega_2 + i \gamma_{nm})(\Omega_{ml} - \omega_1 - i \gamma_{ml})} + \\ & + \frac{\mu_{l,n} \mu_{nm} \mu_{ml}}{(\Omega_{nm} + \omega_1 + \omega_2 + i \gamma_{nm})(\Omega_{ml} - \omega_1 - i \gamma_{ml})} + \\ & + \frac{\mu_{l,n} \mu_{nm} \mu_{ml}}{(\Omega_{ml} + \omega_1 + \omega_2 + i \gamma_{ml})(\Omega_{nl} + \omega_1 + i \gamma_{nl})} + \\ & \left. + \frac{\mu_{l,n} \mu_{nm} \mu_{ml}}{(\Omega_{ml} + \omega_1 + \omega_2 + i \gamma_{ml})(\Omega_{nl} + \omega_2 + i \gamma_{nl})} \right), \quad (8.4.2) \end{aligned}$$

and we will be using the following constants values:

$$\mu = \begin{vmatrix} 1 & 3 \\ -1 & -2 \end{vmatrix}, \Omega = \begin{vmatrix} 3 & 16 \\ 4 & 12 \end{vmatrix}, \gamma = \begin{vmatrix} 1 & 2 \\ -1 & 3 \end{vmatrix}, N = 5, \varepsilon_0 = 1, h = -1$$

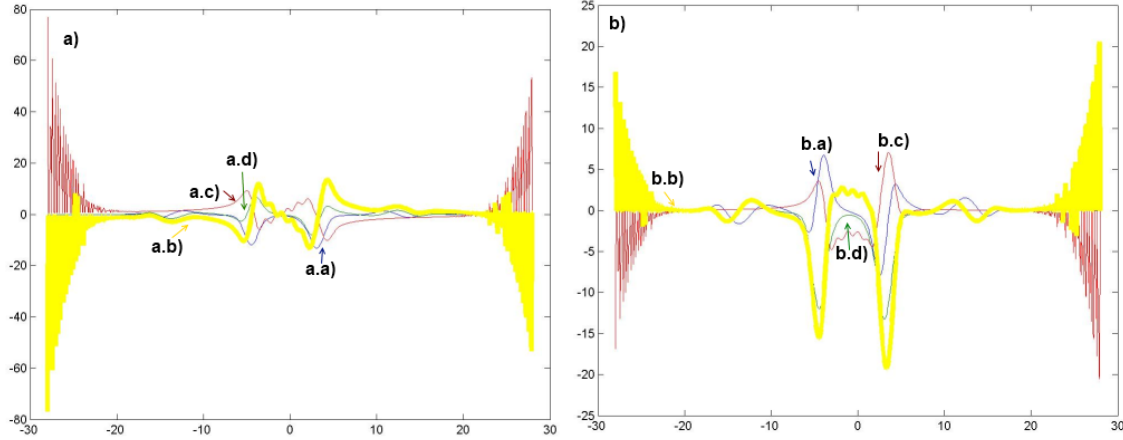


Figure 8.4.2: Results for the second-order quantum perturbative model for Hermite-Hilbert transform transform a.a) The plot of the real part of $\chi_{2,qp}(\omega)$ a.b) absolute error plot (a.d-plot minus a.c-plot) a.c) imaginary part of $\chi_{2,qp}(\omega)$ obtained with the Hermite-Hilbert transform of a.a-plot, a.d) imaginary part of $\chi_{2,qp}(\omega)$ calculated analytically b.a) The plot of the imaginary part of $\chi_{2,qp}(\omega)$ b.b) absolute error plot (b.d-plot minus b.c-plot) b.c) real part of $\chi_{2,qp}(\omega)$ obtained with the Hermite-Hilbert transform of b.a-plot b.d) real part of $\chi_{2,qp}(\omega)$ calculated analytically

Results are presented in the Figure 8.4.2. As for the previous calculations, we can see the model could be invalid because the occurring errors reach up to 100%.

We have checked the HHT method for various parameters, but none of them has gave us better accuracy. We encourage the reader to carry out their own calculations with source code given in Appendix A.5.

9 Fourier-series

9.1 Overview of the Fourier-series based method

The concept of the Hilbert transform evaluation based on the Fourier series also comes from the master thesis by Mathias Johansson [18]. There is an important drawback in this approach - in general it should be applied to the periodical functions, but we will further assume they have a relatively long period.

Fourier series:

Each periodical function can be decomposed into a infinite Fourier series. For a given periodic function f with a given period $2*P$, we will introduce the Fourier coefficients:

$$a_{f,n} = \int_{-P}^P f(x) \cos(n x) dx \quad (9.1.1a)$$

$$b_{f,n} = \int_{-P}^P f(x) \sin(n x) dx \quad (9.1.1b)$$

Not getting deeply into harmonic analysis - we will assume that a series of partial sums:

$$S_{f,N}(x) = \frac{a_{f,0}}{2} + \left(\sum_{n=1}^N (a_{f,n} \cos(n x) + b_{f,n} \sin(n x)) \right) \quad (9.1.2)$$

for a function $f \in L_2(-P, P)$ converges at almost every point to the f , which can be written as:

$$\text{if } S = \{t : \lim_{N \rightarrow \infty} S_{f,N}(t) \neq f(t)\} \text{ then } |S| \leq N_0 \quad (9.1.3)$$

Hilbert transform based on the Fourier series:

After Johansson [18] we state that for any given function f in $L_2(-P, P)$ we can calculate the Hilbert transform using the form of Fourier series for this function. All we need to do, is to make a swap in the 9.1.2 equation - the a_n coefficients should be swapped with b_n coefficients.

$$\begin{aligned} HILBERT(f(x)) &= \lim_{N \rightarrow \infty} \frac{a_{f,0}}{2} + \\ &+ \left(\sum_{n=1}^N (b_{f,n} \cos(n x) + a_{f,n} \sin(n x)) \right) \text{ [at alm. every point x]} \end{aligned} \quad (9.1.4)$$

Algorithm overview:

As mentioned before, we will prepare the algorithm as for the periodic function, but we will try to imply that the period is much longer than the area of interest. We would like to calculate the Hilbert transform for periodical and non-periodical function f . The first step is to calculate the properties of the input X interval, which is the region in which we are interested of both input function f values and the values of its Hilbert transform. The second step is to calculate the Fourier coefficients in a main loop. In the same loop we calculate the next partial sum values. The last step is to extract the inner interval from the extended interval, to omit the numerical errors near the interval edges.

The full source code of this algorithm, has been presented in the appendix A.6.

9.2 Fourier-series for simple linear model

In the Figure 9.2.1 we have presented the results obtained with the Fourier-Hilbert transform for the simple linear model defined in model 3.3.3. As we can see - the Fourier-Hilbert transform comes with poor accuracy, but we would like to put this method into examination with defined models.

9.3 Fourier-series for simple nonlinear model

For the pump-probe and frequency mixing models we have used the same parameters as in chapter 5.3. The results obtained with the Fourier-Hilbert transform has been presented in Figures 9.3.1 and 9.3.2 respectively.

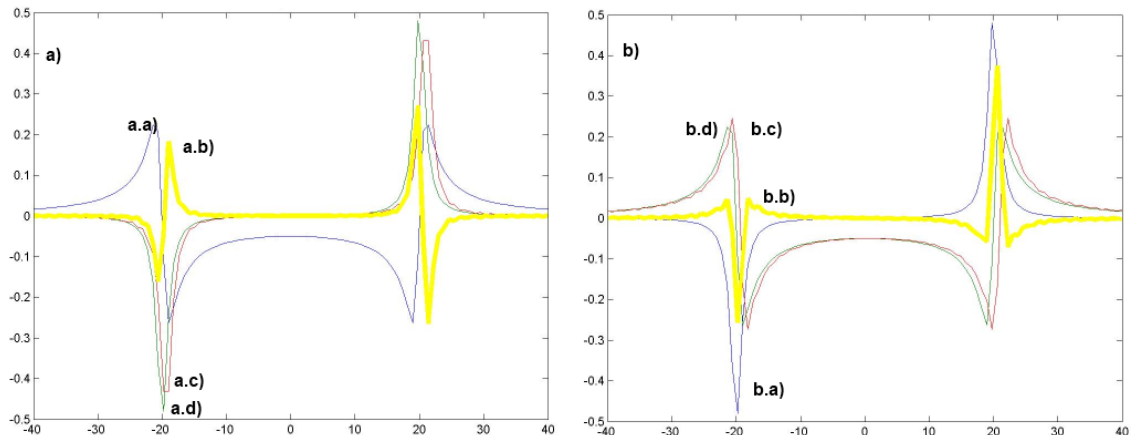


Figure 9.2.1: The Figure presents the results of the Hilbert transform based on the Fourier series method applied to the simple linear model. Results are plotted together: a.a) The plot of the real part of $\chi(\omega)$ a.b) absolute error plot (c-plot minus d-plot) a.c) imaginary part of $\chi(\omega)$ obtained with the Fourier-Hilbert transform of a-plot a.d) imaginary part of $\chi(\omega)$ calculated analytically. b.a) The plot of the imaginary part of $\chi(\omega)$ b.b) absolute error plot (c-plot minus d-plot) b.c) real part of $\chi(\omega)$ obtained with the Fourier-Hilbert transform of a-plot b.d) real part of $\chi(\omega)$ calculated analytically.

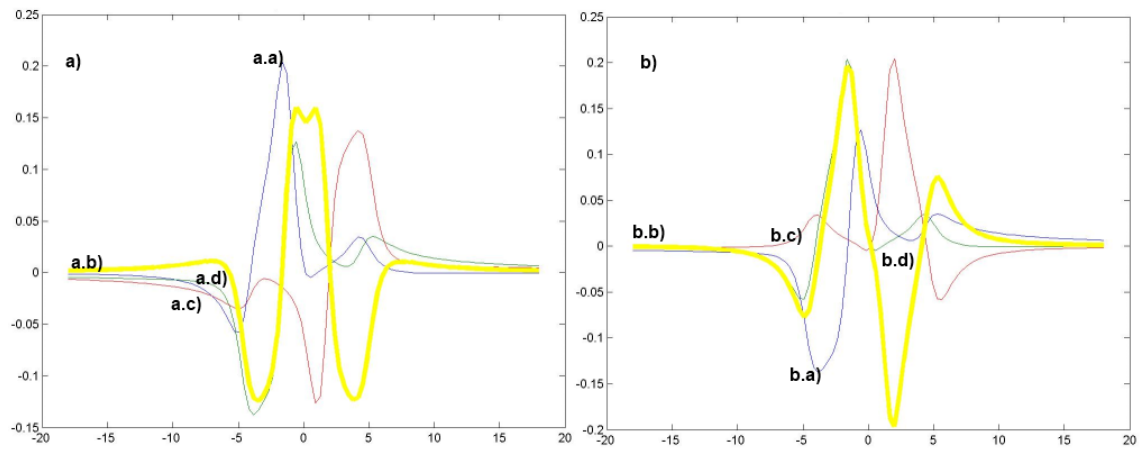


Figure 9.3.1: The Figure presents the results of the Hilbert transform based on the Fourier series method applied to the pump-and-probe model. Results are plotted together: a.a) The plot of the real part of $\chi_{pp}(\delta)$ a.b) absolute error plot (a.d-plot minus a.c-plot) a.c) imaginary part of $\chi_{pp}(\delta)$ obtained with the Fourier-Hilbert transform of a.a-plot, a.d) imaginary part of $\chi_{pp}(\delta)$ calculated analytically b.a) The plot of the imaginary part of $\chi_{pp}(\delta)$ b.b) absolute error plot (b.d-plot minus b.c-plot) b.c) real part of $\chi_{pp}(\delta)$ obtained with the Fourier-Hilbert transform of b.a-plot b.d) real part of $\chi_{pp}(\omega)$ calculated analytically

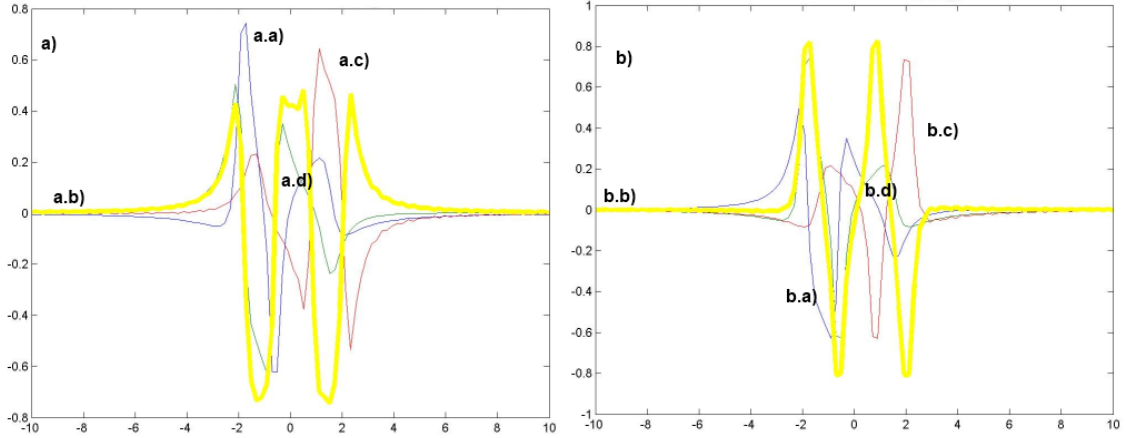


Figure 9.3.2: The Figure presents the results of the Hilbert transform based on the Fourier series method applied to the frequency mixing model. Results are plotted together: a.a) The plot of the real part of $\chi_{mix}(\omega)$ a.b) absolute error plot (a.d-plot minus a.c-plot) a.c) imaginary part of $\chi_{mix}(\omega)$ obtained with the Fourier-Hilbert transform of a.a-plot, a.d) imaginary part of $\chi_{mix}(\omega)$ calculated analytically b.a) The plot of the imaginary part of $\chi_{mix}(\omega)$ b.b) absolute error plot (b.d-plot minus b.c-plot) b.c) real part of $\chi_{mix}(\omega)$ obtained with the Fourier-Hilbert transform of b.a-plot b.d) real part of $\chi_{mix}(\omega)$ calculated analytically

In these results we can draw two conclusions. The method based on the periodical polynomials as Fourier series will give us “zig-zag” like results. The other conclusion is that results obtained seems to be close, but much worst than those obtained with HCCI or FHT.

9.4 Fourier-series for simple quantum-perturbative model

Linear model - results:

As in the Chapter 5.3, we have used the same model to describe the simple linear quantum-perturbative model:

$$\chi_{1,qp}(\omega) = \frac{N}{\varepsilon_0 h} \sum_{n=1}^2 \left(\frac{\mu_{1,n} \mu_{2,n}}{\Omega_n - \omega - i \gamma_n} + \frac{\mu_{2,n} \mu_{1,n}}{\Omega_n + \omega + i \gamma_n} \right) \quad (9.4.1)$$

This time we used the following parameters:

$$\mu = [[3, -0.5], [1.2, 2.4]], \Omega = [-3, 13], \gamma = [0.7, 2.3], N = 8, \varepsilon_0 = 1.4, h = -2.7.$$

Results are presented in the Figure 9.4.1.

Second-order model - results:

We have also used the same model as in 5.3 to describe the second-order susceptibility model:

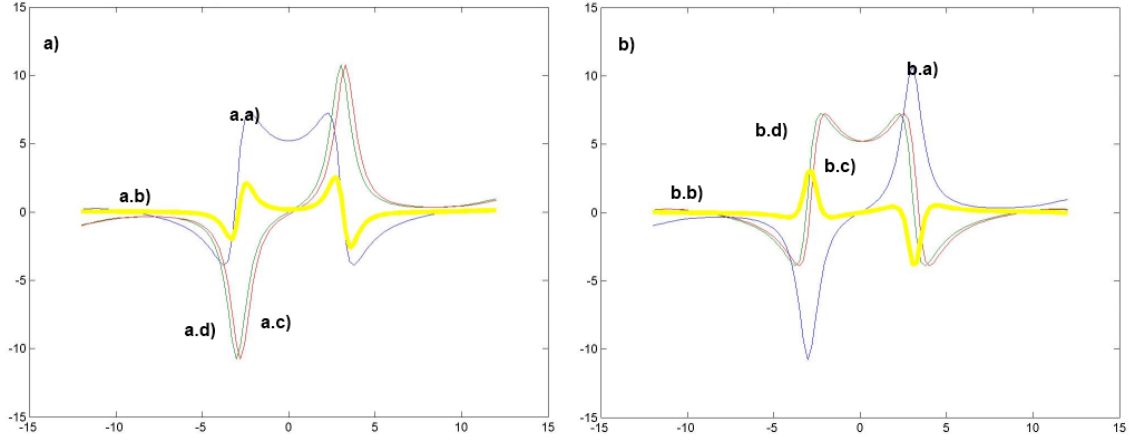


Figure 9.4.1: Results for the linear quantum perturbative model for Fourier-Hilbert transform a.a) The plot of the imaginary part of $\chi_{1,qp}(\omega)$ a.b) absolute error plot (d-plot minus c-plot) a.c) real part of $\chi_{1,qp}(\omega)$ obtained with the Fourier-Hilbert transform of a-plot a.d) real part of $\chi_{1,qp}(\omega)$ calculated analytically b.b) The plot of the real part of $\chi_{1,qp}(\omega)$ b.b) absolute error plot (d-plot minus c-plot) b.c) imaginary part of $\chi_{1,qp}(\omega)$ obtained with the Fourier-Hilbert transform of a-plot b.d) imaginary part of $\chi_{1,qp}(\omega)$ calculated analytically

$$\begin{aligned} \chi_{2,qp}(\omega_1, \omega_2) = & 2N\varepsilon_0 h^2 \sum_{n=1}^2 \sum_{m=1}^2 \sum_{l=1}^2 \left(\frac{\mu_{l,n} \mu_{nm} \mu_{ml}}{(\Omega_{nl} - \omega_1 - \omega_2 - i\gamma_{nl})(\Omega_{ml} - \omega_1 - i\gamma_{ml})} + \right. \\ & + \frac{\mu_{l,n} \mu_{nm} \mu_{ml}}{(\Omega_{nl} - \omega_1 - \omega_1 - i\gamma_{nl})(\Omega_{ml} - \omega_2 - i\gamma_{ml})} + \\ & + \frac{\mu_{l,n} \mu_{nm} \mu_{ml}}{(\Omega_{mn} - \omega_1 - \omega_2 - i\gamma_{mn})(\Omega_{nl} + \omega_2 + i\gamma_{nl})} + \\ & + \frac{\mu_{l,n} \mu_{nm} \mu_{ml}}{(\Omega_{mn} - \omega_1 - \omega_2 - i\gamma_{mn})(\Omega_{nl} + \omega_2 + i\gamma_{nl})} + \\ & + \frac{\mu_{l,n} \mu_{nm} \mu_{ml}}{(\Omega_{nm} + \omega_1 + \omega_2 + i\gamma_{nm})(\Omega_{ml} - \omega_1 - i\gamma_{ml})} + \\ & + \frac{\mu_{l,n} \mu_{nm} \mu_{ml}}{(\Omega_{nm} + \omega_1 + \omega_2 + i\gamma_{nm})(\Omega_{ml} - \omega_1 - i\gamma_{ml})} + \\ & + \frac{\mu_{l,n} \mu_{nm} \mu_{ml}}{(\Omega_{ml} + \omega_1 + \omega_2 + i\gamma_{ml})(\Omega_{nl} + \omega_1 + i\gamma_{nl})} + \\ & \left. + \frac{\mu_{l,n} \mu_{nm} \mu_{ml}}{(\Omega_{ml} + \omega_1 + \omega_2 + i\gamma_{ml})(\Omega_{nl} + \omega_2 + i\gamma_{nl})} \right), \quad (9.4.2) \end{aligned}$$

and we will be using the following constants values: $\mu = \begin{vmatrix} 1 & 3 \\ -1 & -2 \end{vmatrix}$, $\Omega = \begin{vmatrix} 3 & 16 \\ 4 & 12 \end{vmatrix}$, $\gamma = \begin{vmatrix} 1 & 2 \\ -1 & 3 \end{vmatrix}$, $N = 5$, $\varepsilon_0 = 1$, $h = -1$.

Results are presented in the Figure 9.4.2. We can see, that the first model could be valid, while the second model seems to be invalid for consecutively for all Hilbert transform implementations.

We have checked the Fourier-Hilbert method for various parameters, but none of them has gave us better accuracy. We encourage the reader to carry out their own calculations

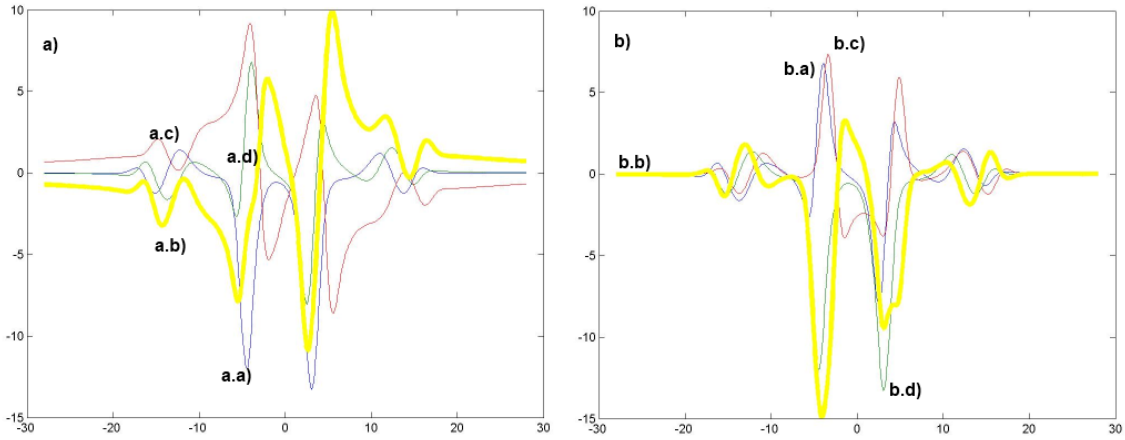


Figure 9.4.2: Results for the second-order quantum perturbative model for Fourier-Hilbert transform transform a.a) The plot of the real part of $\chi_{2,qp}(\omega)$ a.b) absolute error plot (a.d-plot minus a.c-plot) a.c) imaginary part of $\chi_{2,qp}(\omega)$ obtained with the Fourier-Hilbert transform of a.a-plot, a.d) imaginary part of $\chi_{2,qp}(\omega)$ calculated analytically b.a) The plot of the imaginary part of $\chi_{2,qp}(\omega)$ b.b) absolute error plot (b.d-plot minus b.c-plot) b.c) real part of $\chi_{2,qp}(\omega)$ obtained with the Fourier-Hilbert transform of b.a-plot b.d) real part of $\chi_{2,qp}(\omega)$ calculated analytically

with source code given in Appendix A.6.

10 MATLAB ® out-of-the-box functions

10.1 Overview of the MATLAB ® interior functions

Why not take into consideration the already built-in numerical methods from MATLAB?

We compare the results obtained with:

- quadgk() - adaptive Gauss-Kronrod quadrature;
- hilbert() - fast Hilbert transform based on both FFT and IFFT.

Adaptive Gauss-Kronrod quadrature - theory:

The source code of the adaptive Gauss-Kronrod quadrature has been published in the popular Fortran 77 numerical integration QUADPACK library and has been also translated into the MATLAB core language. It is also based on the "quadva" routine described by Lawrence F. Shampine in [36]. The fundamental idea of this numerical integration algorithm is the nested quadrature rule - the more accurate quadrature approximation is calculated from the less accurate one. The algorithm is adaptive and the error estimation is based on the (G-K7,15) pair of the quadrature rules - less and more accurate - the 7-point Gauss rule and the 15-point Kronrod rule with a share nodes. For more information about the theory beneath this algorithm - please read D. Calvetti et al [7] or the chapter 5.5 from the book by David Kahaner [19].

Adaptive Gauss-Kronrod quadrature - short tutorial:

We have used the MATLAB ®R2009b. It comes with built-in quadgk function with four parameters:

'AbsTol'	- absolute error tolerance
'RelTol'	- relative error tolerance
'Waypoints'	- vector of integration waypoints
'MaxIntervalCount'	- maximum number of intervals allowed (default: 650)

The defined models used within the Hilbert transform comes with one, but strong singularity. While the quadgk() method comes with copes with infinities, we have suggested to split the integral into two parts, but not including the small area nearby singularity.

If the models singularity c is taken from the range $[a, b]$, we will divide the range $|b - a|$ by 10000 and calculate the value as defined in equation 10.1.1.

$$\int_{-\infty}^{\infty} \frac{f(x)}{x - c} dx \approx \text{quadgk}\left(\frac{f(x)}{x - c}, -\infty, c - \frac{|b - a|}{10000}, \text{'RelTol'}, 0.001, \text{'AbsTol'}, 0.001\right) \quad (10.1.1)$$

$$+ \text{quadgk}\left(\frac{f(x)}{x - c}, c + \frac{|b - a|}{10000}, +\infty, \text{'RelTol'}, 0.001, \text{'AbsTol'}, 0.001\right)$$

Fast Hilbert transform routine - theory:

The discrete Hilbert transform (DHT) is given by definition after [20] - for a given n-length X vector:

$$\text{DHT}(X_k) = \frac{1}{n} \left(\sum_{s=0}^{n-1} X_s (1 - (-1)^{(k-s)}) \cot\left(\frac{\pi(k-s)}{n}\right) \right) \quad (10.1.2)$$

The other definition by [7] uses the convolution:

$$\text{DHT}(X_k) = X[] * h[] = \sum_{s=0}^{n-1} h_{k-s} X_s \quad (10.1.3a)$$

$$h_k = \frac{1}{n} \left(\cot\left(\frac{\pi k}{n}\right) - \frac{\cos(\pi k)}{\sin(\frac{\pi k}{n})} \right) \quad (10.1.3b)$$

The important issue is that the DHT is closely related to the discrete Fourier transform (DFT). For a given n-length X vector in order to evaluate the DHT(X) we can hire the DFT routine. To start, we must remember that in the continuous case:

$$\text{FOURIER}(\text{HILBERT}(X_k)) = (-i \operatorname{sgn}(\frac{n}{2} - k) \operatorname{sgn}(k)) \text{FOURIER}(X_k), \quad (10.1.4)$$

where we remember that:

$$-i \operatorname{sgn}(\frac{n}{2} - k) \operatorname{sgn}(k) = \text{FOURIER}(\frac{1}{\pi k}). \quad (10.1.5)$$

Therefore, in the discrete case we find the similar equation to 10.1.4 relating the DHT and DFT:

$$\text{DFT}(\text{DHT}(X_k)) = (-i) \operatorname{sgn}(\frac{n}{2} - k) \operatorname{sgn}(k) \text{DFT}(X_k) \quad (10.1.6)$$

From the 10.1.6 we can see, that it is quite easy to operate within the Fourier/frequency domain - because the quite complicate convolution is transformed to a simple

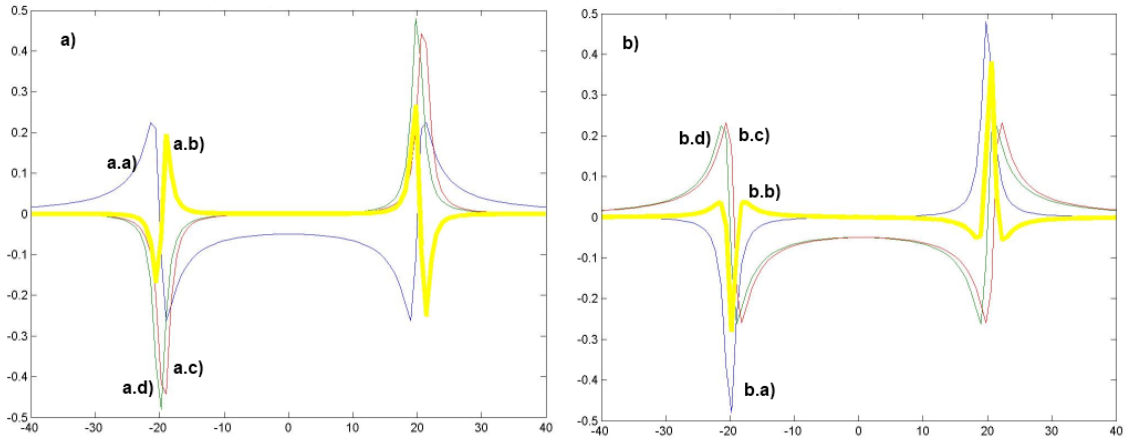


Figure 10.2.1: The Figure presents the results of the `quadgk()` method applied to the simple linear model. Results are plotted together: a.a) The plot of the real part of $\chi(\omega)$ a.b) absolute error plot (c-plot minus d-plot) a.c) imaginary part of $\chi(\omega)$ obtained with the `quadgk()`-Hilbert transform of a-plot a.d) imaginary part of $\chi(\omega)$ calculated analytically. b.a) The plot of the imaginary part of $\chi(\omega)$ b.b) absolute error plot (c-plot minus d-plot) b.c) real part of $\chi(\omega)$ obtained with the `quadgk()`-Hilbert transform of a-plot b.d) real part of $\chi(\omega)$ calculated analytically.

algebraic operations. Also - if we have the quick algorithm to perform both the DFT and inverse-DFT - for example with the fast Fourier transform (FFT) and the inverse fast Fourier transform (IFFT) - the DHT operation will be calculated as follows:

$$\text{DHT}(X_k) = \text{IDFT}\left((-i) \operatorname{sgn}\left(\frac{n}{2} - k\right) \operatorname{sgn}(k) \text{DFT}(X_k)\right) \quad (10.1.7)$$

Fast Hilbert transform routine - short tutorial:

While the hired DFT and IDFT routines are evaluated in complex domain, for a given input n-length X vector we have that:

$$\text{hilbert}(X) \Rightarrow X + i \text{DHT}(X) \quad (10.1.8)$$

In order to obtain the final result we need to take the imaginary part of the MATLAB `hilbert()` function output. The other important issue is that the *MATLAB®* `hilbert()` function has one optional parameter called N - to computer the N-point Hilbert transform. If the input vector X is too short, it will be padded with zeros, otherwise it will be truncated.

10.2 MIF for simple linear model

In two Figures 10.2.1 and 10.2.2 we have gathered the results obtained with the MATLAB `quadgk()` and `hilbert()` functions based Hilbert transforms for the simple linear model defined in model (3.3.3). For each method we can see a acceptable accuracy.

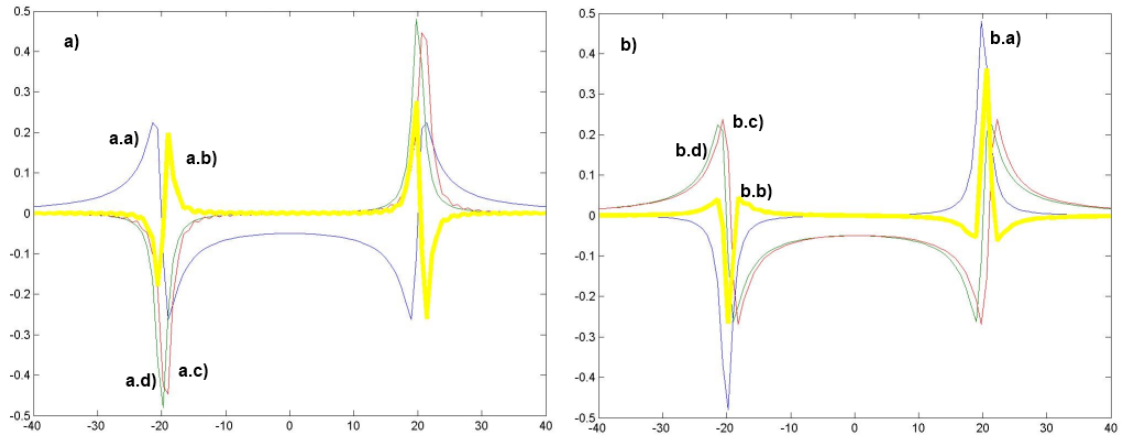


Figure 10.2.2: The Figure presents the results of the `hilbert()` method applied to the simple linear model. Results are plotted together: a.a) The plot of the real part of $\chi(\omega)$ a.b) absolute error plot (c-plot minus d-plot) a.c) imaginary part of $\chi(\omega)$ obtained with the `hilbert()` transform of a-plot a.d) imaginary part of $\chi(\omega)$ calculated analytically. b.a) The plot of the imaginary part of $\chi(\omega)$ b.b) absolute error plot (c-plot minus d-plot) b.c) real part of $\chi(\omega)$ obtained with the `hilbert()` transform of a-plot b.d) real part of $\chi(\omega)$ calculated analytically.

10.3 MIF for simple nonlinear model

In the next four Figures: 10.3.1, 10.3.2, 10.3.3 and 10.3.4 we have gathered the results obtained with the MATLAB® `quadgk()` and `hilbert()` functions based Hilbert transforms for the pump-probe and frequency mixing models with the same parameters as in chapter 5.3.

For each method we can once again see the acceptable accuracy for each method, but we can also observe, that each method comes with noticeable error.

10.4 MIF for simple quantum-perturbative model

We have also put the determined methods onto test with quantum-perturbative models taken from chapter 5.3.

Linear model - results:

In the Figures: 10.4.1 and 10.4.2 we have gathered the results obtained with the MATLAB `quadgk()` and `hilbert()` functions based Hilbert transforms for the linear quantum-perturbative model taken with the same parameters as in chapter 5.3.

We observe quite acceptable results for the investigated model, for both methods applied.

Second-order model - results:

In the Figures: 10.4.3 and 10.4.4 we have gathered the results obtained with the MATLAB `quadgk()` and `hilbert()` functions based Hilbert transforms for the second-order quantum-perturbative model taken with the same parameters as in chapter 5.3.

We observe a huge error as in all previously chapters for the investigated model, for both methods applied.

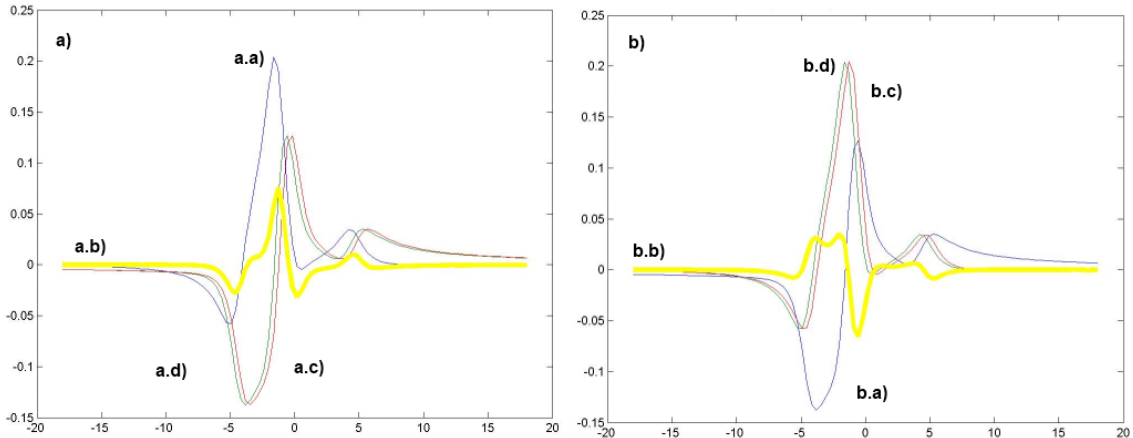


Figure 10.3.1: Results for the pump-probe model using the `quadgk()` Hilbert transform. a.a) The plot of the real part of $\chi_{pp}(\omega)$ a.b) absolute error plot ($a.d$ -plot minus $a.c$ -plot) a.c) imaginary part of $\chi_{pp}(\omega)$ obtained with the `quadgk()` Hilbert transform of $a.a$ -plot, a.d) imaginary part of $\chi_{pp}(\omega)$ calculated analytically b.a) The plot of the imaginary part of $\chi_{pp}(\omega)$ b.b) absolute error plot ($b.d$ -plot minus $b.c$ -plot) b.c) real part of $\chi_{pp}(\omega)$ obtained with the `quadgk()` Hilbert transform of $b.a$ -plot b.d) real part of $\chi_{pp}(\omega)$ calculated analytically

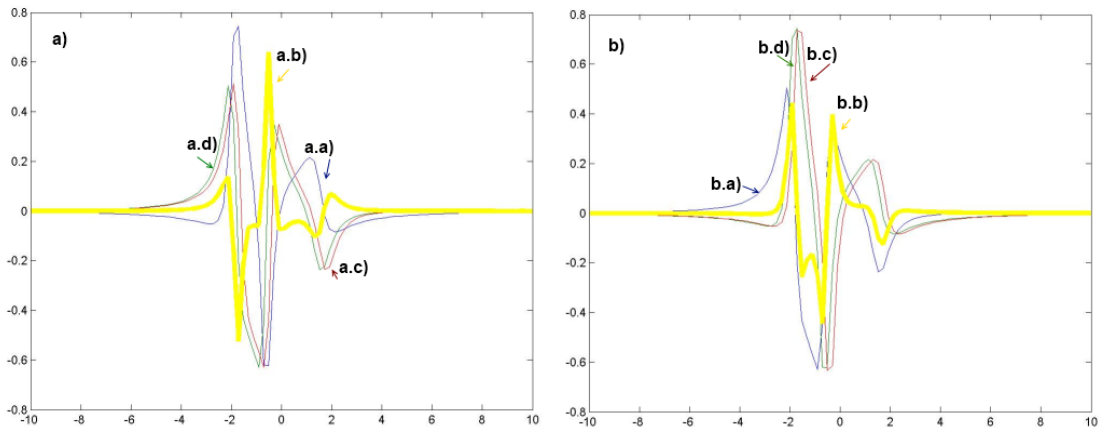


Figure 10.3.2: Results for the frequency model using the `quadgk()` Hilbert transform. a.a) The plot of the real part of $\chi_{pp}(\omega)$ a.b) absolute error plot ($a.d$ -plot minus $a.c$ -plot) a.c) imaginary part of $\chi_{pp}(\omega)$ obtained with the `quadgk()` Hilbert transform of $a.a$ -plot, a.d) imaginary part of $\chi_{pp}(\omega)$ calculated analytically b.a) The plot of the imaginary part of $\chi_{pp}(\omega)$ b.b) absolute error plot ($b.d$ -plot minus $b.c$ -plot) b.c) real part of $\chi_{pp}(\omega)$ obtained with the `quadgk()` Hilbert transform of $b.a$ -plot b.d) real part of $\chi_{pp}(\omega)$ calculated analytically

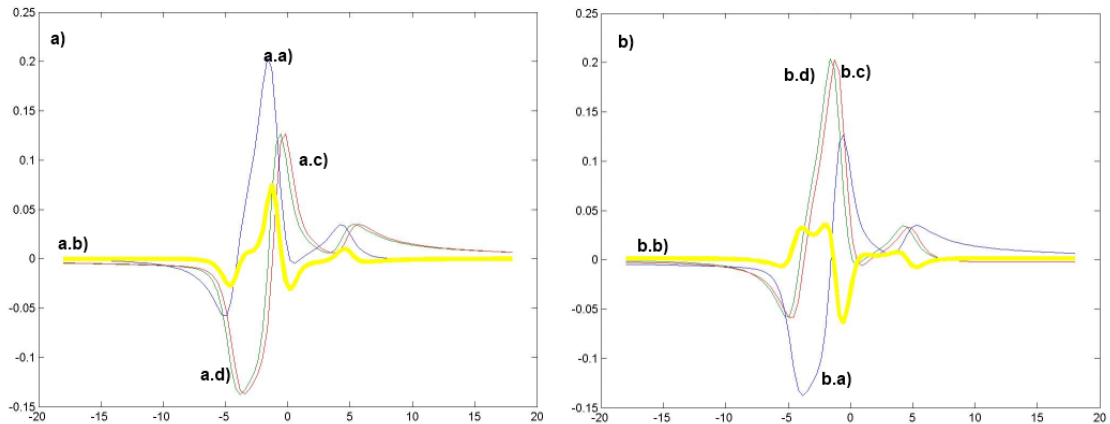


Figure 10.3.3: Results for the pump-probe model using the `hilbert()` transform a.a) The plot of the real part of $\chi_{mix}(\omega)$ a.b) absolute error plot (a.d-plot minus a.c-plot) a.c) imaginary part of $\chi_{mix}(\omega)$ obtained with the `hilbert()` transform of a.a-plot, a.d) imaginary part of $\chi_{mix}(\omega)$ calculated analytically b.a) The plot of the imaginary part of $\chi_{mix}(\omega)$ b.b) absolute error plot (b.d-plot minus b.c-plot) b.c) real part of $\chi_{mix}(\omega)$ obtained with the `hilbert()` transform of b.a-plot b.d) real part of $\chi_{mix}(\omega)$ calculated analytically

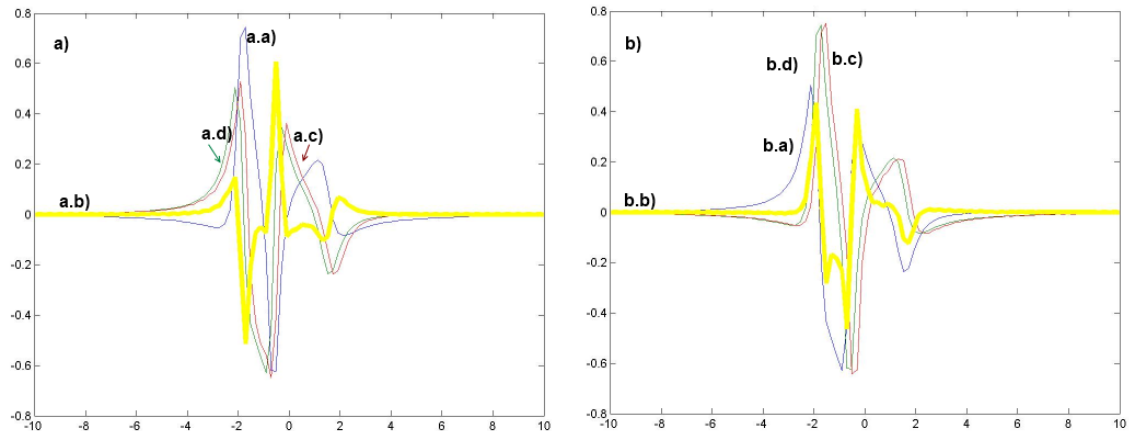


Figure 10.3.4: Results for the frequency mixing model using the `hilbert()` transform a.a) The plot of the real part of $\chi_{pp}(\omega)$ a.b) absolute error plot (a.d-plot minus a.c-plot) a.c) imaginary part of $\chi_{pp}(\omega)$ obtained with the `hilbert()` transform of a.a-plot, a.d) imaginary part of $\chi_{pp}(\omega)$ calculated analytically b.a) The plot of the imaginary part of $\chi_{pp}(\omega)$ b.b) absolute error plot (b.d-plot minus b.c-plot) b.c) real part of $\chi_{pp}(\omega)$ obtained with the `hilbert()` transform of b.a-plot b.d) real part of $\chi_{pp}(\omega)$ calculated analytically

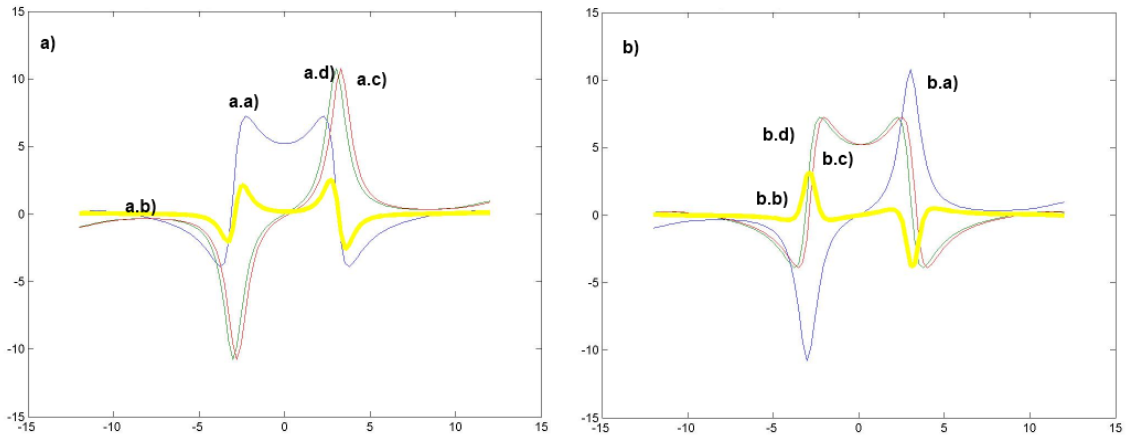


Figure 10.4.1: Results for the linear quantum perturbative model for `quadgk()` Hilbert transform a.a) The plot of the imaginary part of $\chi_{1,qp}(\omega)$ a.b) absolute error plot (d-plot minus c-plot) a.c) real part of $\chi_{1,qp}(\omega)$ obtained with the `quadgk()` Hilbert transform of a-plot a.d) real part of $\chi_{1,qp}(\omega)$ calculated analytically b.b) The plot of the real part of $\chi_{1,qp}(\omega)$ b.b) absolute error plot (d-plot minus c-plot) b.c) imaginary part of $\chi_{1,qp}(\omega)$ obtained with the `quadgk()` Hilbert transform of a-plot b.d) imaginary part of $\chi_{1,qp}(\omega)$ calculated analytically

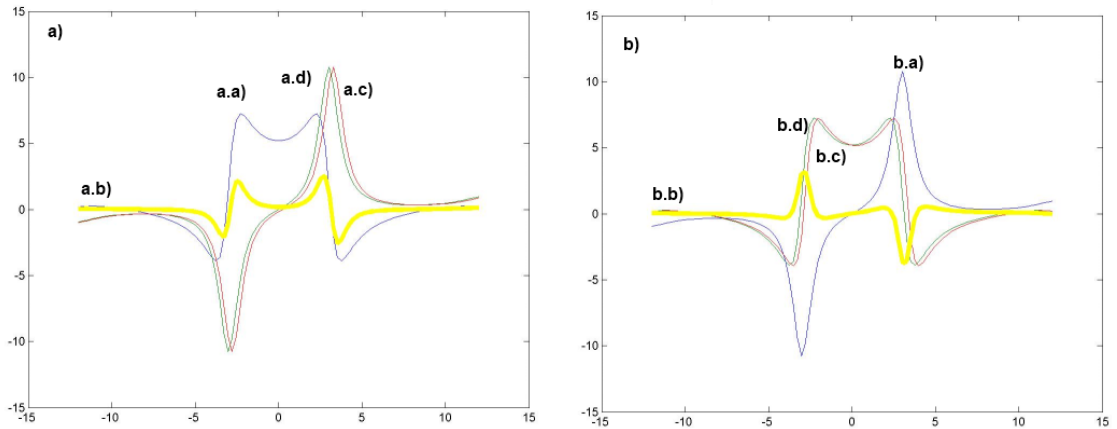


Figure 10.4.2: Results for the linear quantum perturbative model for `hilbert()` transform a.a) The plot of the imaginary part of $\chi_{1,qp}(\omega)$ a.b) absolute error plot (d-plot minus c-plot) a.c) real part of $\chi_{1,qp}(\omega)$ obtained with the `hilbert()` transform of a-plot a.d) real part of $\chi_{1,qp}(\omega)$ calculated analytically b.b) The plot of the real part of $\chi_{1,qp}(\omega)$ b.b) absolute error plot (d-plot minus c-plot) b.c) imaginary part of $\chi_{1,qp}(\delta)$ obtained with the `hilbert()` transform of a-plot b.d) imaginary part of $\chi_{1,qp}(\delta)$ calculated analytically

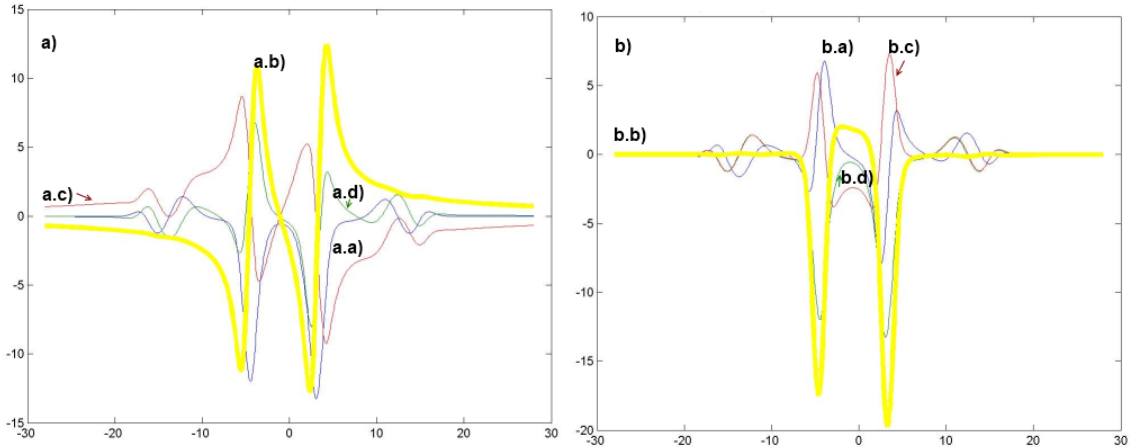


Figure 10.4.3: Results for the second-order quantum perturbative model for `quadgk()` Hilbert transform
 a.a) The plot of the imaginary part of $\chi_{1,qp}(\omega)$ a.b) absolute error plot (d-plot minus c-plot) a.c) real part of $\chi_{1,qp}(\omega)$ obtained with the `quadgk()` Hilbert transform of a-plot a.d) real part of $\chi_{1,qp}(\omega)$ calculated analytically b.b) The plot of the real part of $\chi_{1,qp}(\omega)$ b.b) absolute error plot (d-plot minus c-plot) b.c) imaginary part of $\chi_{1,qp}(\omega)$ obtained with the `quadgk()` Hilbert transform of a-plot b.d) imaginary part of $\chi_{1,qp}(\omega)$ calculated analytically

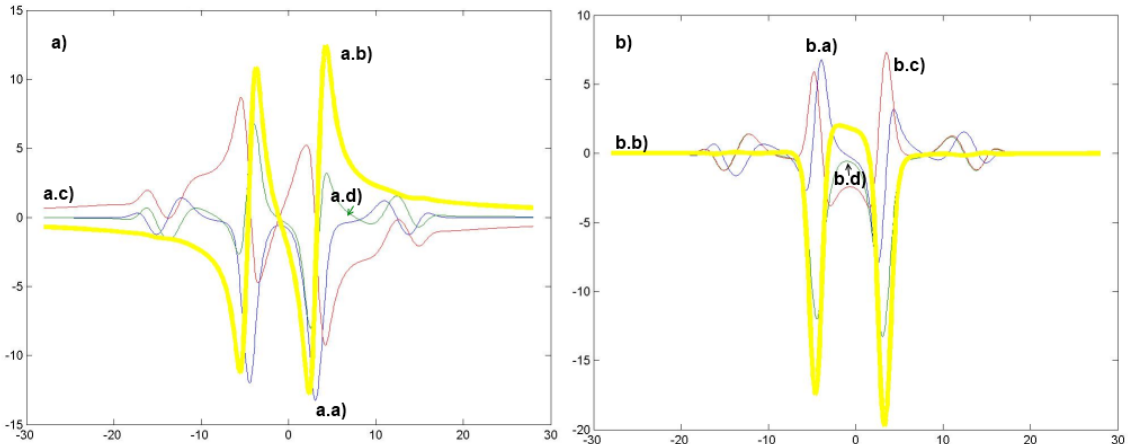


Figure 10.4.4: Results for the second-order quantum perturbative model for `hilbert()` transform a.a) The plot of the imaginary part of $\chi_{1,qp}(\omega)$ a.b) absolute error plot (d-plot minus c-plot) a.c) real part of $\chi_{1,qp}(\omega)$ obtained with the `hilbert()` transform of a-plot a.d) real part of $\chi_{1,qp}(\omega)$ calculated analytically b.b) The plot of the real part of $\chi_{1,qp}(\omega)$ b.b) absolute error plot (d-plot minus c-plot) b.c) imaginary part of $\chi_{1,qp}(\omega)$ obtained with the `hilbert()` transform of a-plot b.d) imaginary part of $\chi_{1,qp}(\omega)$ calculated analytically

Table 2: Time comparison

method name	time used for all 5 models
HTRAN	1.8095s
Newton-Cotes	122.1465s
Clenshaw-Curtis	776.7389s
Hartley	9.5106s
Hermite	6.7423s
Fourier	443.3777s
quadgk()	325.0274s
hilbert()	0.46756s

Table 3: Accuracy comparison

method name	linear	pump-probe	freq. mix.	quant. linear	quant. 2 nd -order
HTRAN	7	5	5	5	2
Newton-Cotes	7	4	4	3	2
Clenshaw-Curtis	9	9	8	7	3
Hartley	8	8	7	6	3
Hermite	6	5	3	3	0
Fourier	6	5	3	3	0
quadgk()	7	7	6	5	3
hilbert()	7	7	6	5	3

11 General comparison of numerical methods used

11.1 Time comparison conclusions:

Until now we have not mention how much time does it take for each of investigated methods to calculate desired results. In the Table 2 we have showed how much time does it take to perform the calculations for all 5 investigated models.

As we can see - the investigated methods come with important timing differences. When preparing experiment data analysis we should choose the appropriate method reasonably.

11.2 Accuracy comparison conclusions:

We have prepare the subjective summary of the accuracy obtained with investigated methods with the zero (bad accuracy) to ten (good accuracy). It is presented in the table 3.

11.3 Application comparison conclusions:

There are two main types of methods - those, which base on the full-vector calculation (like HTRAN, Hartley-Hilbert transform, hilbert()) and those, which require calculation for each point (Newton-Cotes, Clenshaw-Curtis, Hermite-Hilbert, Fourier-Hilbert, quadgk()). The first group comes with relative acceptable accuracy, but still not negligible one.

On the other side we can use the Clenshaw-Curtis based implementation of the Hilbert transform - which has showed as the method with the best accuracy from all investigated methods.

When we would analyze data that has been collected in one dimension - it would be a good idea to hire the accurate, but slow Clenshaw-Curtis Hilbert transform implementation. But we should also prepare a good method for two-dimensional calculation and for such case we should use the fast methods like Hartley-Hilbert transform or built-in MATLAB ®`hilbert()` method.

But what is a good information - all methods can be used in the model analysis and validation process.

12 Conclusion

We have presented a valid implementation of several different approaches to calculate the improper and singular integral used in the Hilbert transform. During the implementation and the literature research we have confirmed, that despite of talking about the complicate Kramers-Kronig relations, we can hire the simpler Hilbert transform.

12.1 Model conclusion

During work on this thesis we have found at least one invalid model - such as second-order quantum-perturbative model. For none of implemented method this model has shown any acceptable type of accuracy. There were more such models, not taken into scope - but with described tools - an experienced research will be able to validate model with the Hilbert transform relations.

The one hypothetical proposal of explanation the failure of the second-order quantum-perturbative model is that this model as the only investigate one - depends on two input frequencies. The theory of multi-dimensional Hilbert transform states, that one point depends on the whole multi-dimensional spectra. What we have done here - was the false assumption - that for such a model we can simple strike on dimension out. This assumption proved to be false.

The multi-dimensional Hilbert transform is beyond the scope of this work and requires the better knowledge of implementation the multi-dimensional singular quadratures.

12.2 Numerical conclusion

1. We have presented several methods and the comparison of their accuracy, convergency and speed. Which method is the best and why? This set of tools should be treated as a numerical tool box - the choice is always depends on the user's choice. 2. The speed-leading methods are based on the full-vector calculations. There are a good candidates for the multi-dimensional hilbert transform integration.

12.3 Z-scan technique conclusion

In our opinion the data collected from the Z-scan experiment can be put into test with all prepared methods. We should also remember, that the phenomena occurring during

this experiment - due to strong energy - shows the complicated nonlinearity, so the multi-dimensional Hilbert transform methods may be required.

12.4 General conclusion

The aim of this work was to:

- Development of numerical methods of the Hilbert transform. It succeeded and the methods are available altogether with their source code and the testing routines. Users can choose among a wide range of methods with described parameters.
- Validation of models given in literature. This succeeded only for the most popular models. There is a wide range of models given in literature for which the Hilbert transform rule simple does not work.
- Carrying out the calculations on multi-dimensional models. It failed. It turned out that such calculations require much more complex numerical methods.

Other conclusions:

1. This thesis is only an introduction into the important, but still not well described, hardly-investigated interdisciplinary problem concerning the investigation of light and matter interaction in area of nonlinear optics.

2. This topic should be continued as the cooperation between various disciplines is the key role to solve many questions stated by nowadays nonlinear optics scientists - so the strong mathematical, numerical, chemical and quantum-mechanical background skills are together required, one person is unable to have it all, so a team should be created (here in Wrocław).

"A major challenge for researchers working in a multidisciplinary area is the need to learn relevant concepts outside their expertise. This may require searching through a vast amount of literature, often leading to frustrations of not being able to extract pertinent information quickly." - P. Prasad [32]

3. We can find many papers in area of Kramers-Kronig for nonlinear optics, but in my opinion - in case of nonlinear optics many of them are false and not properly argued, with wrong or improper mathematical assumptions, numerical errors and sometimes even tendential optimism and non-scepticism, which - especially in area of modern physics - is incomprehensible.

4. We are all in a long run for a Nobel prize :) It's a huge motivation :)

12.5 Further questions and research direction

What should be the continuation of this work?

- The theory which is linking the Hilbert transform with nonlinear optical models should be more deeply investigated. How can the influence of subsequent photons shooting the investigated sample be described with only one equation?
- Many literature models should be validated and a list of both valid and invalid models should be publicated.

- The valid and proper tools for multi-dimensional Hilbert transform should be prepared

Other open questions: 1. Should we always use the Fourier transform when translating between the time-domain and the frequency domain?

2. As the linear model in optical research is quite well described, we need to prepare tools for the nonlinear calculations, which involve operating on the two-dimensional data sets. There are algorithms like 2D-FFT, 2D-FHT, maybe there also can be an algorithm for 2D-hilbert transform.

3. How to efficiently perform calculations for higher dimensional data (f.e. third-order or fifth-order nonlinear phenomena)?

4. We need to make a further research on the topic of the harmonic analysis and Fourier analysis and its application to the spectral analysis.

13 Acknowledgements

I would mostly thank Professor Marek Samo  for introducing me into the magical world of the nonlinear optics. In my opinion there is an important niche between this scientific domain and the numerical analysis, there are also many questions that I am asking now myself (beyond the scope of this thesis) and I would like to find answers in the future.

I would give my acknowledgements for many people from the Wrocław University of Technology, especially:

Katarzyna Matczyszyn, PhD

for inspirations to work between two or more scientific domains and to work for others

Dr. Marcin Nyk, PhD

for a very good mood each time I needed it and for introducing me into the world of real chemical experiments

Chris Corkey, PhD

for Your great smile, great mood and inspiration to travel

All OM-IN-NANO Great TEAM!

I would like to thank You all guys for your hard work and for the great time and experience not only in the real and hard research, but also in a top-science. You are coping with guys! Thank also You for all Your answers to all my (usually simple) questions.

Great honours should be also given for the members of the University of Wrocław. I would like to give my acknowledgements for:

Rafa  Keller, PhD

for supervising me through the hard area of quadratures with singularities

Professor Stanis aw Lewanowicz

for the review of this work, useful comments and inspiration to think outside the cubicle

Grzegorz Karch, Phd

for introducing me into the world of advanced differential and integral calculus

I would also give my thanks for Professor Takemitsu Hasegawa (Fukui, Japan) for useful hints in calculations.

I would also like to thank all those, who has motivated me to finish this thesis.

14 Published Results

K. Parjaszewski, M. Samoć, ”*Understanding the Kramers-Kronig relations in nonlinear optics*”, PANIC 2010 Conference, Wrocław University of Technology

K. Parjaszewski, M. Samoć,”*Understanding and solving the Kramers-Kronig relations in nonlinear optics*”, PANIC 2011 Conference, Wrocław University of Technology

More info: <http://www.organometallics.pwr.wroc.pl/>

15 References

References

- [1] N. Bloembergen. *Nonlinear optics*. World Scientific, 1996.
- [2] Leo I. Bluestein. A linear filtering approach to the computation of the discrete Fourier transform, 1968.
- [3] Robert W. Boyd. *Nonlinear Optics, Third Edition*. Academic Press, 3 edition, April 2008.
- [4] Robert W Boyd, John E Sipe, and Peter W Milonni. Chirality and polarization effects in nonlinear optics. *Journal of Optics A: Pure and Applied Optics*, 6(3):S14, 2004.
- [5] Ronald Newbold Bracewell. *The Fourier Transform and Its Applications*. McGraw Hill, New York, 1965.
- [6] Georg Bruun. z -transform DFT filters and FFTs. *IEEE Transactions on Acoustics, Speech, and Signal Processing*, 26:56–63, 1978. URL: <http://cr.yp.to/bib/entries.html#1978/bruun>.
- [7] Daniela Calvetti, Gene H. Golub, William B. Gragg, and Lothar Reichel. Computation of gauss-kronrod quadrature rules. *Math. Comput.*, 69(231):1035–1052, 2000.
- [8] Demetrios N. Christodoulides, Iam Choon Khoo, Gregory J. Salamo, George I. Stegeman, and Eric W. Van Stryland. Nonlinear refraction and absorption: mechanisms and magnitudes. *Adv. Opt. Photon.*, 2(1):60–200, Mar 2010.
- [9] S. T. Chui, H.-R. Ma, R. V. Kasowski, and W. Y. Hsu. Local-field correction for nonlinear optical coefficients. *Physical Review*, 47(11):6293–6298, March 1993.
- [10] C W Clenshaw and A R Curtis. A method for numerical integration on an automatic computer. *Numerische Mathematik*, 2(1):197–205, 1960.

- [11] James Cooley and John Tukey. An algorithm for the machine calculation of complex fourier series. *Mathematics of Computation*, 19(90):297–301, 1965.
- [12] Newport Corporation. Z-scan for the characterization of transparent optical materials. Application Note 34, Spectra-Physics divistion, Irvine, California, Newport Corporation, Worldwide Headquarters, 1791 Deere Avenue, Irvine, CA 92606, July 2007. MM#00000094 DS-04071.
- [13] Irving J. Good. The interaction algorithm and practical fourier analysis: An addendum. *Journal of the Royal Statistical Society. Series B (Methodological)*, 22:372–375, 1960.
- [14] S.L. Hahn. *Hilbert transforms in signal processing*. Artech House signal processing library. Artech House, 1996.
- [15] T. Hasegawa and T. Torii. An automatic quadrature for Cauchy principal value integrals. *Mathematics of Computation*, 56:741–754, April 1991.
- [16] Peter Henrici. *Applied and Computational Complex Analysis, Discrete Fourier Analysis, Cauchy Integrals, Construction of Conformal Maps, Univalent Functions (Wiley Classics Library) (Volume 3)*. Wiley-Interscience, apr 1993.
- [17] David Crichton Hutchings, M Sheik-Bahae, D J Hagan, and E W Van Stryland. Kramers-kronig relations in nonlinear optics. *Optical and Quantum Electronics*, 24(1):1–30, 1992.
- [18] Mathias Johansson. The hilbert transform. Master’s thesis, Växjö University, March 1999. Mathematics/Applied Mathematics.
- [19] David Kahaner, Cleve Moler, and Stephen Nash. *Numerical methods and software*. Prentice-Hall, Inc., Upper Saddle River, NJ, USA, 1989.
- [20] Subhash C. Kak. Multilayered array computing. In *Proc. 20th Annual Conference on Information Sciences and Systems, Princeton*, pages 436–441, 1986.
- [21] Y. Katznelson. *An introduction to harmonic analysis*. Cambridge mathematical library. Cambridge University Press, 2004.
- [22] M Lamb and V Rouillard. Some issues when using fourier analysis for the extraction of modal parameters. *Journal of Physics: Conference Series*, 181(1):012007, 2009.
- [23] M Levenson and N Bloembergen. Dispersion of the nonlinear optical susceptibility tensor in centrosymmetric media. *Physical Review B*, 10(10):4447–4463, 1974.
- [24] M.D. Licker. *McGraw-Hill Encyclopedia of Science and Technology, 10th Edition*, volume 12. McGraw-Hill, 2007.
- [25] V. Lucarini. *Kramers-Kronig relations in optical materials research*. Springer series in optical sciences. Springer, 2005.

- [26] Marek Samoć, A. Samoć, B. Luther-Davies, M. G. Humphrey, M. P. Cifuentes. Nonlinear absorption: materials and mechanisms. In Agnieszka Popiółek-Masajada, editor, *Proceedings of the Symposium on Photonics Technologies for 7th Framework Program*, pages 230–233, Wrocław, Poland, October 2006. Institute of Physics, Wrocław University of Technology, Centre for Advanced Materials and Nanotechnology, Wrocław University of Technology, Wrocław Centre for Technology Transfer, Oficyna Wydawnicza Politechniki Wrocławskiej.
- [27] Mark G. Kuzyk, Benjamin R. Anderson, Nathan J. Dawson, Sheng-Ting Hung, Wei Lu, Shiva Ramini, Jennifer L. Schei, Shoresh Shafei, Julian H. Smith, Afsoon Soudi, Szymon Steplewski, Xianjun Ye. Nonlinear optics. <http://www.nlosource.com/LectureNotesBook.pdf>, August 2010. Course book.
- [28] Shaul Mukamel. Causal versus noncausal description of nonlinear wave mixing: Resolving the damping-sign controversy. *Phys. Rev. A*, 76:021803, Aug 2007.
- [29] A. Novak. *Identification of Nonlinear Systems in Acoustics*. PhD thesis, Université du Maine, Le Mans, France AND Czech Technical University, Prague, Czech Republic, 2009.
- [30] Palffy-Muhoray. Course materials for lc optics and photonics. <http://mpalffy.lci.kent.edu/Optics/>, Spring 2011. CPHY 6/74495.
- [31] David J. Williams Paras N. Prasad. *Introduction to Nonlinear Optical Effects in Molecules and Polymers*, volume 1. Wiley-Interscience, New York, 01 1991. A Wiley-Interscience publication.
- [32] P.N. Prasad. *Nanophotonics*. Wiley-Interscience, 2004.
- [33] Charles M. Rader. Discrete fourier transforms when the number of data samples is prime. *Proceedings of the IEEE*, 56(6):1107–1108, 1968.
- [34] Marek Samoć. Third-order nonlinear optical materials: practical issues and theoretical challenges. 10.1007/s00894-010-0856-8, 2010.
- [35] Jae-Kuk Seo. *Study of time-resolved measurement of intensity-dependent refractive index change in GaInAsP waveguides*. Doctoral dissertation, Tokyo Institute of Technology, Department of Electrival and Electronic Engineering, 2-12-1 Ookoyama, Meguro-Ku, Tokyo, 152-8552, JAPAN, February 2006. Supervisor: Professor Tetsuya Mizumoto, Report number: 6444.
- [36] L. F. Shampine. Vectorized adaptive quadrature in matlab. *J. Comput. Appl. Math.*, 211:131–140, January 2008.
- [37] Sheik-Bahae, Mansoor and Said, A A and Wei, T H and Hagan, D J and Van Stryland, E W. Sensitive measurement of optical nonlinearities using a single beam. *Quantum*, 26(4):760–769, April 1990.
- [38] Sy-Been Jaw Soo-Chang Pei. Computation of discrete hilbert transform through fast hartley transform. *IEEE Transactions on Circuits and Systems*, 36:1251–1252, September 1989.

- [39] E.C. Titchmarsh. *Introduction to the theory of Fourier integrals*. The Clarendon Press, 1948.
- [40] F. Träger. *Springer handbook of lasers and optics*. Springer, 2007.
- [41] M. Trott. *The Mathematica GuideBook for Programming*. Springer-Verlag, New York, 2004.
- [42] G. Tsigaridas, M. Fakis, I. Polyzos, P. Persephonis, and V. Giannetas. Z-scan technique through beam radius measurements. *Applied Physics B: Lasers and Optics*, 76:83–86, 2003. 10.1007/s00340-002-1067-5.
- [43] H Tuononen, E Gornov, J A Zeitler, J Aaltonen, and K-E Peiponen. Using modified kramers-kronig relations to test transmission spectra of porous media in thz-tds. *Optics Letters*, 35(5):631–633, 2010.
- [44] Ronald F. Ullmann. An algorithm for the fast hartley transform, June 1984. Stanford Exploration Project, 38.
- [45] I. J. Weinberg. Hilbert transform by numerical integration. In-House Report RADC-TR-79-3, Rome Air Development Center, United States Air Force Hanscom AFB, Rome, January 1979. Mass. 01731.
- [46] Eric W. Weisstein. Hilbert transform.
- [47] Honam Yum and Selim M Shahriar. Pump-probe model for the kramers-kronig relations in a laser. Comments: 10 pages, 5 figures, Mar 2010.

Appendix A - The source code

Appendix A.1 - HTRAN

```

function [HT,F] = htran(F,R)
% The algorithm:

% Correcting the input size:
if(size(R,1)>size(R,2)), R=R';end;
if(size(F,1)>size(F,2)), F=F';end;
N = size(R,2);

% Calculating the F middlepoint array:
Fp(1,1:N-1) = 0.5 .* (F(1,1:N-1)+F(1,2:N));
step = F(2)-F(1);

% Build h array (step array for faster calculation) — Simpson's rule combined with
% the trapezoidal rule
h(1) = step/3;
h(1,2:N-1) = 2.*step./3 + mod(1:N-2,2).*2.*step./3;
h(N) = step/3;
if (mod(N,2)==1), h(N-1) = 5*step/6; h(N) = step/2; end;

% Cubic interpolation for the interior values and parabolic interpolation for the
% end values we obtain
% new set of ordinates, to omit the singularity:
Rp = zeros(1,N-1);
Rp(1) = 0.375*R(1) + 0.75*R(2) - 0.125*R(3);
Rp(1,N-1) = -0.125*R(1,N-2) + 0.75*R(1,N-1) + 0.375*R(1,N);
Rp(1,2:N-2) = -0.0625*R(1,1:N-3)+0.5625*R(1,2:N-2)+0.5625*R(1,3:N-1)-0.0625*R(1,4:N);

% Build Yp array — the heart and first step in integration:
Yp = zeros(1,N-1);
for i=1:N-1, Yp(i) = sum(h.*((R-Rp(i))./(F-Fp(i))))/pi; end;

% Build Xp array — the second step in integration:
Xp = -Rp./pi .* log((Fp-Fp(1))./(Fp(N-1)-Fp)) + Yp./pi;

```

```

% Build Xres array - translating the Xp array into Xres array (cubic
% interpolation, as previous) - but this time Xp is smaller than Xres:
Xres = zeros(1,N);
Xres(1)      = 1.875 *Xp(1)      - 1.25 *Xp(2)      + 0.375 *Xp(3);
Xres(1,2)    = 0.375 *Xp(1)      + 0.75 *Xp(2)      - 0.125 *Xp(3);
Xres(1,3:N-2) = -0.0625*Xp(1,1:N-4) + 0.5625*Xp(1,2:N-3) + ..
                  0.5625*Xp(1,3:N-2) - 0.0625*Xp(1,4:N-1);
Xres(1,N-1) = -0.125 *Xp(1,N-3) + 0.75 *Xp(1,N-2) + 0.375 *Xp(1,N-1);
Xres(1,N)    = 0.375 *Xp(1,N-3) - 1.25 *Xp(1,N-2) + 1.875 *Xp(1,N-1);

% We take the real/imag separately:
% Orig = imag(Xres);
HT = Xres;
end

```

Appendix A.2 - HNCX

```

function [H, F] = hncX(fun, a, b, tol, n, cs, pts, wrn, inh)
%% The algorithm:

% Preparation of arguments
if nargin < 3, error('QUADNCX:ParamErr', ...
    'Wrong number of parameter given: fun, a, b are mandatory'); end;
if nargin < 4, tol = 10^(-3); end;
if nargin < 5, n = 8; end;
if nargin < 6, cs = 0.1; end;
if nargin < 7, pts = 200; end;
if nargin < 8, wrn = true; end;
if nargin < 9, h = waitbar(0, 'Please Wait'); closewb= true;
else h = inh; closewb = false; end;

% We would like to integrate within 5 times bigger region
d = b - a;
aMax = a - 2 * d; bMax = b + 2 * d; PTS = 5 * pts;
F = linspace(a, b, PTS); X = linspace(a,b,pts);
Hp = zeros(1, PTS);

% The main hilbert transform loop
for k=1:PTS
    waitbar(k/PTS, h);
    innerfun = @(x) fun(x) ./ (x - F(k));
    Hp(k) = quadncX(@(x) innerfun(x), aMax, F(k) - cs, tol, n, wrn) + ...
        quadncX(@(x) innerfun(x), F(k) + cs, bMax, tol, n, wrn);
end
% finally we are closing the waitbar
if(true==closewb), close(h); end;

Hp = Hp./ pi; H = interp1(F, Hp, X, 'pchip');
end

function res = quadncX(fun, a, b, tol, n, wrn)
nsteps = 100; maxNoSteps = 256*32;
iterates = 1; maxIterate = 256;
M = 1.1;
tab = preevaluateNCTab(n, a, b);

while (iterates < maxIterate);
    nStep = ceil(nsteps * M);
    step1 = doStep(fun, a, b, nsteps, tab);
    step2 = doStep(fun, a, b, nStep, tab);
    res = (4*step2-step1)/3;
    err = abs((step1-res))/max(abs([step1, res, tol]));
    if (err<tol), break;
    else nsteps = nStep; M = M*1.3;
    end;
    if (nsteps >=maxNoSteps), break; end;
    iterates = iterates + 1;
end
if (wrn == true)
    if (iterates >= maxIterate), warning('QUADNCX:MaxIterReached', ...
        'maximum number of iterations reached -- the integral seems to be singular');
    elseif (nsteps >=maxNoSteps), warning('QUADNCX:MaNoSteps', ...
        'maximum number of steps reached -- the integral seems to be singular');
    end;
end
end

function tab = preevaluateNCTab(n, a, b)
%% The algorithm:
maplestr = ['Digits:=40:n:=' num2str(n) ':tab:=evalf(seq((( ' num2str(b) ' )-...
-----(' num2str(a)'))/n*(-1)^(n-k)*1/(factorial(k)*factorial(n-k)) ...
*int(product(t-jj, jj=0..n)/(t-k), t=0..n), k=0..n));'];
maple_string;
tab= str2num(maple(maplestr)); %#ok<ST2NM>
end

function res = doStep(fun, a, b, nsteps, tab)
%% The algorithm:
nc = size(tab, 1);
intervals = linspace(a, b, nsteps);

```

```

% Quadrature is divided into small steps :
M = zeros(nc, nosteps-1);
M(1, :) = intervals(1:nosteps-1);
M(nc, :) = intervals(2:nosteps);
h = (M(nc, :) - M(1, :)) ./ nc;

% Final calculation in two lines using the matrix multiplication :
for k=2:(nc-1), M(k, :) = M(1, :) + (k-1) .* h; end;
res = sum(fun(M') * tab) / nosteps;
end

```

Appendix A.3 - HTRANCC

```

function H = htrancc(fun, X, tol, inh)
    %% The algorithm :

    % We set the default tolerance if not given :
    if nargin<3, tol=10^(-3); end;
    if nargin<4, h = waitbar(0, 'Please wait', 'Name', ...
        'Hilbert-Transform-with-Clebsch-Curtis'); ...
    else h = inh; end;

    a = min(X); b = max(X); NX = length(X); T = abs(b - a);
    A = a - 2 * T; B = b + 2 * T;
    Hh = zeros(1, NX); Y = linspace(a, b, NX);

    % Cubic interpolation routine (N->N-1 points) :
    Yp(1) = 0.375*Y(1) + 0.75*Y(2) - 0.125*Y(3);
    Yp(1, NX-1) = -0.125*Y(1, NX-2) + 0.75*Y(1, NX-1) + 0.375*Y(1, NX);
    Yp(1, 2:NX-2) = -0.0625*Y(1, 1:(NX-3)) + 0.5625*Y(1, 2:(NX-2)) + 0.5625*Y(1, 3:(NX-1)) ...
        - 0.0625*Y(1, 4:NX);

    % Main application loop with the waitbar :
    for n = 1:1:NX-1
        Hh(n) = hcc(fun, Yp(n), tol, A, B);
        waitbar(n/(NX-1), h, 'Please wait');
    end;
    if nargin<4, close(h); end;

    % Reverse cubic interpolation routine (N-1->N points) :
    H = zeros(1,NX);
    H(1) = 1.875 *Hh(1) - 1.25 *Hh(2) + 0.375 *Hh(3);
    H(1,2) = 0.375 *Hh(1) + 0.75 *Hh(2) - 0.125 *Hh(3);
    H(1,3:NX-2) = -0.0625*Hh(1,1:NX-4) + 0.5625*Hh(1,2:NX-3) + 0.5625*Hh(1,3:NX-2) ...
        - 0.0625*Hh(1,4:NX-1);
    H(1,NX-1) = -0.125 *Hh(1,NX-3) + 0.75 *Hh(1,NX-2) + 0.375 *Hh(1,NX-1);
    H(1,NX) = 0.375 *Hh(1,NX-3) - 1.25 *Hh(1,NX-2) + 1.875 *Hh(1,NX-1);

end

function h = hcc(fun, y, tol, a, b)
    %% Central integral
    h = hccside2side(fun, y, tol, a, b);

    %% Left integral
    leftIntVal = 0;

    %% Right integral
    rightIntVal = 0;

    %% Final summation
    h = leftIntVal + h + rightIntVal;
end

function h = hccside2side(fun, y, tol, a, b)
    %% Hilbert transform using the Clebsch-Curtis quadrature for a definite interval
    Period = b - a;
    Center = (b+a)/2;
    d = (y - Center) .* 2 ./ Period;

    ccFun = @(t) (fun(t .* Period./2 + Center));
    h = 1 / pi * newdocc(@(t) ccFun(t), d, tol);
end

```

Appendix A.4 - HFTHILBERT

```

function HY = hfthilbert(Y)
    %% The algorithm :

    % We perform the zero padding to the next power-of-two length
    N = max(size(Y));
    M = 2 ^ ceil(log2(N));
    Y = [Y, zeros(1,M-N)];

    % Discrete Hartley transform boosted-up to O(n log n)
    HF = fht(Y);

    % Defining the HH vector
    O1 = ones(1, floor(M/2)-1); O2 = -ones(1, ceil(M/2)-1); HH = [0, O1, 0, O2];

```

```

% Defining the time reversal of HF
TRHF = HF([1, M:-1:2]);

% Based on the convolution theorem we get the Hartley-Hilbert transform
% of X, so in the last step we need to perform the inverse Hartley
% transform
IHX = TRHF .* HH;

% Inverse Hartley transform boosted-up to O(n log n)
HY = - 1/M .* fht(IHX);

% The final output vector
HY = HY(1:N);
end

function res = fht(X)
%% The algorithm:
N = length(X);

% We precalculate the CAS table for vectors of length less or equal 8:
CAS = cell(8);
CAS{1} = cas(0);
for k=2:8, CAS{k} = cas(2*pi*((0:(k-1))'*(0:(k-1)))/k); end

% Now we are sure, that X vector is of size M which is a power value of 2.
DHT = dofht(X,N,CAS);

% The final vector must be truncated because it was arbitrary enlarged
% to be with length of power of two
res = DHT(1:N);
end

function HY = dofht(X,N,CAS)
% Fast Hartley Transform for N lower than 8
if N<=8,
    HY=X * CAS{N}; % Instant FHT for 8-element array
    return;
end;
% We split the input vector into two equal vectors
X1 = X(1:2:end); X2 = X(2:2:end); % In MATLAB first index equals 1, not 0 -
% but in literature X1 is called even, X2 - odd indices.

% Divide & conquer approach
HT1 = dofht(X1,N/2,CAS);
HT2 = dofht(X2,N/2,CAS);

% We precalculate the lower and upper part of the output array
low = 1:N/2;
revlow = [1, N/2:-1:2];
arg = (2*pi/N).* (low-1);
CS = cos(arg) .* HT2(low) + sin(arg) .* HT2(revlow);
H = HT1(low);

% The lower and upper part of DHT is combined with the following
% radix-2 way
HY = [H + CS, H - CS];
end

function res = cas(X), res = cos(X) + sin(X); end

```

Appendix A.5 - HERHTRANS

```

function [YH, YFun] = herhtrans(fun, X, tol, maxN)
%% The algorithm:

if nargin < 3, tol = 10^(-4); end;
if nargin < 4, maxN = 18; end;
% We set the initial multipliers count on 4, but it shall/may rise
MaxN = min(maxN, 27); InitN = 4; N = InitN;

sum = 0; val = 0;
% Main loop
i=1; AN = zeros(1, N);
Fval = fun(X);
while (i<=N)
    n = i-1; % Select proper Hermite function
    AN(i) = getAN(fun, n, tol);
    HphiVal = hphin(X, n);
    phiVal = phin(X, n);
    multiplier = AN(i) .* HphiVal;
    sum = sum + multiplier;
    val = val + AN(i) .* phiVal;

    % If the current multiplier is not negligable - we need to search further
    err = max(abs((val-Fval)/max(abs([val,Fval,tol]))));
    if ((i > (N-2)) && (err >= tol) && (N<MaxN)), N = N+1; end;
    i = i+1;
end
YH = -real(sum);
YFun = val;
end

```

```

function an = getAN(fun, n, tol)
    pFun = phiFun(n);
    funphi = @(t)^(fun(t)).*pFun(t);

    % We change the integration range from -inf .. inf to -1 .. 1
    ccFun = @(t) ((abs(t)<1) .* funphi(-t./(t.^2-1)) .* (1+t.^2) ./ (-1+t.^2).^2);

    % Main numerical integration
    N = 128;
    prev = docc(ccFun, N/2);
    while (N < 1024*1024)
        an = docc(ccFun, N);
        if (abs(an-prev)<tol), break; else N = 2*N; end;
        prev = an;
    end
end

%% phin, hphin, phiFun, hPhiFun - cached/precalculated function procedures

```

Appendix A.6 - FOURHTRANS

```

function [HY, Y] = fourhtrans(fun, X, m, doccN, inh)
    %% The algorithm:
    if nargin<3,m=1024; end;
    if nargin<4,doccN=4096; end;
    if nargin<5,h=waitbar(0,'Calculations -- Please wait ...','Name', ...
        'Hilbert transform based on the Fourier series');
    closewb = true; else h = inh; closewb = false; end;

    % First we calculate the X boundaries
    a = min(X);
    b = max(X);
    n = length(X);

    % Then we enlarge 5 times the investigated interval:
    down = a-(b-a)*2;
    up = b+(b-a)*2;
    XX = linspace(down, up, 5*n);

    % We measure the important values
    T = (up-down);           % period
    L = T/2;                 % halfperiod

    % Calculation of the first component
    Yp = 1/2 .* docc(fun, doccN, down, up);
    HYp = 0;

    % Main loop:
    for k=1:m
        an = docc(@(x) fun(x) .* cos(k*pi/L .* x), doccN, down, up);
        bn = docc(@(x) fun(x) .* sin(k*pi/L .* x), doccN, down, up);

        cs = cos(k*pi/L .* XX);
        sn = sin(k*pi/L .* XX);

        % Function approximation (on the NX interval)
        Yp = Yp + an .* cs + bn .* sn;
        % Hilbert transform approximation (on the NX interval)
        HYp = HYp + bn .* cs + an .* sn;
        waitbar(k/m,h);
    end;
    if (true==closewb), close(h); end;

    % Finally, we extract the [a, b] part from the [up, down] interval
    INN = (2*n+1):1:3*n;
    Y = Yp(INN);
    HY = HYp(INN);
end

function val = docc(fun, N, a, b)
    %% The algorithm:
    if nargin<4, b = 1; end;
    if nargin<3, a = -1; end;
    if nargin<2, N = 256; end;

    % Mapping [a, b] into [-1, 1]
    C = (b+a)/2;
    T = (b-a)/2;

    % A new function to be integrated from -1 to 1
    newfun = @(x) fun((x .* T) + C);

    % Getting the value with standard -1,1 Clenshaw Curtis integration routine
    val = onetoonecc(newfun,N);
end

function val = onetoonecc(fun, N)
    %% CC integration from -1 to 1:
    N2 = N/2;
    % We make this division once, for faster computation
    ps = 0:1:N2;

```

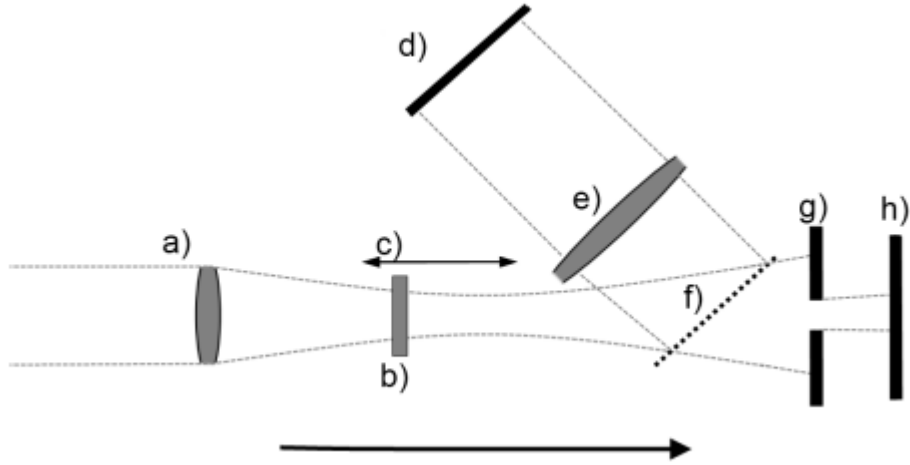


Figure 15.0.1: The schematic diagram of the main measurement part of the z-scan experiment

```
% Array of N/2+1 points (where N2 = N/2)
xn = cos(ps.pi./N);
% N2+1 abscissas from the 0..pi range
yn = fun(xn) + fun(-xn);
% N2+1 ordinates for fun(cos(n*pi/N))
yn(isnan(yn) | (isfinite(yn)==0)) = 0;
% We shall set all NaNs and Infs to zero
g = real(fft(yn(1+[0:N2-(N2-1):-1:1]))/.2;
% Look at quote in the base description about the connection of DCT-I and DFT/FFT
cn = [g(1), g(2:N2)+g(N:-1:N2+2), g(N2+1)];
% We take symmetrical values and add them together (omitting first and last)
dn = [2, 2./(1-(2.*(1:1:(N2-1)).^2), 2./(1-N.^2));
% This is the final vector for multiplying
val = (dn * cn')/ N;
% Final cc integral calculation
end
```

Appendix B - ZScan Measurements

Appendix B.1 - Overview of the z-scan technique

One of the most important questions being the major motivation of this thesis is how the theory of Hilbert transform or the Kramers-Kronig relations can be applied to the data measured with the standard "open aperture" and "closed aperture" z-scan technique. In this chapter we will describe the process of data collection and its translation into the nonlinear absorption coefficient spectra and nonlinear refraction index spectra. As mentioned before, since summer 2010 we have set up the femto-second ($1 \text{ fs} = 10^{-15} \text{ s}$) z-scan system using a Quantronix Integra regenerative amplifier operating at 1 kHz and providing approximately 1 mJ, 100 fs, 800 nanometer ($1 \text{ nm} = 10^{-9} \text{ m}$) pulses. It is used as a pump to the Palitra optical parametric amplifier, which, using several different frequency mixing schemes, can provide the coverage of the 450 - 2000 nm wavelength range. The best way to describe this set up will be to use Figure (15.0.1) and Figure (15.0.2).

Legend for Figures 15.0.1 and 15.0.2

Overview of the main measurement part of the z-scan set-up built at the Wrocław University of Technology and being used since summer 2010.

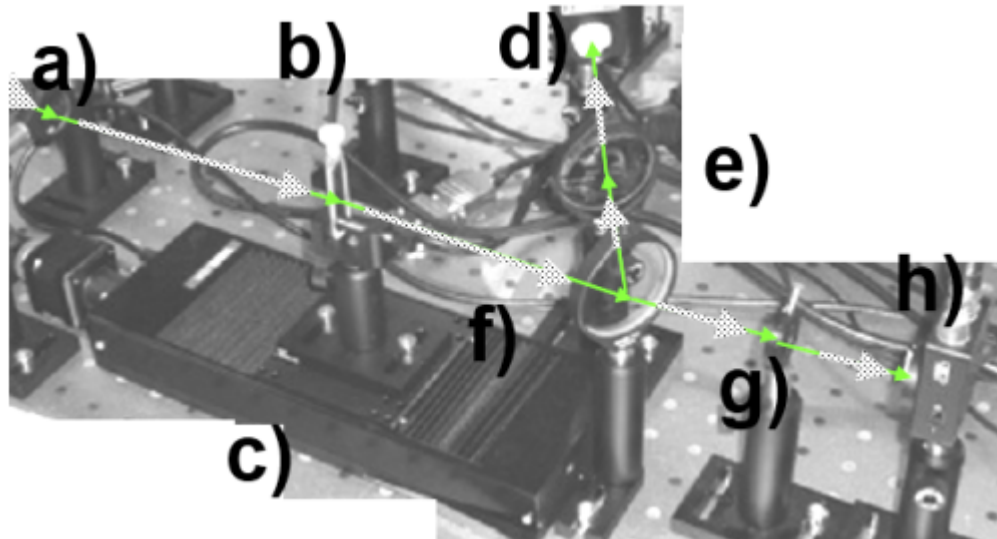


Figure 15.0.2: The photographic diagram of the main measurement part of the z-scan experiment

- (a) FOCUSING LENS - A laser beam goes through focusing a lens.
- (b) SAMPLE IN A CUVETTE - Investigate sample is put into a silica cuvette.
- (c) DYNAMIC (MOBILE) STAGE - During experiment the sample changes its relative position from the lens
- (d) DETECTOR 1 - Finally the beam reaches the “open-aperture” detector
- (e) DEFOCUSING LENS - “Open-aperture” defocusing lens before detector
- (f) BEAM SPLITTER - Laser beam is split to pass both through ”open-aperture” and ”closed aperture” with a beam splitter
- (g) APERTURE - This is the aperture before the “closed-aperture” detector
- (h) DETECTOR 2 - Finally the beam reaches the “closed-aperture” detector

The inventor of the z-scan technique was the Professor Mansoor Sheik-Bahae in 1989 [37] and since then many variants of this technique have been deployed “EZ-Scan”, “White Light z-scan”, “Excite-Probe z-scan” [12]. In a short description - the z-scan technique uses a single laser beam, a mobile stage and two detectors - for the open and closed aperture. Using physical model - we can relate the open-aperture results with the nonlinear absorption and the closed-aperture with the nonlinear refraction index. The mobile stage moves the sample through the position focal point of the focusing lens. We therefore obtain two diagrams - shown on 15.0.1 and 15.0.2.

We must hereby stress that what we obtain with one z-scan measurement is only half a way to calculate one point in the nonlinear spectrum plot - because a typical sample is held inside a silica cuvette and is soluted in some solution (for example chloroform or toluene). So firstly we must measure the solution and an empty silica cuvette z-scan transmittance plots for each monochromatic wavelength and after so - perform the z-scan experiment on the investigated sample.

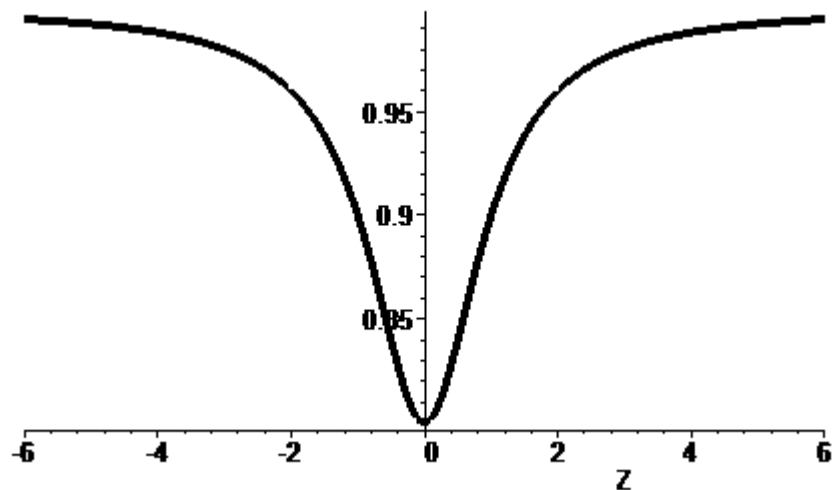


Figure 15.0.3: A typical open-aperture transmittance $\Delta T(Z)$ plot in a z-scan experiment, where
 Z - the position of the stage/sample
0 position - the focal point of focusing lens

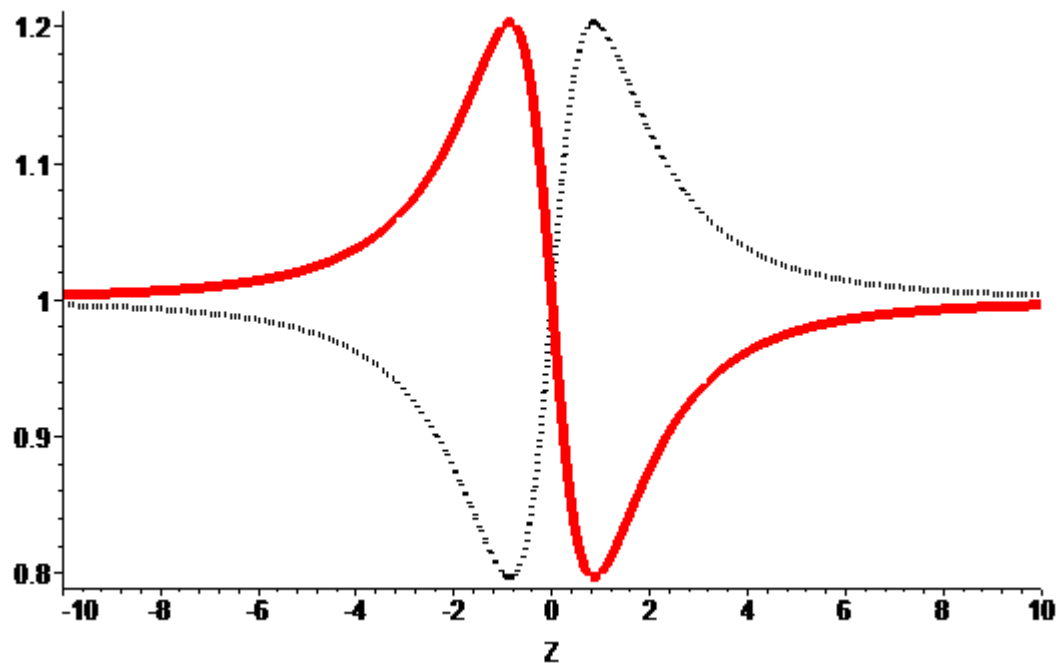


Figure 15.0.4: A typical closed-aperture transmittance $\Delta T(Z)$ plots in a z-scan experiment, where:
 Z - the position of the stage/sample,
0 position - the focal point of focusing lens
red (dashed) plot - material with a positive (negative) refractive index

Appendix B.2 - Overview of the derivation

Calculation of the nonlinear absorption coefficient:

As shown of the 15.0.3 the open-aperture transmittance can be described with the approximation equation:

$$\Delta T(Z) = \frac{\beta I_0 (1 - e^{(-\alpha) L})}{\alpha 2 \sqrt{2}} \left(1 + \frac{Z^2}{(\frac{n \pi w_0^2}{\lambda})^2} \right), \quad (15.0.1)$$

with the following parameters used:

$\Delta T(Z)$ - normalised transmittance of the sample at Z

I_0 - peak on-axis irradiance at focus

L - sample length

β - two-photon absorption coefficient

α - absorption coefficient

n - index of refraction

w_0 - spot size at focus (radius at $\frac{1}{e^2}$)

λ - laser wavelength

Z - position of sample with respect to the focal position

We obtain the two-photon absorption coefficient while standard (f.e. least squares) fitting the measured open-aperture β plot. This is of course also not the complete truth, because with some advanced models we can obtain other absorptive nonlinearities. In a short description - the multi-photon absorption can be assumed when the closed-aperture peak is suppressed, but unfortunately the absorption saturation has just got the opposite effect. So the z-scan technique gives only the simple information about the nonlinear absorption processes.

Calculation of the nonlinear refraction index:

On the Figure 15.0.4 we can see the closed-aperture transmittance plot with respect to the sample position Z . It has a characteristic shape of peak trailing the valley or the valley trailing the peak if the n_2 sign is negative. What now interests us, is the difference between the peak and valley amplitude - we will call it ΔT_{pv} . From this difference we can calculate the on-axis peak nonlinear phase shift with sample at focus $\Delta \Phi_0$

$$|\Delta \Phi_0| = \frac{\Delta T_{pv}}{0.407} (1 - S)^{0.27}, \quad (15.0.2)$$

where: S - fraction of beam transmitted by the aperture
 ΔT_{pv} - change in normalised transmittance between peak and valley.

Now we can estimate the refraction index from equation:

$$n_2 = \frac{\lambda \Delta \Phi_0}{2 \pi I_0} \frac{1 - e^{(-\alpha) L}}{\alpha}, \quad (15.0.3)$$

$\Delta \Phi_0$ - on-axis peak nonlinear phase shift with sample at focus

I_0 - peak on-axis irradiance at focus

where: L - sample length

α - absorption coefficient

λ - laser wavelength

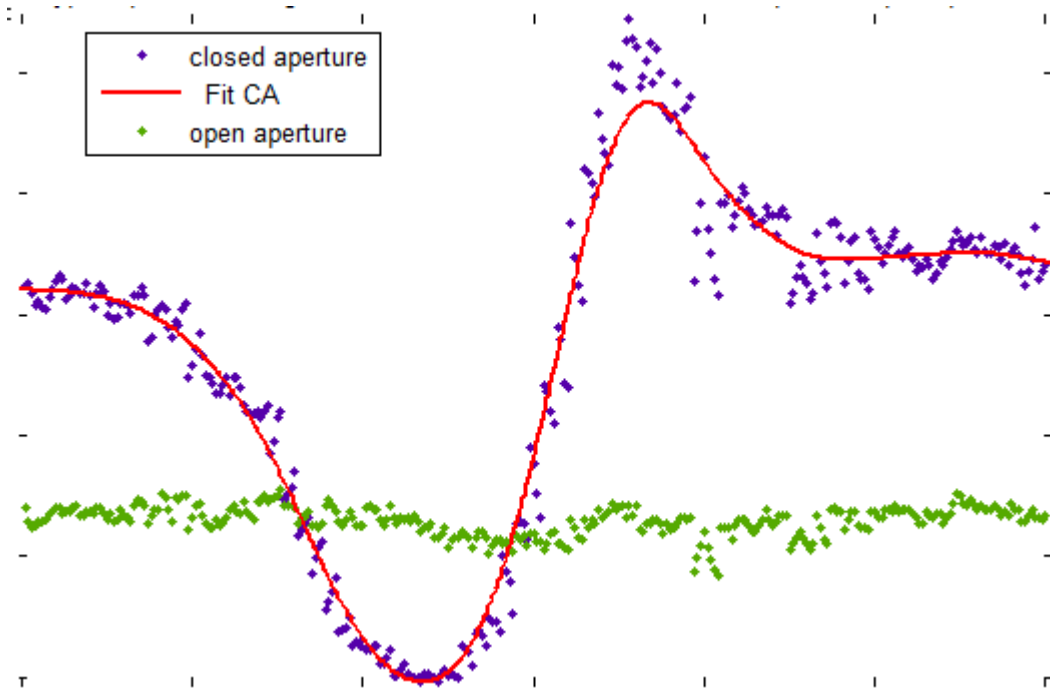


Figure 15.0.5: A typical plot for both close and open aperture with respect to the sample position Z and with the fit spline line

With data points collected for each wavelength we may obtain the full spectral plot for both nonlinear absorption coefficient and nonlinear refraction index - due to the z-scan measurements.

Appendix B.3 - Definition of the main problems

A typical z-scan experiment consists of the measurement routines with number of more or less around 15-20 different wavelength. One z-scan measurement usually takes between 5 to 10 minutes and together with:

- (a) long laser calibration process after each change of wavelength
- (b) silica and empty-solution measurement
- (c) measurement of a typical set of 10-20 measured cuvette samples

The main problems in the z-scan technique concerns the huge amount of time required for one experiment and a dozen factors of uncertainty for each measurement. It may take many days or even weeks to complete one measurement - so even a simple one routine is a time-demanding process and therefore we would like to get as more information from one experiment as possible. Scientists are very interested in optimization of the z-scan method. The physical theory requires better understanding of the process and results requires the better numerical precision, because the general error cumulates with the laser non stability, method approximation error, fitting and numerical calculations error.

A typical plot containing the z-scan measurement for the close aperture, open aperture and the laser reference is shown in the Figure 15.0.5